BioMed Research International

Sepsis: Diagnosis, Pathophysiology, and Novel Therapeutics for Clinical Management

Lead Guest Editor: Anupam Jyoti
Guest Editors: Manash K. Paul, Vijay Kumar Srivastava, and Sanket Kaushik

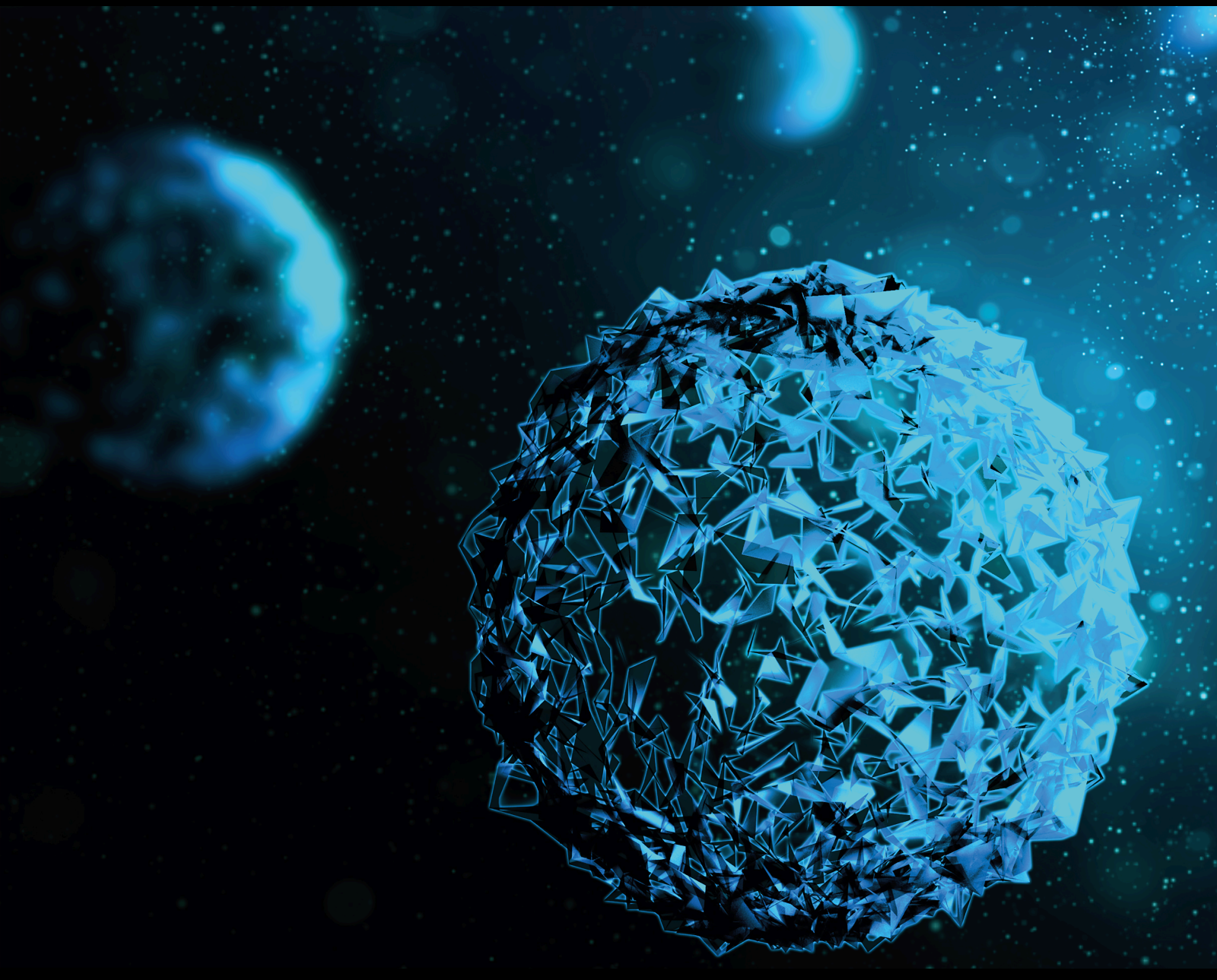

Sepsis: Diagnosis, Pathophysiology, and Novel Therapeutics for Clinical Management

BioMed Research International

Sepsis: Diagnosis, Pathophysiology, and Novel Therapeutics for Clinical Management

Lead Guest Editor: Anupam Jyoti
Guest Editors: Manash K. Paul, Vijay Kumar Srivastava, and Sanket Kaushik

Section Editors

Penny A. Asbell, USA
David Bernardo, Spain
Gerald Brandacher, USA
Kim Bridle, Australia
Laura Chronopoulou, Italy
Gerald A. Colvin, USA
Aaron S. Dumont, USA
Pierfrancesco Franco, Italy
Raj P. Kandpal, USA
Fabrizio Montecucco, Italy
Mangesh S. Pednekar, India
Letterio S. Politi, USA
Jinsong Ren, China
William B. Rodgers, USA
Harry W. Schroeder, USA
Andrea Scribante, Italy
Germán Vicente-Rodriguez, Spain
Momiao Xiong, USA
Hui Zhang, China

Academic Editors

Immunology

Contents

Hindawi
BioMed Research International
Volume 2021, Article ID 9913625, 13 pages
https://doi.org/10.1155/2021/9913625

Research Article

Probing the Peculiarity of *Eh*RabX10, a pseudoRab GTPase, from the Enteric Parasite *Entamoeba histolytica* through In Silico Modeling and Docking Studies

Mrinalini Roy,[1] **Sanket Kaushik**,[1] **Anupam Jyoti**,[2] **and Vijay Kumar Srivastava**[1]

[1]*Amity Institute of Biotechnology, Amity University Rajasthan, Kant Kalwar, NH-11C, Jaipur-Delhi Highway, Jaipur, India*
[2]*Faculty of Applied Sciences and Biotechnology, Shoolini University of Biotechnology and Management Sciences, Bajhol, Solan, Himachal Pradesh 173229, India*

Correspondence should be addressed to Vijay Kumar Srivastava; vksrivastava@jpr.amity.edu

Received 26 May 2021; Revised 8 September 2021; Accepted 23 September 2021; Published 6 October 2021

Academic Editor: Prasanth Manohar

Entamoeba histolytica (*Eh*) is a pathogenic eukaryote that often resides silently in humans under asymptomatic stages. Upon indeterminate stimulus, it develops into fulminant amoebiasis that causes severe hepatic abscesses with 50% mortality. This neglected tropical pathogen relies massively on membrane modulation to flourish and cause disease; these modulations range from the phagocytic mode for food acquisition to a complex trogocytosis mechanism for tissue invasion. Rab GTPases form the largest branch of the Ras-like small GTPases, with a diverse set of roles across the eukaryotic kingdom. Rab GTPases are vital for the orchestration of membrane transport and the secretory pathway responsible for transporting the pathogenic effectors, such as cysteine proteases (*Eh*CPs) which help in tissue invasion. Rab GTPases thus play a crucial role in executing the cytolytic effect of *E. histolytica*. First, they interact with Gal/Nac lectins required for adhering to the host cells, and then, they assist in the secretion of *Eh*CPs. Additionally, amoebic Rab GTPases are vital for encystation because substantial vesicular trafficking is required to create dormant amoebic cysts. These cysts are the infective agent and help to spread the disease. The absence of a "bonafide" vesicular transport machinery in *Eh* and the existence of a diverse repertoire of amoebic Rab GTPases (*Eh*Rab) hint at their contribution in supporting this atypical machinery. Here, we provide insights into a pseudoRab GTPase, *Eh*RabX10, by performing physicochemical analysis, predictive 3D structure modeling, protein-protein interaction studies, and in silico molecular docking. Our group is the first one to classify *Eh*RabX10 as a pseudoRab GTPase with four nonconserved G-motifs. It possesses the basic fold of the P-loop containing nucleotide hydrolases. Through this in silico study, we provide an introduction to the characterization of the atypical *Eh*RabX10 and set the stage for future explorations into the mechanisms of nucleotide recognition, binding, and hydrolysis employed by the pseudo*Eh*Rab GTPase family.

1. Introduction

Membrane dynamics play an indispensable role in not only the transport of molecules through the parasite and its environment, but it is also a requisite for the host-parasite relationship. Membrane dynamics come into play at the first point of contact with the host and eventually support the creation of multiple copies of the parasite inside the host [1, 2]. Phagocytosis is a well-known phenomenon of membrane dynamics observed universally from single-celled amoebas to the complex defences of the human body. *Entamoeba histolytica*, a deadly tropical pathogen, adopts not one but two membrane modulation phenomena, namely, phagocytosis and trogocytosis, to create a severe prognosis of invasive amoebic colitis [3].

This seemingly simple organism takes more than 55,000 human lives each year and is the leading cause of death by diarrhoea in children below 5 years of age in low-income countries. It often lurks silently inside the human body until one day under the right stimulus; it manifests itself as severe amoebic colitis with a mortality rate of more than 50%. This makes it imperative for us to understand more about the

pathogenesis of *E. histolytica*, focusing on the attachment, invasion, and cytolytic abilities of the pathogen; all these processes are governed by vesicular trafficking [4, 5].

The various steps of the membrane dynamics in a cell are coordinated by small GTPases that are essentially GTP/GDP molecular switches. According to their sequence, structure, and reactivity to botulinum toxin C3, they are divided into five families and subsequent subfamilies. Rab is the largest subfamily of the Ras-like GTPase superfamily. Different Rab GTPases are localized in different cellular compartments and orchestrate the vesicular trafficking seamlessly [3, 6–8]. The genome of the pathogenic amoeba *E. histolytica* has 102 annotated genes encoding a stupendous number of 91 Rab GTPases, yet the highest documented number in the available genomes of the eukaryotic kingdom. Some of these are perfect homologues to classical GTPases and others largely divergent. The vigorous and atypical endocytosis machinery observed in *E. histolytica* (*Eh*) provides support to the existence of a wide variety of Rab GTPases required to regulate this delicate machinery [9, 10].

The G-domain in the Rab GTPases facilitates shuttling between GTP- and GDP-bound stages. It belongs to the most common protein fold in the natural world, the P-loop containing fold family of nucleotide hydrolases [11]. The five motifs of this universal fold are designated G1 to G5 with highly conserved sequences—GDSGVGKS (G1/P-loop), T (G2/switch I), DTAGQ (G3/switch II), GNKCDL (G4), and SAK (G5), pivotal to the functioning of the GTPase. Previous studies have reported that 52 out of the 91 *Eh*Rab enzymes have more than 40% identity to human, yeast, and amoebic homologues. However, the remaining 39 are peculiar in their G-domain sequences and do not show substantial identity to other eukaryotic small GTPases. Thus, a separate group was created for these 39 Rab GTPases. Three of these were previously discovered (*Eh*RabA, *Eh*RabB, and *Eh*RabH) and 36 were newly identified proteins (*Eh*RabX members) [12, 13]. Surprisingly, only nine amoebic GTPases have been characterized to date and even fewer are well understood [14–18]. One cannot stress enough the importance of investigating this huge repertoire of small molecular switches in amoebic protozoans, which underpin the complex vesicular arrangements seen in *E. histolytica* and probably aid in making it a notorious pathogen [19]. It was initially believed that *E. histolytica* lacks endoplasmic reticulum and Golgi system; however, more recent studies have provided proof of the presence of an ER-Golgi system albeit not of the conventional type. The ER is distributed uniformly in the amoebic cytosol and not clustered together near the nucleus. Another unexpected observation was the continuous synthesis and movement of new proteins through the cell even after the collapse of Golgi. This indicates the presence of an atypical membrane transport system involving the diversified collection of Rab GTPases in the pathogenic amoeba [9, 20, 21].

The applications of vesicular dynamics can have a direct impact on creating therapeutics to control amoebiasis, currently managed only by the nitroimidazoles which do not come without their barrage of toxic side effects [4]. One such application is mentioned in a recent paper communicating that proanthocyanidins via manipulation of the multivesicular body (MVB) pathway act as effective antitrypanosomal compounds displaying low toxicity in humans [22]. Taking the lead from here, we decided to characterize the grossly underrepresented master membrane regulators, amoebic Rab GTPases. We selected a greatly divergent protein from the atypical *Eh*RabX family, *Eh*RabX10, and subjected it to computational biology delving into the physicochemical analysis, protein structure modeling, molecular docking, and protein-protein interaction (PPI) analysis to explore the premise of discovering the functioning of this atypical GTPase in the vesicular transport machinery of pathogenic *E. histolytica*.

2. Materials and Methods

2.1. Accession of Protein Sequence. EhRabX10 (*EHI_096440, AB197094*) protein sequence for *Entamoeba histolytica* (*Eh*) was retrieved from Amoeba DB (https://amoebadb.org/amoeba/app) and subjected to further analysis.

2.2. Physicochemical Characterization. The physicochemical properties of the target protein sequence were assessed on molecular weight, isoelectric point (pI), extinction coefficient, instability index, aliphatic index, and the GRAVY (grand average of hydropathicity) index using the Expasy ProtParam tool (https://web.expasy.org/protparam/) [23].

2.3. Sequence Alignment and Conserved Motif Identification. The Clustal W 2.0 [24] tool at the NPS server was used to obtain multiple alignments of the *Eh*RabX10 sequence with the other proteins of relevance. The identification of conserved domains was done through the NCBI Conserved Domain Database [25].

2.4. Structure Modeling and Validation. The information regarding the structure of EHI_096440 is not available in the RCSB PDB database [26]. Thus, we utilized homology modeling to generate a protein structure of EHI_096440 (*Eh*RabX10). Protein templates for in silico modeling of *Eh*RabX10 were obtained by running a BLAST search through the PDB, NCBI, I-TASSER, and SWISS-MODEL databases [26–28]. The sequence similarity and query coverage cut-offs were 30% and 70%, respectively. The normalised Z-score (template-target alignment score) and global model quality estimate (GMQE) cut-offs were 1.0 and 0.5, respectively. The templates above the cut-off values were used for homology modeling of *Eh*RabX10, through SWISS-MODEL via the Expasy web server [29]. The homology models were then analyzed for their quality via the SWISS-MODEL server. Further quality analysis was done by assessing the structural deviation (RMSD) between the template and the model, through PyMOL Molecular Graphics System (http://www.pymol.org). The final selected model of *Eh*RabX10 was subjected to validation of the structural quality using the Ramachandran plot [30] through the PDBSUM server (http://www.ebi.ac.uk/thornton-srv/databases/pdbsum/Generate.html) [31, 32].

2.5. Protein-Protein Interaction Study. To find out the interacting partners of our protein of interest, *Eh*RabX10 (EHI_096440), we used the STRING version 11.0 (http://string-db.org/). It generated a network view of the interacting proteins.

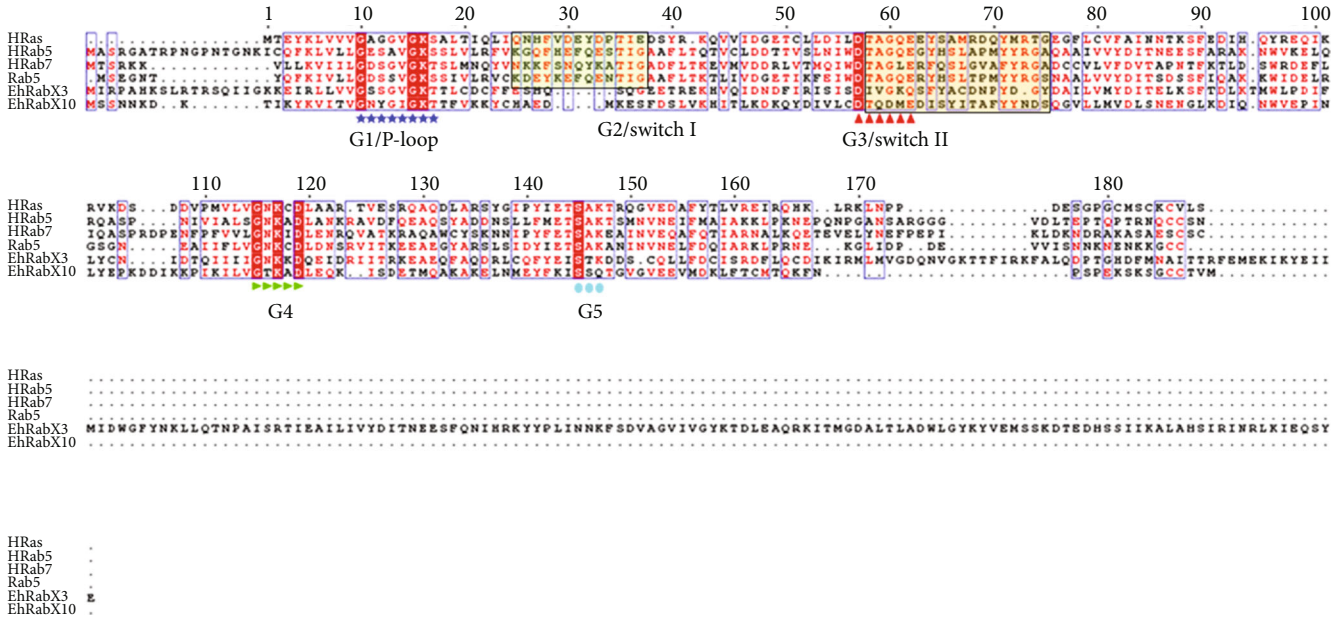

(a)

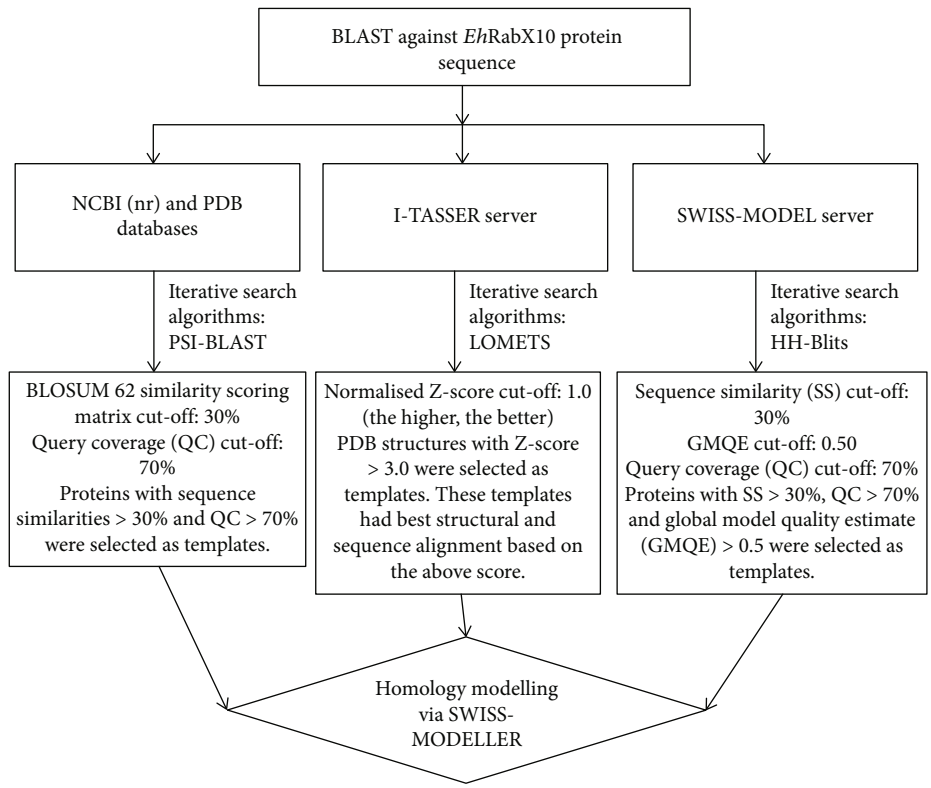

(b)

Figure 1: Continued.

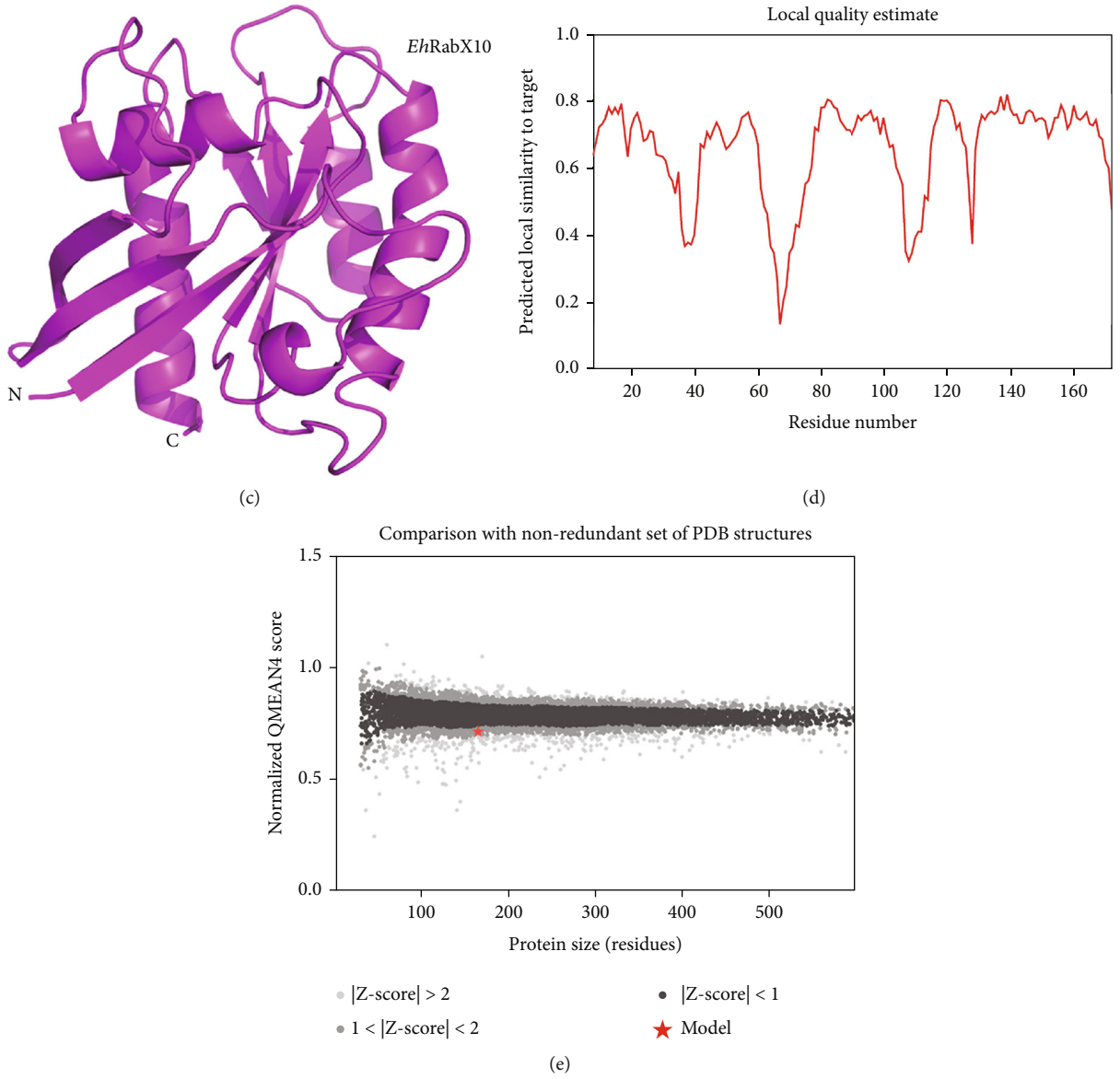

Figure 1: Decoding the sequence features of *Eh*RabX10 and constructing its 3D model through *in silico* methods. (a) Sequence alignment of *Eh*RabX10 with the canonical GTPases HRas (human), HRab5 (human), HRab7 (human), and Rab5 (*E. histolytica*) and the noncanonical GTPase *Eh*RabX3 (*E. histolytica*). The divergent motifs in *Eh*RabX10 are G2/switch I (absent), G3/switch II (DTQDME), G4 (TKAD), and G5 (SSQ). (b) Flowchart describing the selection of templates for homology modeling of *Eh*RabX10. (c) The modeled 3D structure of *Eh*RabX10. (d) The local quality estimate plot of the model showing the appreciable strength of local similarities between the target (*Eh*RabX10) and the template (PDB: 6O62). (e) QMEAN plot of *Eh*RabX10 is a mean of *Z*-scores that describes the "degree of nativeness" of the structural features observed in the model on a global scale. QMEAN *Z*-scores closer to zero indicate good nativeness. Our model falls in the range $1 < Z\text{-score} < 2$; thus, it is in agreement with structural conformations of crystal structures of similar-sized proteins.

These interacting proteins were displayed as nodes, with the node edges indicating the confidence scores. The confidence scores were generated by integrative STRING algorithms that collect and compute information from seven evidence parameters; these are experiments, text mining, cooccurrence, gene fusion, coexpression, conserved neighbourhood, and databases. The multiple coloured lines in the network map represent the seven evidence parameters supporting the interaction [33, 34].

2.6. Docking Studies. The proteins with high confidence interactions were subjected to molecular docking via the ClusPro server 2.0 (https://cluspro.org) [35]. None of the interacting partners of *Eh*RabX10 had their three-dimensional structure defined in the databases. Since only the PDB format is accepted as input in ClusPro, we subjected the interacting proteins to homology modeling via the SWISS-MODEL server. We performed the docking of *Eh*RabX10 with the 3D structures of the interacting partners and the algorithm generated eighty docked sets. These docked sets were based on the ClusPro PIPER algorithm energy terms: hydrophobic and electrostatic interactions, Van der Waals forces, and interatomic charges. The low-energy docked structures were

Table 1: Comparative analysis of the templates for homology modeling of *Eh*RabX10.

PDB ID (name)	Query coverage (%)	GMQE (global model quality estimate)	Sequence similarity (%)	Method of structure determination of template	Model QMEAN	RMSD between template and model
6O62 (Rab GTPase Sec4p, *Candida albicans*)	86	**0.61**	34	X-ray diffraction, 1.88 Å	**-1.51**	**0.124** Å
6S5F (Ras-related protein Rab39B, *Homo sapiens*)	87	0.54	34	X-ray diffraction, 1.70 Å	-2.25	0. 292 Å
4DSU (GTPase Kras isoform 2B, *Homo sapiens*)	94	0.59	32	X-ray diffraction, 1.70 Å	-1.97	2.78 Å
4DST (GTPase Kras isoform 2B, *Homo sapiens*)	94	0.58	32	X-ray diffraction, 2.3 Å	-1.21	2.078 Å
1KY3 (GTP-binding protein YPT7P, *Saccharomyces cerevisiae*)	90	0.49	35	X-ray diffraction, 1.35 Å	-3.34	0.58 Å

subjected to rigorous qualitative and quantitative analysis via PyMOL (v.1.2r3pre; Schrodinger LLC) and Protein Interaction Calculator (http://pic.mbu.iisc.ernet.in/), respectively [36].

3. Results

3.1. Sequence-Based Investigation of EhRabX10 (EHI_096440). The EHI_096440 (UniProt ID: Q5NT06) protein, commonly known as *Eh*RabX10, consists of 188 amino acid residues. The physicochemical properties of molecular mass and isoelectric point (pI) are 21.45 kDa and 5.32, respectively. The extinction coefficient is 19160 M^{-1} cm^{-1} at 280 nm, measured in water. The physicochemical indices including instability, aliphatic, and GRAVY index were calculated to be 30.63, 76.65, and −0.49, respectively. By the careful investigation of the sequence through the NCBI conserved domain database and Expasy ProtParam tool, we found that this protein has four motifs indicative of Rab GTPases, namely, G1 motif (residues 18-25), G3 motif (residues 61-66), G4 motif (residues 122-126), and G5 motif (residues 151-153). It also houses a coiled-coil domain at residues 124-144. The G1 motif (GxxxGKS/T) is conserved; however, the G2 box threonine, an extremely conserved residue in canonical Rab GTPases such as HRas [37] and HRab5 [38], is absent in *Eh*RabX10. It was also observed that three out of the four motifs (G3-G5) in *Eh*RabX10 have nonconserved sequences. The conserved sequences of these motifs are G3 (DxxGQE), G4 (NKxD), and G5 (SAK) for canonical GTPases [39] as seen in Figure 1(a); however, *Eh*RabX10 houses divergent sequences in these motifs which are G3 (DTQDME), G4 (TKAD), and G5 (SSQ).

3.2. Molecular Modeling of EhRabX10 (EHI_096440), Proteins from Entamoeba histolytica. To better understand the relevance of EHI_096440, a structure was needed and the absence of a three-dimensional X-ray structure of EHI_096440 in the PDB database necessitated homology modeling of the protein. A thorough search for ideal templates was done via the servers of NCBI, PDB, I-TASSER, and SWISS-MODEL. The templates were selected based on the highest similarity to the sequence and the structural folds (secondary protein structures), predicted model quality, and percent query coverage (QC) (Figure 1(b)). The following templates scored higher than the cut-off values as mentioned in Section 2.4 and were selected for homology modeling: Rab GTPase Sec4p of *Candida albicans* (PDB ID: 6O62) [40], Ras-related protein Rab39B of *Homo sapiens* (PDB ID: 6S5F) [41], GTPase Kras isoform 2B of *Homo sapiens* (PDB ID: 4DSU) [42], GTPase Kras isoform 2B of *Homo sapiens* (PDB ID: 4DST) [42], and GTP-binding protein YPT7P of *Saccharomyces cerevisiae* (PDB ID: 1KY3) [43]. Homology models, based on all the above templates, were subjected to further scrutiny by assessing the QMEAN, GMQE (global model quality estimate), and RMSD (root mean square deviation) values (Table 1). Models with QMEAN scores closer to zero are of better quality, and models with QMEAN scores below −4.0 are rejected. Additionally, models with higher GMQE scores are considered of higher quality. Furthermore, a good model has a very low (closer to zero) root mean square deviation (RMSD) from the template.

Here, we observed the highest GMQE score (0.61) and the least RMSD value (0.124 Å) for the model built on the template, Rab GTPase Sec4p of *Candida albicans* (PDB ID: 6O62). The query coverage (QC) was good (86%), covering all the crucial G-motifs of the G-domain barring only the terminal residues (1-8 and 174-188) of the *Eh*RabX10 sequence. Additionally, it also had a good model QMEAN score of −1.51 which is closer to zero (Table 1). All these factors indicate the 6O62-based *Eh*RabX10 model to be of the most credible quality [44]. This model of size 18.15 kDa was selected as final, and all further assessments were done using this model (Figures 1(c)–1(e)). The analysis of the structural quality of the *Eh*RabX10 model was done through the Ramachandran plot (Figure 2(a)). The plot computed that 90.8% residues of the *Eh*RabX10 structure lay in the most-favoured regions, 7.9% in the additionally allowed regions, 1.3% in the generously allowed regions, and none in the disallowed regions indicating the modeled structure to be of high quality when compared to the stereochemistry of protein structures experimentally decoded to date [30, 45].

The topological model generated by PROCHECK (Figure 2(b)) revealed our protein to possess the classical

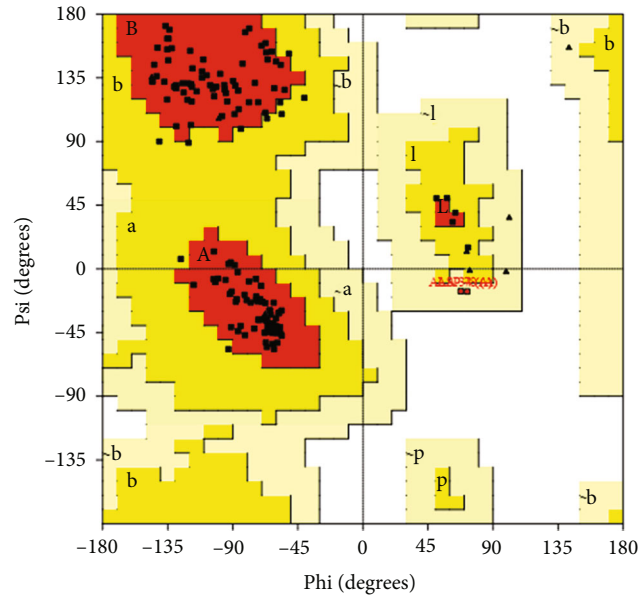

(a)

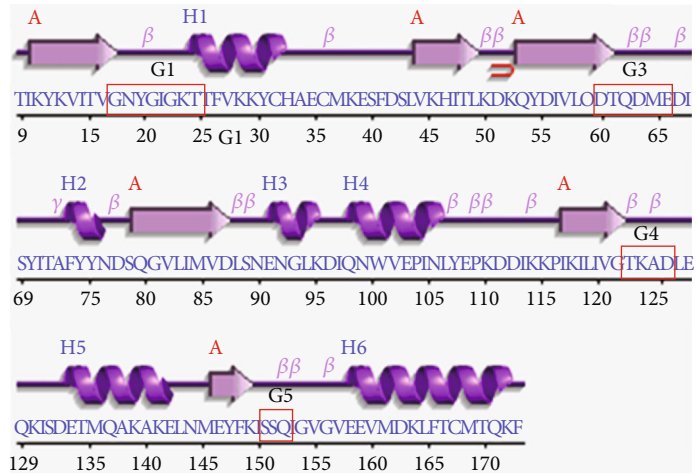

(b)

Figure 2: Continued.

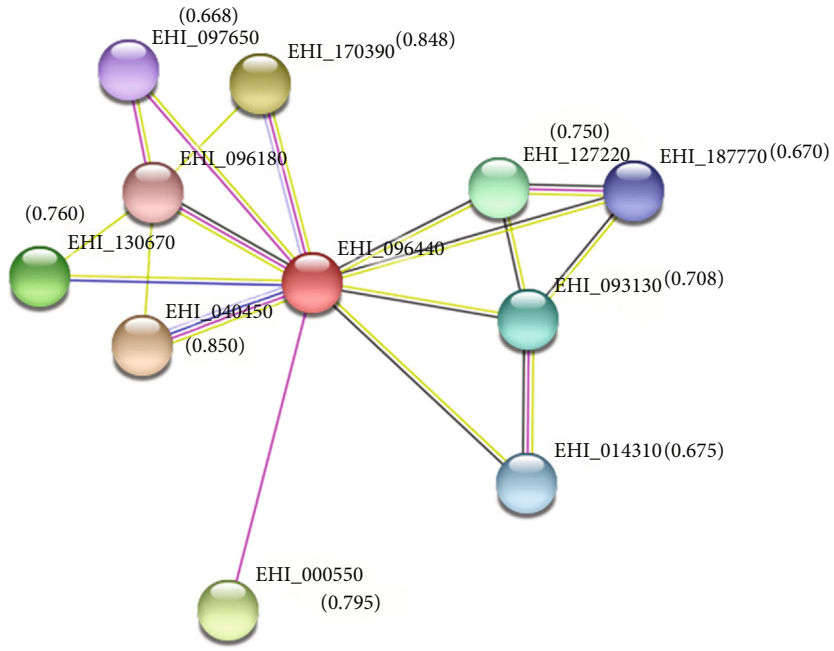

(c)

Figure 2: Structure quality assessment and the protein interactome of *Eh*RabX10. (a) Ramachandran plot of *Eh*RabX10 computed through PROCHECK. (b) Topology of the secondary structures of *Eh*RabX10 aligned with the FASTA sequence of *Eh*RabX10. The G-domain motifs are marked with red boxes. (c) STRING network of predicted interacting partners of EHI_096440 (*Eh*RabX10). The nodes represent the proteins, and the lines represent the functional evidence links between the proteins. The combined confidence scores are highlighted in the brackets over the nodes.

Table 2: Interactome parameters of EHI_096440 (*Eh*RabX10).

Accession no.	Annotation	Confidence score	Evidence of interaction	Amenable to homology modeling
EHI_040450	Rab family GTPase; *Eh*RabK2	0.850	Experiments, cooccurrence, text mining, homology	Yes
EHI_170390	Rab family GTPase; *Eh*RabC8	0.848	Experiments, text mining, homology	Yes
EHI_000550	Myb-like DNA-binding domain-containing protein	0.795	Experiments	No
EHI_130670	Rab family GTPase; *Eh*RabX35	0.760	Cooccurrence, text mining	Yes
EHI_127220	Synapsin, putative	0.750	Coexpression, text mining	Yes
EHI_093130	*Eh*Sec1; Syntaxin-binding protein, putative; belongs to STXBP/unc-18/SEC1 family	0.708	Coexpression, text mining	Yes
EHI_014310	Calcium-gated potassium channel protein, putative	0.675	Coexpression, text mining	No
EHI_187770	SH3 domain protein	0.670	Coexpression, text mining	Yes
EHI_097650	Rab family GTPase; *Eh*RabN2	0.668	Experiments, text mining	Yes
EHI_096180	Ras family protein	0.664	Experiments, coexpression, text mining	Yes

fold of the Rab GTPase family. This fold is composed of a six-stranded β-sheet with one antiparallel and five parallel strands which are interspersed by five distinct α-helices. In agreement with the convention, the four Rab motifs of the G-domain (G1-G5), except the G2 box (absent), are located in the loops connecting the α-helices and β-strands, and this can be observed in the modeled structure (Figure 2(b)).

3.3. Interactome. The STRING v11.0 server provided an interactive network (Figure 2(c)) composed of ten predicted interactions with the protein of interest, *Eh*RabX10 (EHI_096440). Each of these interacting proteins had a combined confidence score computed by combining the individual scores of each of the seven evidence parameters mentioned in Section 2.5. Indeed, all the interactions had a combined confidence score

Table 3: Homology modeling of interacting partners that have high confidence interaction score.

Accession number	Annotation	Sequence similarity (%)	Query coverage (%)	GMQE (global model quality estimate)	Combined confidence score of interaction
EHI_093130	*Eh*Sec1; syntaxin-binding protein, putative; belongs to STXBP/unc-18/SEC1 family	35	**93**	**0.62**	0.708
EHI_170390	Rab family GTPase; *Eh*RabC8	39	**88**	**0.60**	0.848
EHI_040450	Rab family GTPase; *Eh*RabK2	40	80	0.54	0.850
EHI_127220	Synapsin, putative	40	93	0.70	0.750
EHI_130670	Rab family GTPase; *Eh*RabX35	39	85	0.56	0.760

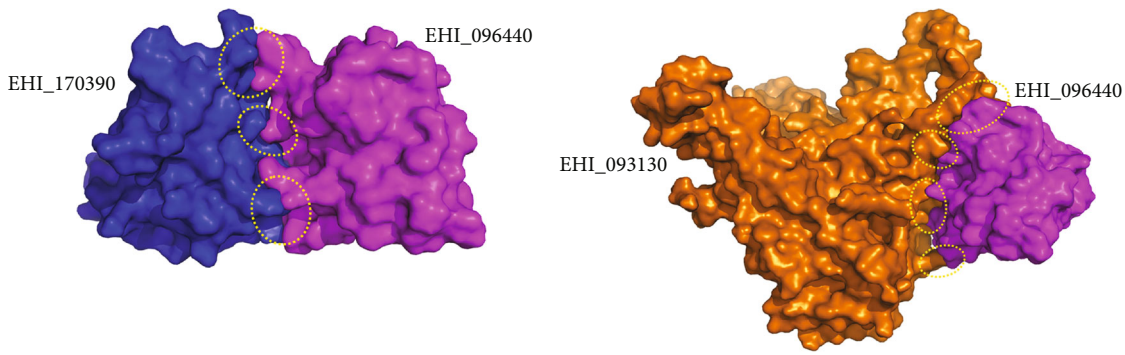

Figure 3: Assessment of the protein-protein interactions of *Eh*RabX10 with its partner proteins. Docked complexes of EHI_096440 (magenta) with (a) EHI_170390 (blue) and (b) EHI_093130 (orange) visualised through PyMOL. Interacting interface marked in dotted circles. (c) The complete sequence of *Eh*RabX10 displaying the diagnostic G-domain motifs and RabF regions required for the specificity of interacting effectors. The sequences are colour coded as red for the G-domain (G1-G5) motifs, blue for the RabF3 region, pink for the RabF4 region, and green for the RabF5 region. The interacting partners EHI_017390 and EHI_093130 both docked at the switch II region (G3, RabF3, and RabF4) of EHI_096440 (*Eh*RabX10).

greater than 66% indicating a low chance of false positives (Table 2). We selected the protein partners with high confidence scores (>70%) for molecular docking studies (Table 3). Since none of the predicted interacting partners had a 3D structure resolved, we resorted to homology modeling and those providing the highest quality structures were used for the docking studies in ClusPro 2.0 server. Among the six, high confidence interactions, Myb-like DNA-binding domain-containing protein (EHI_000550) was not amenable to predictive modeling; however, the other five were able to produce protein structures of reliable standard (Table 2). Out of these five, we selected two proteins for further studies: the Rab family GTPase *Eh*RabC8 (EHI_170390) and the syntaxin-binding protein, *Eh*Sec1 (EHI_093130). These proteins were subjected to docking after a final structural quality check where both fared excellently with high GMQE scores of 0.62 and 0.60 of EHI_093130 and EHI_170390, respectively (Table 3). The functional links of these docked partners of *Eh*RabX10 were supported by the STRING evidence parameters of in vitro experiments, text mining, homology, and coexpression.

3.4. Assessment of the Docked Complexes. The modeled 3D structures of interacting partners, EHI_170390 and EHI_093130, were fed into ClusPro 2.0 server as receptor proteins and EHI_096440 (*Eh*RabX10) as the ligand. The low-energy docked complexes were rendered into four groups of energy coefficients; these are balanced, electrostatically favoured, hydrophobic favoured, and Van der Waals. We assessed the top 10 complexes from each group using PyMOL and supplemented the assessment with quantitative data from

Table 4: Interactions between EHI_096440 (*Eh*RabX10; chain A) and EHI_170390 (chain B) within 5 Å.

(a)

Position	Residue	Chain	Position	Residue	Chain
41	PHE	A	62	TRP	B
41	PHE	A	77	TYR	B
65	MET	A	45	PHE	B
65	MET	A	62	TRP	B
68	ILE	A	47	PHE	B

(b)

Protein-protein side chain-side chain hydrogen bonds							
Donor				Acceptor			
Position	Chain	Residue	Atom	Position	Chain	Residue	Atom
25	A	THR	OG1	77	B	TYR	OH
38	A	LYS	NZ	72	B	ASN	OD1
67	A	ASP	OD1	3	B	GLN	OE1
67	A	ASP	OD1	3	B	GLN	OE1
3	B	GLN	OE1	67	A	ASP	OD1
3	B	GLN	OE1	67	A	ASP	OD1
58	B	LYS	NZ	67	A	ASP	OD1
58	B	LYS	NZ	67	A	ASP	OD2
77	B	TYR	OH	39	A	GLU	OE1
79	B	ARG	NH1	42	A	ASP	OD1
79	B	ARG	NH1	42	A	ASP	OD1
79	B	ARG	NH2	42	A	ASP	OD1
79	B	ARG	NH2	42	A	ASP	OD1
79	B	ARG	NH2	42	A	ASP	OD2
79	B	ARG	NH2	42	A	ASP	OD2

Protein Interaction Calculator (PIC) server for both the receptor proteins (Figures 3(a) and 3(b)). After careful examination of ~80 docked sets, we identified the interacting residues of EHI_096440 to fall mainly in the switch II region composed of G3 box (DTQDME), RabF3 box (DISYIT), and RabF4 box (YY), for both the partners, EHI_170390 and EHI_093130 (Figure 3(c)). As established for classical Rab GTPases, the switch II region is involved in interaction with Rab effectors and regulators [11, 46]. Thus, we can speculate from the molecular docking data that this region might also serve the same function in *Eh*RabX10.

The interacting residues of EHI_170390 (*Eh*RabC8) are positioned at residue 3 Gln (N-terminus) and residues 45-79 (mainly in RabF1 and RabF3 regions) (Figure 1(a), Table 4). The interacting residues of EHI_093130 are positioned at the C-terminal (485-521) (Table 5). Singularly, we also found residues 41 Phe and 42 Asp of *Eh*RabX10 to participate in hydrophobic and ionic interactions with the partner proteins. Based on the multiple alignment data (Figure 1(a)), these two residues fall in the region annotated as RabF1 in canonical Rab GTPases but have not yet been annotated for *Eh*RabX10. This observation should be explored in future studies.

Table 5: Interactions between EHI_096440 (*Eh*RabX10; chain A) and EHI_093130 (chain B) within 5 Å.

(a)

Position	Residue	Chain	Position	Residue	Chain
20	TYR	A	495	PHE	B
20	TYR	A	496	ALA	B
20	TYR	A	499	PRO	B
37	MET	A	188	PRO	B
65	MET	A	495	PHE	B
74	PHE	A	485	PRO	B
75	TYR	A	490	LEU	B

(b)

Protein-protein side chain-side chain hydrogen bonds							
Donor				Acceptor			
Position	Chain	Residue	Atom	Position	Chain	Residue	Atom
67	A	ASP	OD2	520	B	GLN	NE2
67	A	ASP	OD2	520	B	GLN	NE2
70	A	TYR	OH	520	B	GLN	OE1
75	A	TYR	OH	483	B	GLU	OE1
75	A	TYR	OH	483	B	GLU	OE2
110	A	LYS	NZ	486	B	GLU	OE1
110	A	LYS	NZ	486	B	GLU	OE2
183	B	ARG	NH2	65	A	MET	SD
183	B	ARG	NH2	65	A	MET	SD
187	B	LYS	NZ	39	A	GLU	OE1
187	B	LYS	NZ	39	A	GLU	OE2
449	B	ARG	NE	35	A	GLU	OE1
449	B	ARG	NE	35	A	GLU	OE2
449	B	ARG	NH1	35	A	GLU	OE2
449	B	ARG	NH1	35	A	GLU	OE2
453	B	LYS	NZ	39	A	GLU	OE1
478	B	ARG	NH1	42	A	ASP	OD2
478	B	ARG	NH1	42	A	ASP	OD2
478	B	ARG	NH2	42	A	ASP	OD1
478	B	ARG	NH2	42	A	ASP	OD1
478	B	ARG	NH2	42	A	ASP	OD2
478	B	ARG	NH2	42	A	ASP	OD2
520	B	GLN	NE2	67	A	ASP	OD2
520	B	GLN	NE2	67	A	ASP	OD2
520	B	GLN	OE1	70	A	TYR	OH
520	B	GLN	OE1	70	A	TYR	OH
521	B	LYS	NZ	70	A	TYR	OH

4. Discussion

Rab family members, though sharing the conventional G-domain of P-loop containing nucleotide hydrolases, are distinguished from the other small GTPases by virtue of the Rab family regions (RabF) flanking the G-domain motifs. Moreover, these regions are bracketed by Rab subfamily

specific regions (RabSF) which provide for the specificity of the diverse Rab community across eukaryotes [46]. The discovery of these regions aided in the identification and classification of new Rab GTPases, among which lies our enzyme of interest, *Eh*RabX10, of the pathogen *Entamoeba histolytica* [12].

With nothing known about this novel GTPase, we started with the physicochemical characterization based on the amino acid sequence of *Eh*RabX10, where the instability, aliphatic, and GRAVY indices were calculated. The instability index (II) indicates the stability of a protein in a test tube. *Eh*RabX10 has an II of less than 40.0; it is stable in vitro. The aliphatic index (AI) is the relative volume occupied by the aliphatic side chains, and a high value of 76.65 signifies our protein to be thermostable. Apart from being stable, it is also essential for a protein to be pure for its study and applications, thus underlining the importance of knowing the extinction coefficient of a protein. This coefficient conveys the amount of light a protein absorbs at a certain wavelength. The extinction coefficient of *Eh*Rabx10 was 19160 M^{-1} cm^{-1} at 280 nm, measured in water, a value of importance when considering the spectrophotometric analysis of purified protein at 280 nm. The negative GRAVY index of hydropathicity defines our protein as globular and hydrophilic, which endorses the small GTPase annotation of *Eh*Rabx10.

However, an interesting contrast during sequence-based evaluation revealed the absence of the prominent G2 box threonine, vital for binding guanine nucleotide and Mg^{+2} ion in small GTPases and is the most conserved motif of the GTPase fold [37]. In addition, a massive divergence was noted in the other conserved motifs of the globular G-domain through sequence assessment. Multiple alignment of *Eh*RabX10 with classical Rab GTPases of humans (HRas [37]and HRab5 [38]) and *Entamoeba histolytica* (Rab5 [47]) and another nonclassical GTPase (*Eh*RabX3 [48]) revealed maximum deviations in the G3, G4, and G5 motifs (Figure 1(a)). The conserved residues of G3 (DxxGQE), G4 (NKxD), and G5 (SAK) are crucial for GTP/GDP state switching and hydrolysis and such significant alterations in the G-domain might affect the enzymes functioning greatly [37, 49]. We thus have labelled *Eh*RabX10 as a pseudoRab GTPase possessing noncanonical G-motifs.

Homology modeling was necessitated by the absence of the crystal structure of EHI_096440 (*Eh*RabX10). It was a rigorous process in the bid to create the best possible predictive 3D model. After iterative examination of several templates and their corresponding models, Rab GTPase Sec4p of *Candida albicans* (PDB ID: 6O62) was used as a template to model EHI_096440. The crystal structure of 6O62 protein was itself resolved at a high resolution of 1.88 Å, thus providing a detailed and reliable template for creating our model. Consequently, the predicted structure was of a high standard as mentioned in Section 3.2; none of the residues lay in the disallowed region of the Ramachandran plot, illustrating the feasibility of the phi and psi dihedral angles of all residues in our structure. Extended proof of template credibility was exhibited by the low structural deviation (RMSD 0.124 Å) between the template and the model. The model was approximately 18.15 kDa in size, which supports its

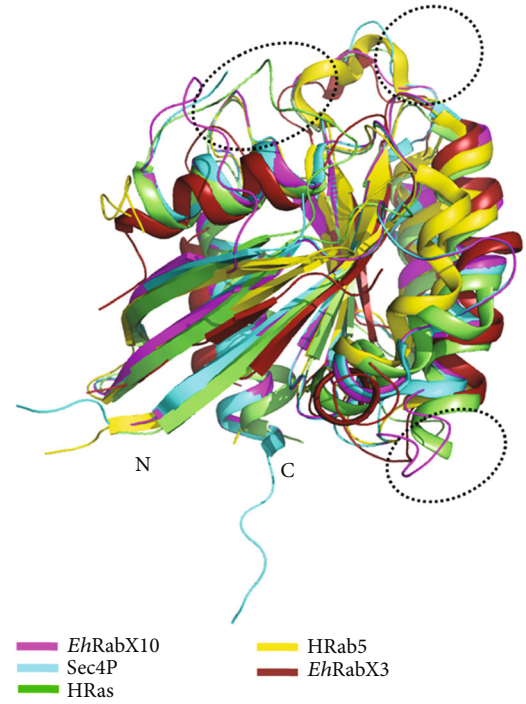

Figure 4: Superposition of target *Eh*RabX10 (magenta) over template Sec4p (PDB: 6O62) (cyan) and with other notable Rab GTPases: HRas (PDB ID: 6ZL3) [55] (lime green), HRab5 (PDB ID: 1TU4) [38] (yellow), and *Eh*RabX3 (PDB ID: 5C1T) [48] (raspberry) to assess the structural alignments. The dotted circles indicate the loops of maximum deviation between the structures.

annotation of a small Rab GTPase. The *Eh*RabX10 structure was also aligned with other notable Rab GTPases, among which *Eh*RabX3 was of consequence (Figure 4), being the only documented pseudoRab GTPase with its structure defined through X-ray diffraction by Srivastava et.al [48]. Quite unexpectedly, the least deviation was observed in *Eh*RabX10 alignment with HRab5 (RMSD 1.978), not *Eh*RabX3 (Table 6), and this implies that all noncanonical Rab enzymes are not identical in their structural arrangements. More research is needed to better understand the pseudoGTPase family.

In agreement with the classical Rab fold [37], *Eh*RabX10 houses six β-strands inside a partial shell of five α-helices with the loops connecting the secondary structures (Figure 1(c)). These loops contain the functional motifs (G1-G5), albeit the motifs are quite divergent as compared to the conserved sequences of conventional Rab GTPases. To explore the effects of these altered sequences on the enzyme functionality and interaction with other biomolecules, we generated an interactome of *Eh*RabX10 (EHI_096440) through the STRING v11.0 server. The interacting partners predicted with high confidence fell mostly in the category of fellow Rab GTPases and one in the syntaxin-binding protein (STXBP) family that regulate vesicle docking and fusion [50, 51] (Table 3). High-quality structures of *Eh*RabC8 (EHI_170390) and *Eh*Sec1 (EHI_093130) were built through SWISS-MODEL and were then used for docking studies in ClusPro 2.0. Experimental evidence acquired from STRING v11.0 demonstrated a strong

Table 6: Root mean square deviation (RMSD) of *Eh*RabX10 from HRas, HRab5, *Eh*RabX3, and the template Sec4p.

Name of protein	Method of structure determination	RMSD (from *Eh*RabX10 model)
Human Ras GTPase (HRas)	X-ray diffraction	3.042 Å
Human Rab GTPase (HRab5)	X-ray diffraction	1.978 Å
Entamoeba histolytica GTPase (EhRabX3)	X-ray diffraction	3.432 Å
Candida albicans Rab GTPase (Sec4p)	X-ray diffraction	**0.124 Å**

functional link between EHI_170390 and *Eh*RabX10 (EHI_096440). It was based on affinity chromatography and tandem affinity purification assays. Coexpression evidence in the interactome showed that the STXBP partner (EHI_093130) is often coexpressed with Rab GTPases and controls the late-stage vesicular trafficking. Thus, we selected these two proteins for docking studies [50].

As described in the opening of this discussion, the RabF and RabSF regions are diagnostic for the diverse Rab GTPases found in the eukaryotic kingdom. These regions are clustered in the switch I and II regions of the GTPase [46]. In-depth tracking of residues of the protein-protein interaction complexes showed that the G3 box, RabF3, and RabF4 regions comprising the switch II loop were engaged in the docked interface of EHI_096440 (Figure 3(c)). Accordingly, it can be speculated that the diverged G-motifs may not render *Eh*RabX10 inactive and it may function as an atypical GTPase similar to the known functionally active hydrolase, *Eh*RabX3, which also lacks the G2 domain. However, the altered G4 motif in *Eh*RabX10 could considerably affect the nucleotide recognition potential of this pseudoGTPase [16, 48, 52]. A closer inspection is required to validate these hypotheses.

Previous literature has shown that the yeast homologue of Rab8, the Sec4 protein, plays a regulatory role in the late-stage vesicular secretory pathway [1]; *Eh*RabX10 is modeled using a template that is a Sec4 protein (PDB: 6O62). Additionally, *Eh*RabX10 is predicted to interact with syntaxin-binding protein of the Sec1 family (EHI_093130). These observations suggest the putative involvement of *Eh*RabX10 in the cascade of Rab-Sec signalling in the late-stage vesicular pathway [53]. There is limited knowledge about the role of amoebic Rab GTPases, except *Eh*Rab5, in the early stages of the endocytic pathway [15, 47]. In addition, there is a huge gap in understanding the orchestration of the secretion of various virulence factors such as amoebic cysteine proteases (*Eh*CPs). *E. histolytica* (*Eh*) houses a huge arsenal of *Eh*CPs, and these are the major contributors to the cytolytic potential of *E. histolytica* (*Eh*) [8, 54]. *Eh* also contains a complex and unique system of vesicle-based de novo protein trafficking that continues to function even after the collapse of the Golgi complex [20]. This compels us to explore the role of these noncanonical Rab GTPases in regulating the stages of vesicle trafficking and the *de novo* synthesis of virulence factors in the peculiar vesicular transport system of *E. histolytica* [9, 20]. The absence of these pseudoRab GTPases (*Eh*RabX family) in humans hallmarks them as targets for future exploration and justifies extensive research in discovering their mechanisms of nucleotide recognition, binding, and hydrolysis which may throw new light on the complex membrane dynamics of enteric amoebic protozoa.

Data Availability

Others will be able to access these data in the same manner as the authors. The authors did not have any special access privileges that others would not have.

Conflicts of Interest

The authors declare that they have no known competing financial interests or personal relationships that could have appeared to influence the work reported in this review.

Authors' Contributions

MR and VKS were involved in the conception and design of this article and played prime roles in literature curation, writing, and revising the manuscript. SK and AJ critically reviewed and evaluated the manuscript. All authors had final approval of the submitted and published versions.

Acknowledgments

We extend our appreciation towards Amity University Rajasthan, Jaipur, India, for its valuable support throughout the work.

References

[1] A. H. Hutagalung and P. J. Novick, "Role of Rab GTPases in membrane traffic and cell physiology," *Physiological Reviews*, vol. 91, no. 1, pp. 119–149, 2011.

[2] M.-T. Gabe Lee, A. Mishra, and D. G. Lambright, "Structural mechanisms for regulation of membrane traffic by Rab GTPases," *Traffic*, vol. 10, no. 10, pp. 1377–1389, 2009.

[3] K. Verma, V. K. Srivastava, and S. Datta, "Rab GTPases take centre stage in understandingEntamoeba histolyticabiology," *Small GTPases*, vol. 11, no. 5, pp. 320–333, 2020.

[4] A. Rawat, P. Singh, A. Jyoti, S. Kaushik, and V. K. Srivastava, "Averting transmission: a pivotal target to manage amoebiasis," *Chemical Biology & Drug Design*, vol. 96, no. 2, pp. 731–744, 2020.

[5] M. Kantor, A. Abrantes, A. Estevez et al., "*Entamoeba histolytica*: updates in clinical manifestation, pathogenesis, and vaccine development," *Canadian Journal of Gastroenterology & Hepatology*, vol. 2018, article 4601420, pp. 1–6, 2018.

[6] H. Stenmark, "Rab GTPases as coordinators of vesicle traffic," *Nature Reviews. Molecular Cell Biology*, vol. 10, no. 8, pp. 513–525, 2009.

[7] S. R. Pfeffer, "Rab GTPases: master regulators that establish the secretory and endocytic pathways," *Molecular Biology of the Cell*, vol. 28, no. 6, pp. 712–715, 2017.

[8] A. Rawat, M. Roy, A. Jyoti, S. Kaushik, K. Verma, and V. K. Srivastava, "Cysteine proteases: battling pathogenic parasitic protozoans with omnipresent enzymes," *Microbiological Research*, vol. 249, article 126784, 2021.

[9] D. Perdomo, N. Aït-Ammar, S. Syan, M. Sachse, G. D. Jhingan, and N. Guillén, "Cellular and proteomics analysis of the endomembrane system from the unicellular *Entamoeba histolytica*," *Journal of Proteomics*, vol. 112, pp. 125–140, 2015.

[10] E. Orozco, A. Betanzos, C. Bañuelos, R. Javier-Reyna, and G. García-Rivera, "Vesicular trafficking in *Entamoeba histolytica* is essential for its virulence," in *Eukaryome Impact on Human Intestine Homeostasis and Mucosal Immunology*, pp. 275–290, Springer International Publishing, 2020.

[11] O. Pylypenko, H. Hammich, I. M. Yu, and A. Houdusse, "Rab GTPases and their interacting protein partners: structural insights into Rab functional diversity," *Small GTPases*, vol. 9, no. 1-2, pp. 22–48, 2018.

[12] Y. Saito-Nakano, B. J. Loftus, N. Hall, and T. Nozaki, "The diversity of Rab GTPases in *Entamoeba histolytica*," in *Experimental Parasitology. Vol 110*, pp. 244–252, Academic Press Inc., 2005.

[13] D. D. Leipe, Y. I. Wolf, E. V. Koonin, and L. Aravind, "Classification and evolution of P-loop GTPases and related ATPases[1]," *Journal of Molecular Biology*, vol. 317, no. 1, pp. 41–72, 2002.

[14] B. N. Mitra, Y. Saito-Nakano, K. Nakada-Tsukui, D. Sato, and T. Nozaki, "Rab11B small GTPase regulates secretion of cysteine proteases in the enteric protozoan *parasiteEntamoeba histolytica*," *Cellular Microbiology*, vol. 9, no. 9, pp. 2112–2125, 2007.

[15] K. Verma, Y. Saito-Nakano, T. Nozaki, and S. Datta, "Insights into endosomal maturation of human holo-transferrin in the enteric *parasiteEntamoeba histolytica*: essential roles of Rab7A and Rab5 in biogenesis of giant early endocytic vacuoles," *Cellular Microbiology*, vol. 17, no. 12, pp. 1779–1796, 2015.

[16] M. Chandra, M. Mukherjee, V. K. Srivastava, Y. Saito-Nakano, T. Nozaki, and S. Datta, "Insights into the GTP/GDP cycle of RabX3, a novel GTPase fromEntamoeba histolyticawith tandem G-domains," *Biochemistry*, vol. 53, no. 7, pp. 1191–1205, 2014.

[17] K. Verma and S. Datta, "Rab35 Participates in E. histolytica Phagocytosis," *The Journal of Biological Chemistry*, vol. 292, no. 12, pp. 4960–4975, 2017.

[18] P. Juárez, R. Sanchez-Lopez, R. P. Stock, A. Olvera, M. A. Ramos, and A. Alagón, "Characterization of the _Eh_ rab8 gene, a marker of the late stages of the secretory pathway of *Entamoeba histolytica*," *Molecular and Biochemical Parasitology*, vol. 116, no. 2, pp. 223–228, 2001.

[19] E. Herman, M. A. Siegesmund, M. J. Bottery et al., "Membrane Trafficking Modulation during _Entamoeba_ Encystation," *Scientific Reports*, vol. 7, no. 1, pp. 1–17, 2017.

[20] R. Manning-Cela, C. Marquez, E. Franco, P. Talamas-Rohana, and I. Meza, "BFA-sensitive and insensitive exocytic pathways in *Entamoeba histolytica* trophozoites: their relationship to pathogenesis," *Cellular Microbiology*, vol. 5, no. 12, pp. 921–932, 2003.

[21] J. Santi-Rocca, S. Smith, C. Weber et al., "Endoplasmic reticulum stress-sensing mechanism is activated in *Entamoeba histolytica* upon treatment with nitric oxide," *PLoS One*, vol. 7, no. 2, 2012.

[22] B. K. Kubata, K. Nagamune, N. Murakami et al., "Kola acuminata proanthocyanidins: a class of anti-trypanosomal compounds effective against *Trypanosoma brucei*," *International Journal for Parasitology*, vol. 35, no. 1, pp. 91–103, 2005.

[23] E. Gasteiger, C. Hoogland, A. Gattiker et al., "Protein identification and analysis tools on the ExPASy server," in *The Proteomics Protocols Handbook*, pp. 571–607, Humana Press, 2005.

[24] M. A. Larkin, G. Blackshields, N. P. Brown et al., "Clustal W and Clustal X version 2.0," *Bioinformatics*, vol. 23, no. 21, pp. 2947-2948, 2007.

[25] A. Marchler-Bauer, M. K. Derbyshire, N. R. Gonzales et al., "CDD: NCBI's conserved domain database," *Nucleic Acids Research*, vol. 43, no. D1, pp. D222–D226, 2015.

[26] P. W. Rose, B. Beran, C. Bi et al., "The RCSB Protein Data Bank: redesigned web site and web services," *Nucleic Acids Research*, vol. 39, Suppl. 1, 2011.

[27] C. Camacho, G. Coulouris, V. Avagyan et al., "BLAST+: architecture and applications," *BMC Bioinformatics*, vol. 10, no. 1, pp. 1–9, 2009.

[28] M. Steinegger, M. Meier, M. Mirdita, H. Vöhringer, S. J. Haunsberger, and J. Söding, "HH-suite3 for fast remote homology detection and deep protein annotation," *BMC Bioinformatics*, vol. 20, no. 1, pp. 1–15, 2019.

[29] A. Waterhouse, M. Bertoni, S. Bienert et al., "SWISS-MODEL: homology modelling of protein structures and complexes," *Nucleic Acids Research*, vol. 46, no. W1, pp. W296–W303, 2018.

[30] G. N. Ramachandran, C. Ramakrishnan, and V. Sasisekharan, "Stereochemistry of polypeptide chain configurations," *Journal of Molecular Biology*, vol. 7, no. 1, pp. 95–99, 1963.

[31] R. A. Laskowski, "PDBsum: summaries and analyses of PDB structures," *Nucleic Acids Research*, vol. 29, no. 1, pp. 221-222, 2001.

[32] R. A. Laskowski, M. W. MacArthur, D. S. Moss, and J. M. Thornton, "PROCHECK: a program to check the stereochemical quality of protein structures," *Journal of Applied Crystallography*, vol. 26, no. 2, pp. 283–291, 1993.

[33] D. Szklarczyk, A. L. Gable, D. Lyon et al., "STRING v11: protein-protein association networks with increased coverage, supporting functional discovery in genome-wide experimental datasets," *Nucleic Acids Research*, vol. 47, no. D1, pp. D607–D613, 2019.

[34] C. von Mering, L. J. Jensen, B. Snel et al., "STRING: known and predicted protein-protein associations, integrated and transferred across organisms," *Nucleic Acids Research*, vol. 33, pp. D433–D437, 2004.

[35] D. Kozakov, D. R. Hall, B. Xia et al., "The ClusPro web server for protein-protein docking," *Nature Protocols*, vol. 12, no. 2, pp. 255–278, 2017.

[36] K. G. Tina, R. Bhadra, and N. Srinivasan, "PIC: protein interactions calculator," *Nucleic Acids Research*, vol. 35, pp. W473–W476, 2007.

[37] J. Colicelli, "Human RAS superfamily proteins and related GTPases," *Science's STKE*, vol. 2004, no. 250, p. RE13, 2004.

[38] G. Zhu, P. Zhai, J. Liu, S. Terzyan, G. Li, and X. C. Zhang, "Structural basis of Rab5-Rabaptin5 interaction in

endocytosis," *Nature Structural & Molecular Biology*, vol. 11, no. 10, pp. 975–983, 2004.

[39] K. Nakada-Tsukui, Y. Saito-Nakano, A. Husain, and T. Nozaki, "Conservation and function of Rab small GTPases in *Entamoeba*: Annotation of *E. invadens* Rab and its use for the understanding of *Entamoeba* biology," *Experimental Parasitology*, vol. 126, no. 3, pp. 337–347, 2010.

[40] P. J. Stogios, T. Skarina, R. Di Leo, A. Savchenko, and Center for Structural Genomics of Infectious Diseases (CSGID), *Crystal structure of Sec4p, a Rab family GTPase from Candida albicans*, 2019.

[41] L. Diaz-Saez, S. Jung, F. von Delft et al., *Structure of the human RAB39B in complex with GMPPNP*, 2019.

[42] T. Maurer, L. S. Garrenton, A. Oh et al., "Small-molecule ligands bind to a distinct pocket in Ras and inhibit SOS-mediated nucleotide exchange activity," *Proceedings of the National Academy of Sciences*, vol. 109, no. 14, pp. 5299–5304, 2012.

[43] A. T. Constantinescu, A. Rak, K. Alexandrov, H. Esters, R. S. Goody, and A. J. Scheidig, "Rab-subfamily-specific regions of Ypt7p are structurally different from other RabGTPases," *Structure*, vol. 10, no. 4, pp. 569–579, 2002.

[44] P. Benkert, M. Biasini, and T. Schwede, "Toward the estimation of the absolute quality of individual protein structure models," *Bioinformatics*, vol. 27, no. 3, pp. 343–350, 2011.

[45] A. L. Morris, M. W. MacArthur, E. G. Hutchinson, and J. M. Thornton, "Stereochemical quality of protein structure coordinates," *Proteins: Structure, Function, and Genetics*, vol. 12, no. 4, pp. 345–364, 1992.

[46] J. B. Pereira-Leal and M. C. Seabra, "The mammalian Rab family of small GTPases: definition of family and subfamily sequence motifs suggests a mechanism for functional specificity in the Ras superfamily[1]," *Journal of Molecular Biology*, vol. 301, no. 4, pp. 1077–1087, 2000.

[47] V. K. Srivastava, S. Kaushik, and A. Jyoti, "A comparativein silicoanalysis of Rab5 proteins from pathogenic species to find its role in the pathogenesis," *Journal of Molecular Recognition*, vol. 32, no. 12, article e2808, 2019.

[48] V. K. Srivastava, M. Chandra, Y. Saito-Nakano, T. Nozaki, and S. Datta, "Crystal Structure Analysis of Wild Type and Fast Hydrolyzing Mutant of *Eh* RabX3, a Tandem Ras Superfamily GTPase from *Entamoeba histolytica*," *Journal of Molecular Biology*, vol. 428, no. 1, pp. 41–51, 2016.

[49] M. A. White, C. Nicolette, A. Minden et al., "Multiple ras functions can contribute to mammalian cell transformation," *Cell*, vol. 80, no. 4, pp. 533–541, 1995.

[50] J. Jorgačevski, M. Potokar, S. Grilc et al., "Munc18-1 tuning of vesicle merger and fusion pore properties," *The Journal of Neuroscience*, vol. 31, no. 24, pp. 9055–9066, 2011.

[51] J. Jorgačevski, M. Kreft, and R. Zorec, "Exocytotic pore in a SNARE," *Oncotarget*, vol. 8, no. 24, pp. 38082-38083, 2017.

[52] V. Kumar Srivastava, M. Chandra, and S. Datta, "Crystallization and preliminary X-ray analysis of RabX3, a tandem GTPase from *Entamoeba histolytica*," *Acta Crystallographica Section F Structural Biology Communications*, vol. 70, no. 7, pp. 933–937, 2014.

[53] S. Batra, P. Pancholi, M. Roy et al., "Exploring insights of syntaxin superfamily proteins fromEntamoeba histolytica: a prospective simulation,protein-proteininteraction, and docking study," *Journal of Molecular Recognition*, vol. 34, no. 6, pp. 1–13, 2021.

[54] M. Espinosa-Cantellano, A. Marti'nez, and M. Marti'nez-Palomo, "Pathogenesis of intestinal amebiasis: from molecules to disease. Vol 13," December 2020, http://cmr.asm.org/.

[55] D. Kessler, A. Bergner, J. Böttcher et al., "Drugging all RAS isoforms with one pocket," *Future Medicinal Chemistry*, vol. 12, no. 21, pp. 1911–1923, 2020.

Hindawi
BioMed Research International
Volume 2021, Article ID 5550387, 11 pages
https://doi.org/10.1155/2021/5550387

Review Article

The Accuracy of 16S rRNA Polymerase Chain Reaction for the Diagnosis of Neonatal Sepsis: A Meta-Analysis

Ying Wang,[1] **Jingyi Zhao**,[2] **Yinhui Yao**,[1] **Lan Yang**,[3] **Dan Zhao**,[4] **and Shiquan Liu**[5]

[1]*Department of Pharmacy, The Affiliated Hospital of Chengde Medical College, Chengde 067000, China*
[2]*Department of Functional Center, Chengde Medical College, Chengde 067000, China*
[3]*Institute of Chinese Materia Medica, Chengde Medical College, Chengde 067000, China*
[4]*Department of Intensive Care Unit, The Affiliated Hospital of Chengde Medical College, Chengde 067000, China*
[5]*Department of Thoracic Surgery, The Affiliated Hospital of Chengde Medical College, Chengde 067000, China*

Correspondence should be addressed to Yinhui Yao; yaoyh_gc@163.com

Received 26 February 2021; Accepted 29 April 2021; Published 15 May 2021

Academic Editor: Sanket Kaushik

Objective. To determine the accuracy of 16S rRNA polymerase chain reaction (PCR) for the diagnosis of neonatal sepsis through a systematic review and meta-analysis. *Methods*. Studies involving 16S rRNA PCR tests for the diagnosis of neonatal sepsis were searched in the PubMed, Medline, Embase, and Cochrane Library databases. The methodological quality of the identified studies was evaluated using the Quality Assessment of Diagnostic Accuracy Studies-2 (QUADAS-2), and the sensitivity, the specificity, the positive likelihood ratio (PLR), the negative likelihood ratio (NLR), the diagnostic odds ratio (DOR), and the area under the curve (AUC) of operator characteristic (SROC) curves were determined. Heterogeneity between studies was analyzed by metaregression. Stata 14.0 and Meta-disc 1.4 software were used for the analyses. *Results*. This meta-analysis included 19 related studies. The analysis found a sensitivity of 0.98 (95% CI: 0.85-1), specificity of 0.94 (95% CI: 0.87-0.97), PLR of 16.0 (95% CI: 7.6-33.9), NLR of 0.02 (95% CI: 0.00-0.18), DOR of 674 (95% CI: 89-5100), and AUC of 0.99 (95% CI: 0.97-0.99). Metaregression analysis identified Asian countries, arterial blood in blood samples, and sample size > 200 as the main sources of heterogeneity. This meta-analysis did not uncover publication bias. Sensitivity analysis showed that the study was robust. Fagan's nomogram results showed clinical usability. *Conclusions*. The results from this meta-analysis indicate that 16S rRNA PCR testing is effective for the rapid diagnosis of neonatal sepsis.

1. Introduction

Neonatal sepsis, a systemic inflammatory reaction to the invasion of bacteria, viruses, fungi, and other pathogens in a newborn's blood, produces toxins and is the most common form of infectious disease among newborns [1]. Globally, neonatal sepsis has an intimate connection with a 2.2% morbidity rate and a mortality rate of 11-19%, with higher mortality in developing countries [2, 3]. Clinical signs of neonatal sepsis are often aspecific, which limits initial diagnosis. Late diagnosis leads to disease progression, resulting in multiple organ failure and even death. Thus, early diagnosis of sepsis and early treatment are key to successful outcomes.

The gold standard for the diagnosis of neonatal sepsis is through culture of the microorganisms from patient blood or other body fluids, such as urine, and cerebrospinal fluid. However, due to factors such as insufficient samples, maternal use of antibiotics, and antibiotic use before sampling, this method may give false negative results [4, 5]. Various biomarkers, including C-reactive protein (CRP), procalcitonin (PCT), neutrophil CD64, interleukin-8, and interleukin-27, are used for sepsis diagnosis [6–11]. However, these biomarkers may also be elevated in noninfectious conditions such as premature rupture of membranes, fetal distress, dystocia, and perinatal asphyxia, resulting in false positive results and low specificity for neonatal sepsis [6]. Thus, there is an urgent need for faster, more sensitive tests for neonatal sepsis diagnosis.

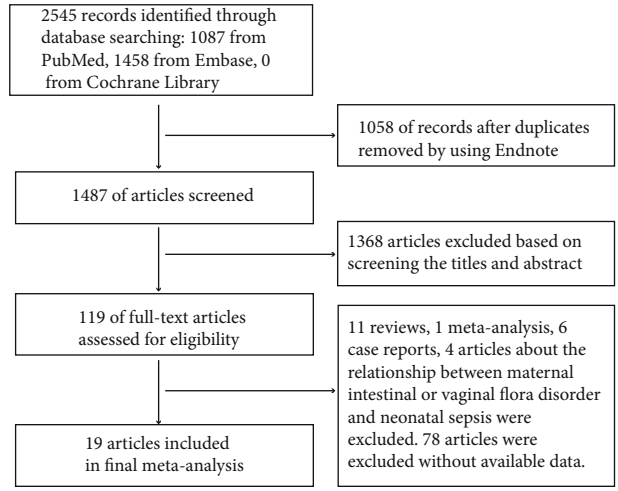

Figure 1: Study selection flow chart.

Table 1: The important features of the 19 articles included in this meta-analysis.

Author	Year	Country	TP	TN	FN	FP	Specimen	Center	Threshold
İstanbullu K [25]	2019	Turkey	1	2	5	92	Blood	Single	Florescence
EL-Amir [26]	2019	Egypt	51	0	13	11	Venous	Single	380 base pairs and 212
Yu R [12]	2020	China	31	25	0	4	Blood	Single	1380 bp
Punia H [27]	2017	India	66	3	0	31	Blood	Single	203 bp
Midan DA [28]	2016	Egypt	28	4	0	8	Intravenous	Single	Fluorescent sensor
Rohit A [29]	2016	India	28	27	6	36	Peripheral	Single	996 bp
El Gawhary S [30]	2015	Egypt	10	6	6	40	Peripheral	Single	200 bp
Dutta S [31]	2009	India	50	7	2	183	Blood	Single	380 bp
Liu CL [32]	2014	China	95	28	0	583	Venous	Multicenter	630 and 216 bp
Fujimori M [33]	2010	Japan	6	9	0	24	Arterial	Single	NA
Ohlin A [34]	2008	Sweden	21	12	29	233	Intravenous	Single	CP value with a range
Wu YD [35]	2007	China	20	23	0	787	Venous	Single	CT values ≤ 35 cycles
Jordan JA [36]	2006	USA	7	30	10	1186	Venous	Single	380 bp
Makhoul IR [37]	2005	Israel	9	0	4	202	Venous	Single	997 bp
Shang S [38]	2005	China	8	9	0	155	Venous	Single	371 bp
Yadav AK [13]	2005	India	9	4	0	87	Venous	Single	861 bp
Tong MQ [39]	2004	China	8	9	0	268	Venous	Single	371 bp
Shang S [40]	2001	China	26	0	0	30	Blood & CFS	Single	371 bp
Laforgia N [41]	1997	Italy	4	2	0	27	Venous	Single	861 bp

Recently, the PCR technique has been universal deployed in clinical diagnoses, which makes it possible to diagnose infectious diseases caused by microorganisms quickly and accurately. Moreover, numerous studies have shown that 16S rRNA PCR can diagnose neonatal sepsis [12–17]. The 16S rRNA gene is 1500 nucleotides long and encodes the 30S ribosomal subunit in all prokaryotes. The 16S rRNA gene is highly conserved and does not change over time. Within a certain range, the 16S rRNA gene can accurately identify specific bacteria based on gene-specific signatures [18, 19]. Relative to culture techniques, 16S rRNA PCR is cost-effective and rapid [20]. Here, we conducted a systematic review and meta-analysis of published studies to determine the utility of 16S rRNA PCR in neonatal sepsis diagnosis.

2. Methods

2.1. Search Strategy. Two authors independently performed literature searches of PubMed, Medline, Embase, and the Cochrane Library using the search terms 16S rRNA, 16S ribosomal ribonucleic acid, septic, septicemia, and neonatal sepsis. No restrictions were applied on the search, which included studies published until 13 January 2021. To ensure comprehensive literature identification, we manually searched relevant references in the identified studies.

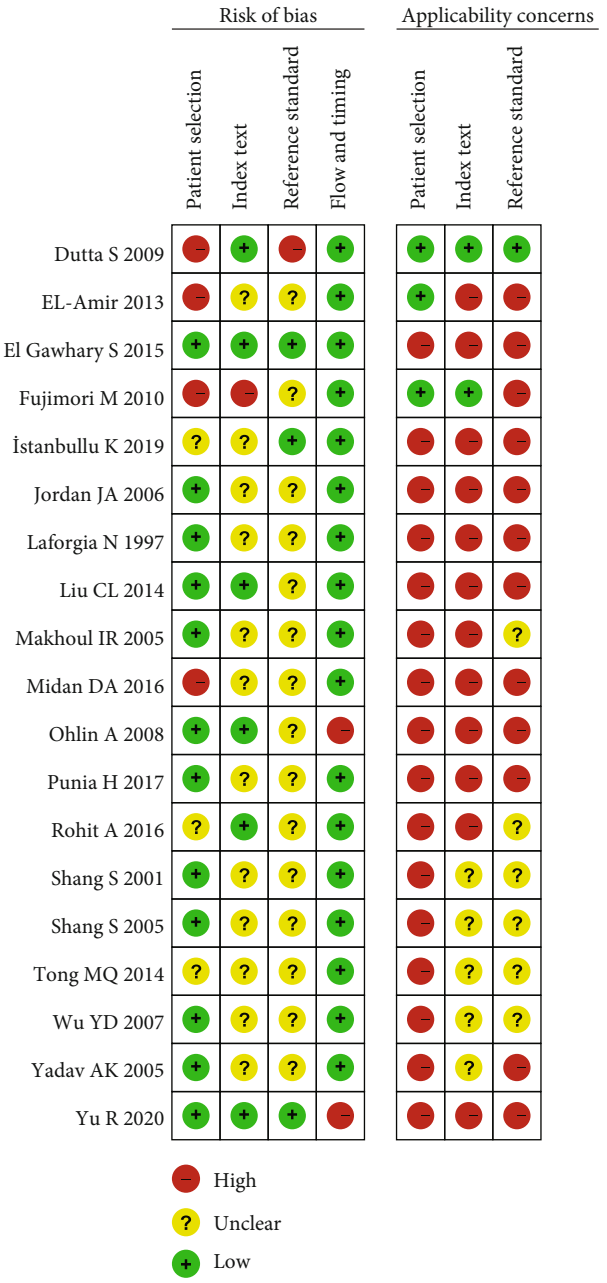

Figure 2: Risk of bias and applicability concerns in the included studies.

2.2. Study Selection. The following inclusion criteria were used: (1) samples were neonatal blood; (2) true positive (TP), true negative (TN), false positive (FP), and false negative (FN) values could be directly or indirectly obtained; (3) all data were derived from 16S rRNA PCR tests for neonatal sepsis diagnosis. The exclusion criteria were as follows: (1) literature in the form of review, meta-analysis, case report, or letter; (2) studies that were not clearly defined as involving neonates; (3) studies in with insufficient data for meta-analysis; and (4) studies involving nonblood samples.

2.3. Data Extraction. The following data were extracted by 2 authors: first author name, publication year, region, TN, FN, TP, FP, test method, and test sample. Disagreements were resolved by a 3rd author.

2.4. Quality Assessment. The inclusion criteria and methodological quality of selected articles were evaluated by 2 independent authors using QUADAS-2 [21], and disagreements were resolved by a 3rd author.

2.5. Statistical Analysis. Study heterogeneity was evaluated by I^2 test. Heterogeneity due to the threshold effect was evaluated by the Spearman model. When study heterogeneity was statistically significant ($I^2 > = 50\%$ or $p = <0.05$), the random effect model was used; otherwise, a fixed effects model was used [22, 23]. To evaluate 16S rRNA PCR

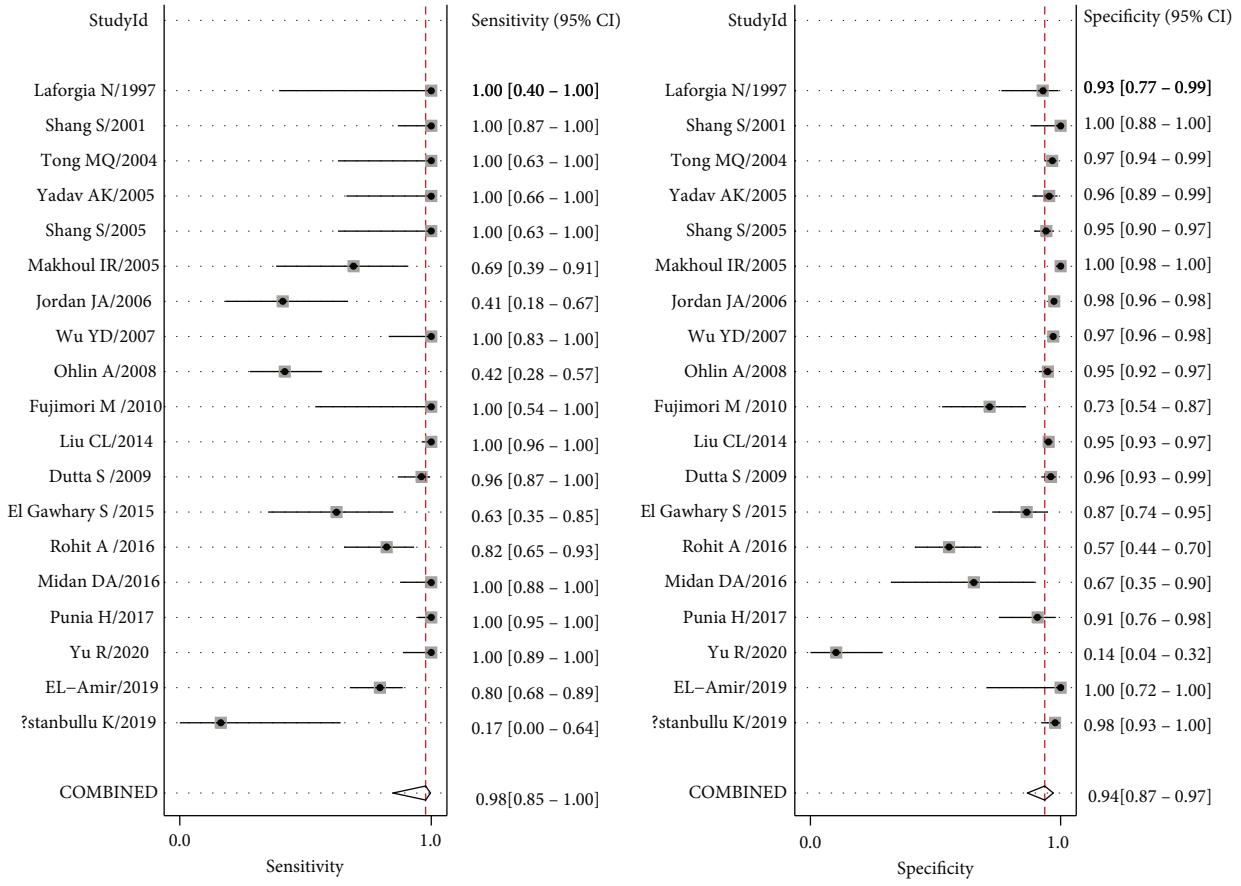

Figure 3: Forest plots for pooled sensitivity and specificity of neonatal sepsis diagnosis by 16S rRNA PCR.

potential and accuracy in neonatal sepsis diagnosis, sensitivity, specificity, PLR, NLR, DOR, and AUC of SROC curve analyses were used. Metaregression analysis was used to determine heterogeneity sources. Deeks' funnel plot asymmetry test was used to evaluate publication bias [24]. Sensitivity analysis was used to evaluate the robustness of this study. Statistical analyses were performed by Stata 14.0 and Meta-disc 1.4.

3. Results

3.1. Study Characteristics. A total of 2545 studies were identified, and 1058 duplicate studies were eliminated. Upon title and abstract review, 1368 studies were excluded, and 119 were subjected to full-text review. Of these, 100 were excluded because valid data could not be extracted, and the remaining 19 articles were included in our study [12, 13, 25–41] (Figure 1).

The19 articles incorporated into in our study involved a comparison between the diagnostic value of 16S rRNA PCR and blood culture for pathogenic microorganism identification in neonatal sepsis patients. The important features of the 19 articles are displayed in Table 1. They involved a total of 4740 neonatal blood samples, of which 553 were positive and 4187 were negative. The included studies were from Turkey (1), China (6), Egypt (3), India (4), Israel (1), the US (1), Japan (1), Italy (1), and Sweden (1). 16S rRNA amplification was achieved by PCR.

3.2. Quality Assessment. Methodological quality and risk of bias in the included studies were assessed using QUADAS-2. All studies used a prospective study design to avoid inappropriate exclusion (Figure 2). Five studies did not specify whether patients were continuously enrolled or not [25, 26, 28–30]. The remaining studies specified continuous enrollment. The reference standard in all studies was pathogenic microorganism blood culture. Some studies did not report sufficient data on indicator tests and/or reference criteria, so these items were used as ambiguous risk of bias scores. QUADAS-2 did not include an overall bias score, but the overall quality of the studies included in the analysis was moderate to high.

3.3. Heterogeneity Analysis and Diagnostic Accuracy. The sensitivity I^2 was 99.95 (95% CI: 99.94-99.55), $p \leq 0.001$. And the specificity I^2 was 99.32 (95% CI: 99.23-99.42), $p \leq 0.001$. Because the results point out heterogeneity among the studies, the random effect model was adopted. Analysis results were displayed in Figure 3. The overall sensitivity and specificity of the 19 studies were 0.98 (95% CI: 0.85-1.00) and 0.94 (95% CI: 0.87-0.97), respectively. The PLR was 16.0 (95% CI: 7.6-33.9), the NLR was 0.02 (95% CI: 0.00-0.18), and the DOR was 674 (95% CI: 89-5100). The

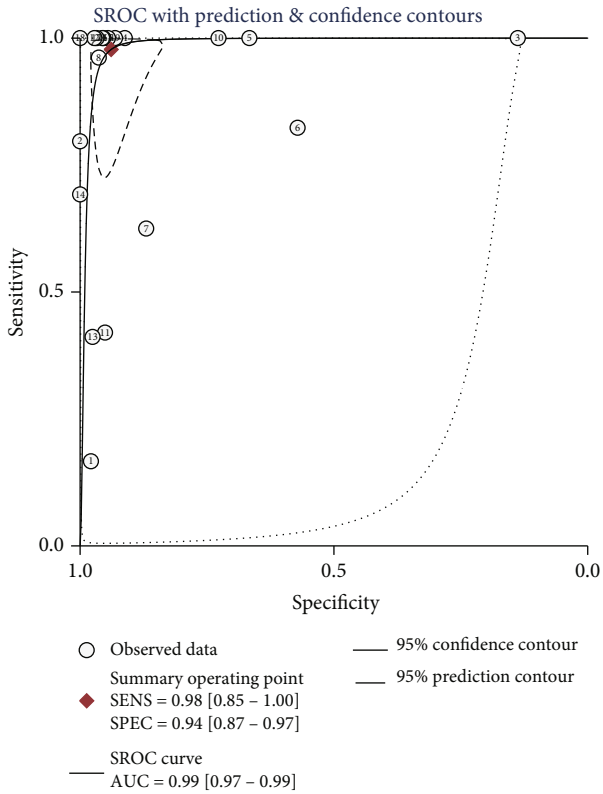

Figure 4: 16S rRNA symmetrical summary receiver operator characteristic (SROC) curve for all 19 studies.

SROC curve analysis of the 16S rRNA gene PCR test accuracy in neonatal sepsis diagnosis revealed an AUC of 0.99 (95% CI: 0.97-0.99; Figure 4).

3.4. Subgroup Analysis and Metaregression. In order to investigate the potential sources of heterogeneity, we conducted threshold effect analysis using Meta-disc 1.4 and obtained a Spearman correlation coefficient of 0.262 ($p = 0.279$), indicating that the threshold effect was not the source of the heterogeneity. Next, metaregression analysis was used to divide the subgroups into location (Asian vs. non-Asian), specimen (arterial vs. nonarterial blood), center (single center vs. multicenter), and sample size (≥200 vs. <200) (Figure 5). The main sources of sensitivity heterogeneity were location, specimen, center, and sample size. Specificity heterogeneity was mainly due to sample size.

3.5. Sensitivity Analysis. Sensitivity analysis was used to evaluate the reliability and robustness of the analysis results. The validity and robustness of the models involved in the statistical analyses were verified by goodness-of-fit and bivariate normality analysis (Figures 6(a) and 6(b)). Influence analysis (Figure 6(c)) showed 3 influence studies, and outlier detection (Figure 6(d)) found 1 outlier study. Sequential exclusion of influencing factors and outliers did not significantly alter the overall results (Table 2).

3.6. Clinical Utility of the Index Test. To evaluate posttest probabilities, Fagan's nomogram could be used to calculate the posttest probability of 16S rRNA PCR for neonatal sepsis diagnosis. When the pretest probability was set at 11%, it was found that the probability of neonatal sepsis was 0.66 if the results were positive and 0 if the results were negative (Figure 7). A likelihood ratio scatter plot showed that 16S rRNA PCR was effective for neonatal sepsis diagnosis (positive) and exclusion (negative), with the summary point of the probability ratio in the upper left quadrant (Figure 8).

3.7. Publication Bias. Deeks' funnel plot asymmetry test on the 19 included studies found no publication bias (Figure 9, $p = 0.09$).

4. Discussion

Past studies demonstrated the high potential of 16S rRNA PCR tests for diagnosing bloodstream infections. This strategy has been suggested to be effective and fast for screening sepsis [42]. In this meta-analysis, we evaluated the performance of 16S rRNA PCR for neonatal sepsis diagnosis relative to blood culture techniques. 16S rRNA PCR tests have the potential to accelerate neonatal sepsis diagnosis, thereby ensuring timely and effective treatment.

Our analysis found that the sensitivity and specificity of 16S rRNA PCR tests for neonatal sepsis diagnosis were 0.98 (95% CI: 0.85-1.00) and 0.94 (95% CI: 0.87-0.97), respectively, indicating high diagnostic effectiveness. The SROC curve showed the trade-off between the sensitivity and specificity of diagnostic research, and the AUC of the SROC curve is a measure of the integrity of the diagnostic testing ability, providing a precise basis for the overall study [43]. Our analysis revealed an AUC of 0.99 (95% CI: 0.97-0.99), indicating that 16S rRNA PCR is highly accurate for neonatal sepsis diagnosis. The DOR is a way of the usefulness of a diagnostic test and is given as a value between 0 and ∞, and a higher value means better performance. Conversely, a value of <1 indicates that the test lacks the ability to distinguish between outcomes [44]. Our analysis revealed a DOR value of 674 (95% CI: 89-5100), indicating high accuracy. The likelihood ratio fully reflects the diagnostic value of a screening test and is very stable. The DOR comprises the PLR (ratio of true positive rate to false positive rate, where the larger the ratio is, the greater the likelihood of a true positive test result) and the NLR (ratio of false negative rate to true negative rate, where the smaller the ratio is, the greater the chance of a true negative test result). Our pooled results revealed a PLR of 16.0 (95% CI: 7.6-33.9) and NLR of 0.02 (95% CI: 0.00-0.18), indicating that 16S rRNA PCR has good diagnostic ability.

Although the 16S rRNA PCR test was effective, there was significant heterogeneity in this meta-analysis. Different regions were also major sources of heterogeneity in this study. In the Asian population relative to the non-Asian populations, the sensitivity, specificity, PLR, NLR, DOR, and AUC were 1.00 (0.89-1.00) vs. 0.71 (0.41-0.89), 0.91 (0.79-0.97) vs. 0.96 (0.89-0.98), 11.5 (4.4-30.3) vs. 16.7 (7.0-39.5), 0 (0-0.14) vs. 0.31 (0.13-0.72), 4297 (64-289895) vs. 55 (17-180), and 1.00 (0.99-1.00) vs. 0.95

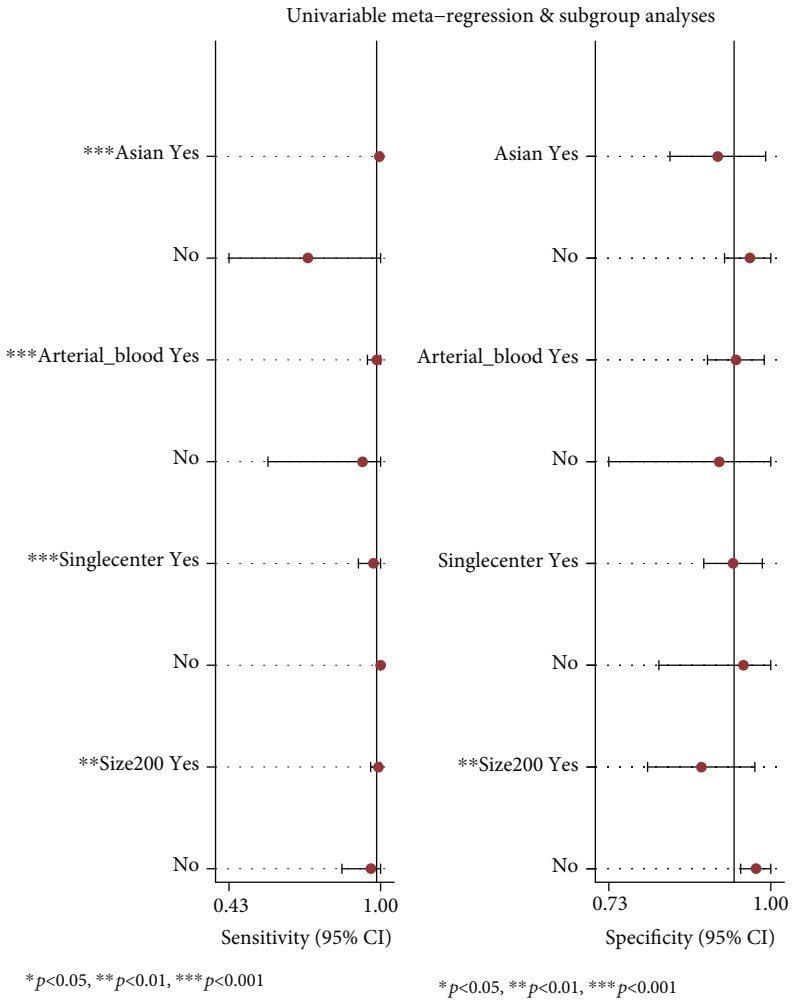

Figure 5: Univariable metaregression and subgroup analyses.

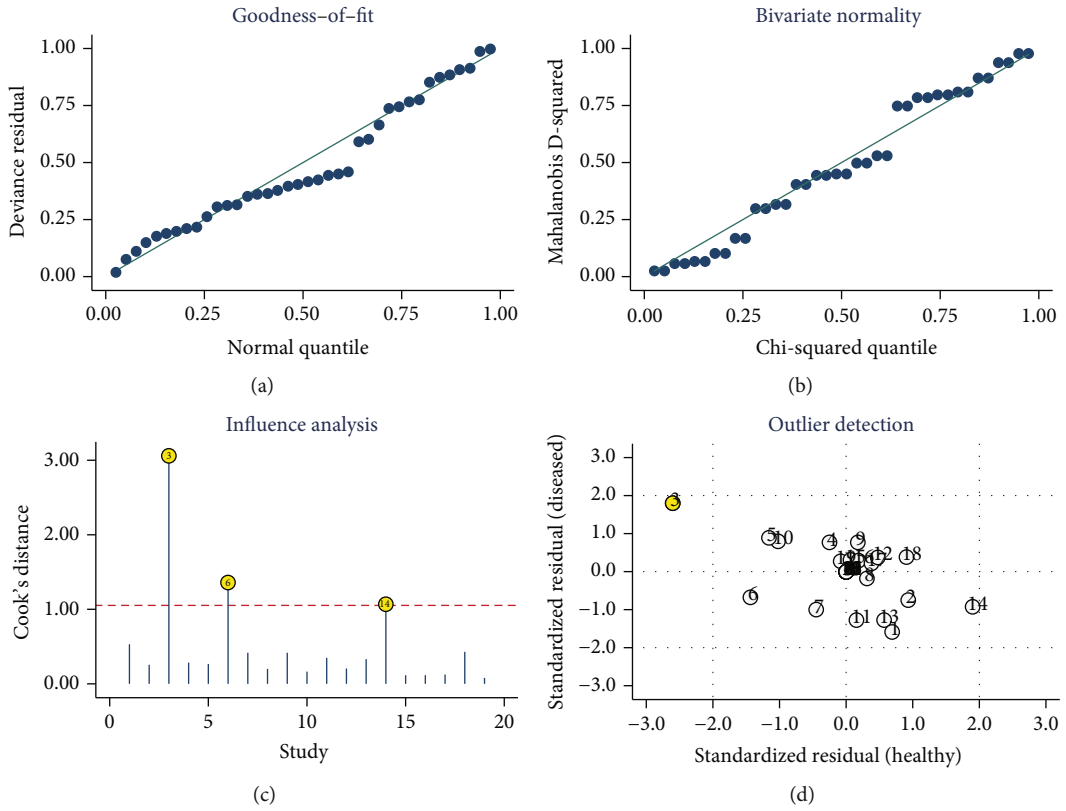

Figure 6: Stability and robustness analysis of the included studies.

Table 2: Summary estimates of the diagnostic performance of 16S rRNA PCR in neonatal sepsis diagnosis.

Analysis	Number of studies	Sensitivity (95% CI)	Specificity (95% CI)	PLR (95% CI)	NLR (95% CI)	DOR (95% CI)	AUC (95% CI)
Overall	19[12, 13, 25-41]	0.98 (0.85-1.00)	0.94 (0.87-0.97)	16.0 (7.6-33.9)	0.02 (0.00-0.18)	674 (89-5100)	0.99 (0.97-0.99)
Influence studies excluded	16[13, 25-28, 30-36, 38-41]	0.99 (0.84-1.00)	0.95 (0.92-0.97)	19.5 (12.9-29.4)	0.01 (0.00-0.20)	1464 (103-20881)	0.98 (0.96-0.99)
Outlier excluded	18[13, 25-41]	0.97 (0.83-1.00)	0.95 (0.91-0.97)	19.2 (10.6-34.7)	0.03 (0.00-0.20)	612 (87-4290)	0.98 (0.97-0.99)

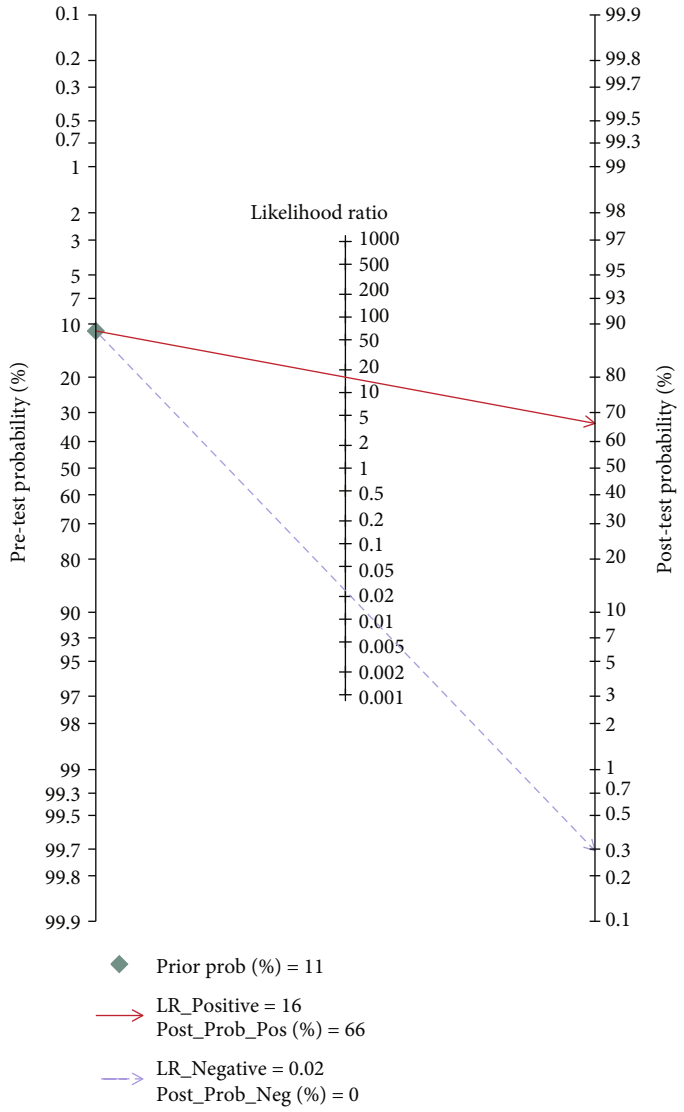

Figure 7: Fagan's nomogram for calculating the post-test probabilities of 16S rRNA PCR for neonatal sepsis diagnosis.

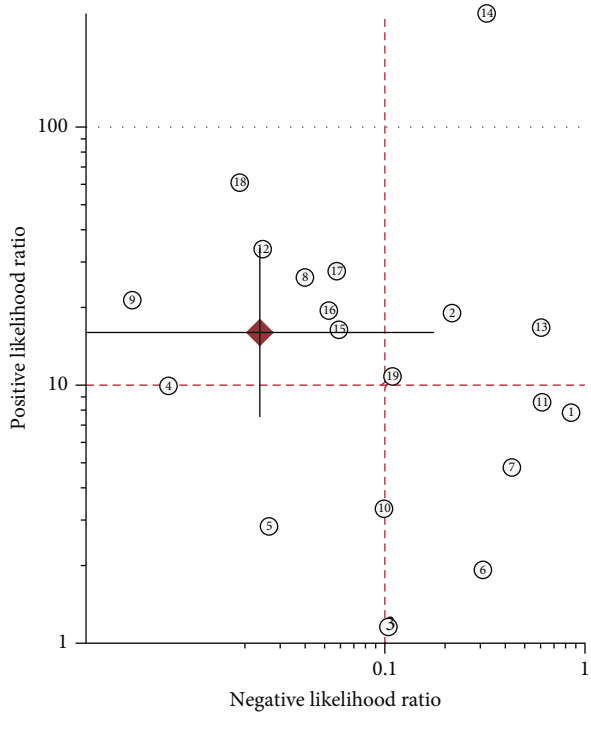

Figure 8: Likelihood ratio scatter gram.

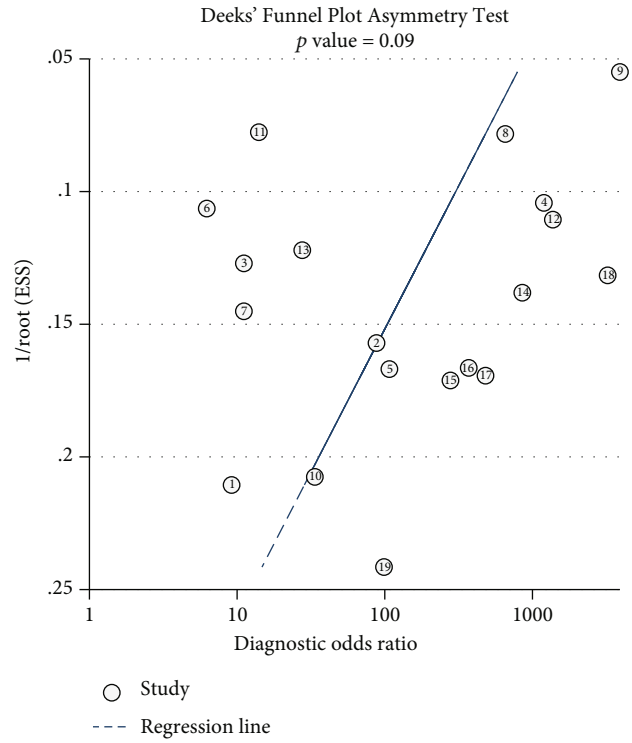

Figure 9: Deeks' funnel plot for identifying publication bias.

(0.93-0.97), respectively. Blood sample sources, sample sizes, and single- or multicenter studies were also sources of heterogeneity. However, because there were few multicenter studies, more standardized multicenter studies are needed to better understand the value of 16S rRNA PCR tests in neonatal sepsis diagnosis [45].

Our meta-analysis has some limitations. First, the included studies defined sepsis using different criteria, which may be reflected in different clinical symptoms and routine blood tests for the included patients. Although blood culture, the gold standard for sepsis diagnosis, was used in all studies, the associated false positive rate was high [4]. Second, the kits and testing tools used for blood cultures and testing were manufactured by different companies, and there are no studies on whether the results vary by kit manufacturer. Third, most studies included in this meta-analysis did not distinguish between early-onset sepsis and late-onset sepsis. Thus, we could not carry out subgroup analysis between early-onset sepsis and late-onset sepsis.

5. Conclusions

In summary, this meta-analysis shows that 16S rRNA PCR tests are effective for rapid neonatal sepsis diagnosis. However, PCR amplification methods are not fully defined, and future prospective studies should carry out subgroup analysis of PCR methods.

Data Availability

The data of Table 1 used to support the findings of this study are included within the article (see References).

Conflicts of Interest

No conflicts of interest are declared.

Acknowledgments

This project was sponsored by the Science and Technology Planning Project of Chengde (grant nos. 202006A049 and 202006A088).

References

[1] F. Kim, R. A. Polin, and T. A. Hooven, "Neonatal sepsis," *BMJ*, vol. 371, article m3672, 2020.

[2] Y. Dong, R. Basmaci, L. Titomanlio, B. Sun, and J. C. Mercier, "Neonatal sepsis: within and beyond China," *Chinese Medical Journal*, vol. 133, no. 18, pp. 2219–2228, 2020.

[3] C. Fleischmann-Struzek, D. M. Goldfarb, P. Schlattmann et al., "The global burden of paediatric and neonatal sepsis: a

systematic review," *The Lancet Respiratory Medicine*, vol. 6, no. 3, pp. 223–230, 2018.

[4] I. O. Odabasi and A. Bulbul, "Neonatal Sepsis," *Sisli Etfal Hastan Tip Bul*, vol. 54, no. 2, pp. 142–158, 2020.

[5] M. Satar, A. E. Arısoy, and I. H. Celik, "Turkish Neonatal Society guideline on neonatal infections-diagnosis and treatment," *Turk Pediatri Ars*, vol. 53, no. 1, pp. S88–S100, 2018.

[6] M. Tsokos, U. Reichelt, A. Nierhaus, and K. Püschel, "Serum procalcitonin (PCT): a valuable biochemical parameter for the post-mortem diagnosis of sepsis," *International Journal of Legal Medicine*, vol. 114, no. 4-5, pp. 237–243, 2001.

[7] A. V. Raveendran, A. Kumar, and S. Gangadharan, "Biomarkers and newer laboratory investigations in the diagnosis of sepsis," *The Journal of the Royal College of Physicians of Edinburgh*, vol. 49, no. 3, pp. 207–216, 2019.

[8] J. Zhao, S. Zhang, L. Zhang et al., "Serum procalcitonin levels as a diagnostic marker for septic arthritis: A meta-analysis," *The American Journal of Emergency Medicine*, vol. 35, no. 8, pp. 1166–1171, 2017.

[9] Y. Song, Y. Chen, X. Dong, and X. Jiang, "Diagnostic value of neutrophil CD64 combined with CRP for neonatal sepsis: A meta-analysis," *The American Journal of Emergency Medicine*, vol. 37, no. 8, pp. 1571–1576, 2019.

[10] M. Zhou, S. Cheng, J. Yu, and Q. Lu, "Interleukin-8 for diagnosis of neonatal sepsis: a meta-analysis," *PLoS One*, vol. 10, no. 5, article e0127170, 2015.

[11] Y. Wang, J. Zhao, Y. Yao, D. Zhao, and S. Liu, "Interleukin-27 as a Diagnostic Biomarker for Patients with Sepsis: A Meta-Analysis," *BioMed Research International*, vol. 2021, Article ID 5516940, 7 pages, 2021.

[12] R. Yu, Q. Zhou, S. Jiang, Y. Mei, and M. Wang, "Combination of 16S rRNA and procalcitonin in diagnosis of neonatal clinically suspected sepsis," *Journal of International Medical Research*, vol. 48, no. 3, article 030006051989241, 2020.

[13] A. K. Yadav, C. G. Wilson, P. L. Prasad, and P. K. Menon, "Polymerase chain reaction in rapid diagnosis of neonatal sepsis," *Indian Pediatrics*, vol. 42, no. 7, pp. 681–685, 2005.

[14] J. A. Jordan and M. B. Durso, "Real-time polymerase chain reaction for detecting bacterial DNA directly from blood of neonates being evaluated for sepsis," *The Journal of Molecular Diagnostics*, vol. 7, no. 5, pp. 575–581, 2005.

[15] C. Oeser, M. Pond, P. Butcher et al., "PCR for the detection of pathogens in neonatal early onset sepsis," *PLoS One*, vol. 15, no. 1, article e0226817, 2020.

[16] A. Ohlin, A. Bäckman, U. Ewald, J. Schollin, and M. Björkqvist, "Diagnosis of neonatal sepsis by broad-range 16S real-time polymerase chain reaction," *Neonatology*, vol. 101, no. 4, pp. 241–246, 2012.

[17] C. S. Buhimschi, V. Bhandari, Y. W. Han et al., "Using proteomics in perinatal and neonatal sepsis: hopes and challenges for the future," *Current Opinion in Infectious Diseases*, vol. 22, no. 3, pp. 235–243, 2009.

[18] D. L. Church, L. Cerutti, A. Gürtler, T. Griener, A. Zelazny, and S. Emler, "Performance and Application of 16S rRNA Gene Cycle Sequencing for Routine Identification of Bacteria in the Clinical Microbiology Laboratory," *Clinical Microbiology Reviews*, vol. 33, no. 4, 2020.

[19] K. Fukuda, M. Ogawa, H. Taniguchi, and M. Saito, "Molecular Approaches to Studying Microbial Communities: Targeting the 16S Ribosomal RNA Gene," *Journal of UOEH*, vol. 38, no. 3, pp. 223–232, 2016.

[20] R. M. Hassan, M. G. El Enany, and H. H. Rizk, "Evaluation of broad-range 16S rRNA PCR for the diagnosis of bloodstream infections: two years of experience," *Journal of Infection in Developing Countries*, vol. 8, no. 10, pp. 1252–1258, 2014.

[21] P. F. Whiting, A. W. Rutjes, M. E. Westwood et al., "QUADAS-2: a revised tool for the quality assessment of diagnostic accuracy studies," *Annals of Internal Medicine*, vol. 155, no. 8, pp. 529–536, 2011.

[22] T. B. Huedo-Medina, J. Sánchez-Meca, F. Marín-Martínez, and J. Botella, "Assessing heterogeneity in meta-analysis: Q statistic or I2 index?," *Psychological Methods*, vol. 11, no. 2, pp. 193–206, 2006.

[23] F. L. Schmidt, I. S. Oh, and T. L. Hayes, "Fixed- versus random-effects models in meta-analysis: model properties and an empirical comparison of differences in results," *The British Journal of Mathematical and Statistical Psychology*, vol. 62, no. 1, pp. 97–128, 2009.

[24] J. J. Deeks, P. Macaskill, and L. Irwig, "The performance of tests of publication bias and other sample size effects in systematic reviews of diagnostic test accuracy was assessed," *Journal of Clinical Epidemiology*, vol. 58, no. 9, pp. 882–893, 2005.

[25] K. İstanbullu, N. Köksal, M. Çetinkaya et al., "The potential utility of real-time PCR of the 16S-rRNA gene in the diagnosis of neonatal sepsis," *The Turkish Journal of Pediatrics*, vol. 61, no. 4, pp. 493–499, 2019.

[26] M. I. El-Amir, M. A. El-Feky, D. A. Abo Elwafa, and E. A. Abd-Elmawgood, " Rapid diagnosis of neonatal sepsis by PCR for detection of 16S rRNA gene, while blood culture and PCR results were similar in E.coli-predominant EOS cases ," *Infect Drug Resist*, vol. 12, pp. 2703–2710, 2019.

[27] H. Punia, G. Gathwala, D. B. Dhaulakhandi, and M. Aamir, "Diagnosis of neonatal sepsis using 16S rRNA polymerase chain reaction," *Tropical Doctor*, vol. 47, no. 4, pp. 336–339, 2017.

[28] D. A. Midan, W. M. M. Abo El Fotoh, and A. H. El Shalakany, "The potential role of incorporating real-time PCR and DNA sequencing for amplification and detection of 16S rRNA gene signatures in neonatal sepsis," *The Journal of Maternal-Fetal & Neonatal Medicine*, vol. 30, no. 12, pp. 1476–1483, 2017.

[29] A. Rohit, B. Maiti, S. Shenoy, and I. Karunasagar, "Polymerase chain reaction-restriction fragment length polymorphism (PCR-RFLP) for rapid diagnosis of neonatal sepsis," *The Indian Journal of Medical Research*, vol. 143, no. 1, pp. 72–78, 2016.

[30] S. el Gawhary, M. el-Anany, R. Hassan, D. Ali, and E. Q. el Gameel, "The Role of 16S rRNA Gene Sequencing in Confirmation of Suspected Neonatal Sepsis," *Journal of Tropical Pediatrics*, vol. 62, no. 1, pp. 75–80, 2016.

[31] S. Dutta, A. Narang, A. Chakraborty, and P. Ray, "Diagnosis of neonatal sepsis using universal primer polymerase chain reaction before and after starting antibiotic drug therapy," *Archives of Pediatrics & Adolescent Medicine*, vol. 163, no. 1, pp. 6–11, 2009.

[32] C. L. Liu, H. W. Ai, W. P. Wang et al., "Comparaison entre l'ARNr 16S et l'hemoculture pour le diagnostic de septicemie neonatale," *Archives de Pédiatrie*, vol. 21, no. 2, pp. 162–169, 2014.

[33] M. Fujimori, K. Hisata, S. Nagata et al., "Efficacy of bacterial ribosomal RNA-targeted reverse transcription-quantitative

PCR for detecting neonatal sepsis: a case control study," *BMC Pediatrics*, vol. 10, no. 1, p. 53, 2010.

[34] A. Ohlin, A. Bäckman, M. Björkqvist, P. Mölling, M. Jurstrand, and J. Schollin, "Real-time PCR of the 16S-rRNA gene in the diagnosis of neonatal bacteraemia," *Acta Paediatrica*, vol. 97, no. 10, pp. 1376–1380, 2008.

[35] Y. D. Wu, S. Q. Shang, J. P. Li et al., "A broad-range 16S rRNA gene real-time PCR assay for the diagnosis of neonatal septicemia," *Zhonghua Er Ke Za Zhi*, vol. 45, no. 6, pp. 446–449, 2007.

[36] J. A. Jordan, M. B. Durso, A. R. Butchko, J. G. Jones, and B. S. Brozanski, "Evaluating the near-term infant for early onset sepsis: progress and challenges to consider with 16S rDNA polymerase chain reaction testing," *The Journal of Molecular Diagnostics*, vol. 8, no. 3, pp. 357–363, 2006.

[37] I. R. Makhoul, T. Smolkin, P. Sujov et al., "PCR-based diagnosis of neonatal staphylococcal bacteremias," *Journal of Clinical Microbiology*, vol. 43, no. 9, pp. 4823–4825, 2005.

[38] S. Shang, G. Chen, Y. Wu, L. Du, and Z. Zhao, "Rapid diagnosis of bacterial sepsis with PCR amplification and microarray hybridization in 16S rRNA gene," *Pediatric Research*, vol. 58, no. 1, pp. 143–148, 2005.

[39] M. Q. Tong, S. Q. Shang, Y. D. Wu, and Z. Y. Zhao, "Rapid diagnosis of neonatal sepsis by 16SrRNA genes PCR amplification and genechip hybridization," *Zhonghua Er Ke Za Zhi*, vol. 42, no. 9, pp. 663–667, 2004.

[40] S. Shang, Z. Chen, and X. Yu, "Detection of bacterial DNA by PCR and reverse hybridization in the 16S rRNA gene with particular reference to neonatal septicemia," *Acta Paediatrica*, vol. 90, no. 2, pp. 179–183, 2001.

[41] N. Laforgia, B. Coppola, R. Carbone, A. Grassi, A. Mautone, and A. Iolascon, "Rapid detection of neonatal sepsis using polymerase chain reaction," *Acta Paediatrica*, vol. 86, no. 10, pp. 1097–1099, 1997.

[42] G. Su, Z. Fu, L. Hu, Y. Wang, Z. Zhao, and W. Yang, "16S Ribosomal Ribonucleic Acid Gene Polymerase Chain Reaction in the Diagnosis of Bloodstream Infections: A Systematic Review and Meta-Analysis," *PLoS One*, vol. 10, no. 5, article e0127195, 2015.

[43] S. D. Walter, "Properties of the summary receiver operating characteristic (SROC) curve for diagnostic test data," *Statistics in Medicine*, vol. 21, no. 9, pp. 1237–1256, 2002.

[44] F. Tuzun, H. Ozkan, M. Cetinkaya et al., "Is European Medicines Agency (EMA) sepsis criteria accurate for neonatal sepsis diagnosis or do we need new criteria?," *PLoS One*, vol. 14, no. 6, article e0218002, 2019.

Hindawi
BioMed Research International
Volume 2021, Article ID 5535562, 11 pages
https://doi.org/10.1155/2021/5535562

Research Article

β-Sitosterol Alters the Inflammatory Response in CLP Rat Model of Sepsis by Modulation of NFκB Signaling

Sara Kasirzadeh,[1,2] **Mohammad Hossein Ghahremani**,[1] **Neda Setayesh**,[3] **Fereshteh Jeivad**,[1] **Amir Shadboorestan**,[4] **Ali Taheri**,[5] **Abbas Beh-Pajooh**,[1] **Armin Azadkhah Shalmani**,[1] **Alireza Ebadollahi-Natanzi**,[6] **Alamgir Khan**,[7] **Samin Sabzevari**,[1,2] **and Omid Sabzevari**[1,2]

[1]*Department of Toxicology and Pharmacology, Faculty of Pharmacy, Tehran University of Medical Sciences, Tehran, Iran*
[2]*Toxicology and Poisoning Research Centre, Tehran University of Medical Sciences, Tehran, Iran*
[3]*Department of Pharmaceutical Biotechnology, Faculty of Pharmacy and Biotechnology Research Center, Tehran University of Medical Sciences, Tehran, Iran*
[4]*Department of Toxicology, Faculty of Medical Sciences, Tarbiat Modares University, Tehran, Iran*
[5]*Biopharmaceutics and Pharmacokinetics Division, Department of Pharmaceutics, Faculty of Pharmacy, Tehran University of Medical Sciences, Tehran, Iran*
[6]*Medicinal Plants Department, Imam Khomeini Higher Education Center, Agricultural Research, Education and Extension Organization (AREEO), Karaj, Iran*
[7]*Australian Proteome Analysis Facility (APAF), Level 4, Building F7B, Research Park Drive, Macquarie University, Sydney, NSW 2109, Australia*

Correspondence should be addressed to Omid Sabzevari; omid@tums.ac.ir

Received 18 February 2021; Revised 29 March 2021; Accepted 17 April 2021; Published 30 April 2021

Academic Editor: Vijay Kumar Srivastava

Purpose. Sepsis originates from the host inflammatory response, especially to bacterial infections, and is considered one of the main causes of death in intensive care units. Various agents have been developed to inhibit mediators of the inflammatory response; one prospective agent is β-sitosterol (βS), a phytosterol with a structure similar to cholesterol. This study is aimed at evaluating the effects of βS on the biomarkers of inflammation and liver function in cecal ligation and puncture- (CLP-) induced septic rats. *Methods*. Thirty male Wistar rats were divided equally into six groups as follows: sham, CLP, CLP+dexamethasone (DX, 0.2 mg/kg), CLP+βS (1 mg/kg), CLP+imipenem (IMI, 20 mg/kg), and CLP+IMI (20 mg/kg)+βS (1 mg/kg). Serum levels of IL-1β, IL-6, IL-10, AST, ALT, and liver glutathione (GSH) were assessed by ELISA. Liver expression levels of TNF-α and NF-κBi mRNAs were evaluated by RT-qPCR. *Results*. Serum concentrations of IL-1β, IL-6, IL-10, ALT, and AST and mRNA levels of TNF-α and NF-κBi were all significantly higher in septic rats than in normal rats ($p < 0.05$). Liver GSH content was markedly lower in the CLP group than that in the sham group. βS-treated rats had remarkably lower levels of IL-1β, IL-6, IL-10, TNF-α, NF-κBi, AST, and ALT (51.79%, 62.63%, 41.46%, 54.35%, 94.37%, 95.30%, 34.87%, and 46.53% lower, respectively) and greater liver GSH content (35.71% greater) compared to the CLP group ($p < 0.05$). *Conclusion*. βS may play a protective role in the septic process by mitigating inflammation. This effect is at least partly mediated by inhibition of the NF-κB signaling pathway. Thus, βS can be considered as a supplementary treatment in septic patients.

1. Introduction

Sepsis is a life-threatening critical illness caused by the invasion of microbial pathogens into the bloodstream. It remains one of the major causes of death specifically in intensive care units. According to the World Health Organization (WHO), sepsis affects more than 30 million people each year, causing approximately six million deaths worldwide [1]. Excessive and uncontrolled response to infection, septic shock, and acute failure of one or multiple organs such as the liver, kidney, and lungs can occur and may result in death in sepsis patients [2, 3]. It has been reported that liver

dysfunction is a subsequent result of sepsis, confirmed by higher serum levels of aspartate aminotransferase (AST) and alanine aminotransferase (ALT), and lower glutathione (GSH) content [3].

Cytokines, defined as a group of endogenous inflammatory and immune-modulating proteins, play a dominant role in sepsis syndrome. Exacerbated production of both pro- and anti-inflammatory cytokines results in a situation called "cytokine cascade." A cytokine cascade is initiated when a host is targeted by stimuli such as bacterial endotoxins, which induce the production of early cytokines including tumor necrosis factor-alpha (TNF-α) and interleukin 1-beta (IL-1β). Overproduction of early cytokines has been associated with multiple end-organ dysfunction and mortality [4]. Along with endotoxins, these cytokines are able to stimulate the production of later cytokines, such as interleukin 6 (IL-6). Interestingly, IL-6 is responsible for the downregulation of TNF-α and IL-1β, which might be vital in limiting the cytokine cascade [2]. Nuclear factor-kappa B (NF-κB) also plays a regulatory role in the cytokine cascade and is activated in numerous cell types by endotoxins, TNF-α, and IL-1β. Activation of NF-κB is a pivotal step for the transcription of many cytokines including TNF-α, IL-1β, IL-6, and IL-8. However, as activation of NF-κB increases, the transcription of NF-κB inhibitor (NF-κBi) also rises. The protein product of NF-κBi, IκBα, is an indicator of NF-κB activation. Newly synthesized IκBα translocates into the nucleus and terminates NF-κB activation by binding to the activated dimer. NF-κBi level increases in response to inflammation and decreases when appropriate treatment is given [5]. Furthermore, the NF-κB signaling pathway has been reported to play a role in hepatic injury [6]. In addition to the cytokine cascade, several studies have demonstrated that the balance between pro- and anti-inflammatory cytokines is a major factor determining the severity of sepsis [7, 8]. *In vitro* studies have shown that the anti-inflammatory cytokine interleukin 10 (IL-10) is a regulatory factor that blocks TNF-α, IL-1β, and IL-8 [4] and many studies have found higher concentrations of IL-10 in patients with sepsis [9, 10] (Figure 1).

Many natural plants contain pharmacologically active compounds that possess immunomodulating and anti-inflammatory properties and can potentially inhibit the cytokine cascade [11]. β-Sitosterol (βS) is a phytosterol found in various plants and has a chemical structure similar to that of cholesterol [12]. Several *in vitro* studies have revealed βS to possess anti-inflammatory properties. βS has been shown to have antiatherogenic potential through its anti-inflammatory action on human aortic endothelial cells [13]. Similarly, it has been reported that βS causes a dose-dependent inhibition of IL-6 and TNF-α in endotoxin-activated human monocytes [13, 14]. It has been found that βS has beneficial effects on the immune system by increasing the number of viable peripheral blood mononuclear cells (PBMCs) and activating the swine dendritic cells (DCs) [15]. Moreover, βS has been evaluated as an anti-inflammatory agent in a number of animal models in *in vivo* experiments. Anti-inflammatory and immunomodulatory properties of βS have been demonstrated in several animal models, including fattener pigs after receiving a modified live porcine reproductive and respiratory syndrome virus (PRRSV) vaccine [15], rats with oxazolone-induced contact-delayed type hypersensitivity [16], and mice with ovalbumin-induced lung inflammation [17]. Clinical studies represented the potential immunomodulatory effects of βS in patients with pulmonary tuberculosis, human immunodeficiency virus (HIV), human papillomavirus (HPV), stress-induced immune suppression, rheumatoid arthritis, and allergic rhinitis and sinusitis [14].

Our research is aimed at evaluating the effects of βS administration on the biomarkers of inflammation and liver function in cecal ligation and puncture (CLP) rats as a gold standard animal model of sepsis.

2. Methods

2.1. Animals. Thirty male Wistar rats, weighing 210-250 g, were acquired from the Animal House, Faculty of Pharmacy, Tehran University of Medical Sciences, Tehran, Iran. The animals were housed in a temperature-controlled environment ($25 \pm 3^{\circ}$C) on a 12 h light/dark cycle (lights on at 08:00 AM) and were provided with water and standard diet ad libitum. The rats did not fast before CLP surgery (Section 2.3.). All animals were acclimated to the laboratory environment for seven days before surgery. Experimental procedures were conducted according to the Institutional Animal Care and Use Committee (IACUC) guidelines and were approved by the Animal Ethics Committee of Tehran University of Medical Sciences, Tehran, Iran (Code: IR.TUMS.REC.1394.1837).

2.2. Study Design. Animals were randomly divided into six groups of five rats each. The first group was the sham group and received 5 mL normal saline (NS) as fluid resuscitation at 6 h and 24 h after sham surgery. CLP surgery was performed in all other groups. The second group (CLP group) received NS at 6 h and 24 h after surgery. The third group (DX group) received NS and dexamethasone (DX, 0.2 mg/kg) at 6 h and 24 h after surgery. The fourth group (βS group) received NS and βS (1 mg/kg) at 6 h and 24 h after surgery. The fifth group (IMI group) received NS and imipenem reconstituted in NS (IMI, 20 mg/kg) at 6 h, 24 h, 36 h, and 48 h after surgery. The sixth group (IMI+βS group) received NS, IMI (20 mg/kg), and βS (1 mg/kg) at 6 h, 24 h, 36 h, and 48 h after surgery. DX and IMI were obtained from 13Aban Pharmacy (Tehran, Iran), and βS was purchased from Zardband Company (Tehran, Iran), with 95.41% purity as assessed by high-performance liquid chromatography at 208 nm by the manufacturer (Zardband Company, Tehran, Iran). All animals in the sham, CLP, DX, and βS groups were euthanized 48 h after surgery, and those in the IMI and IMI+βS groups were euthanized 72 h after surgery by ketamine (160 mg/kg) and xylazine (20 mg/kg). Liver tissue was removed and washed thoroughly with cold-sterile phosphate-buffered saline (PBS) to remove blood residues. It was then snap-frozen in liquid nitrogen for real-time quantitative polymerase chain reaction (RT-qPCR).

2.3. CLP. The animals were anesthetized under aseptic conditions by intraperitoneal (i.p.) administration of ketamine

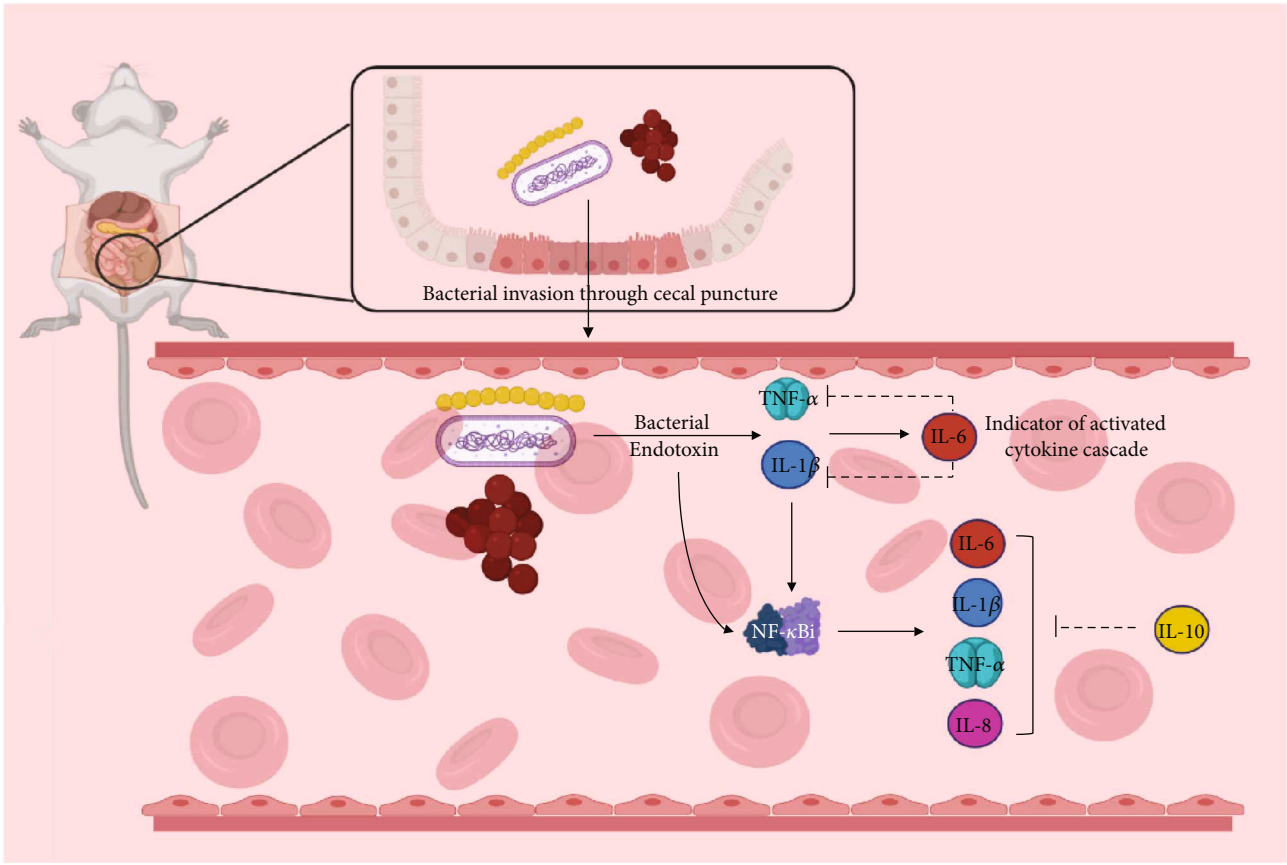

Figure 1: Cytokine cascade after CLP induction. Invasion of stimuli (bacterial endotoxin) to the blood is the trigger of cytokine cascade. An increase in the early proinflammatory elements (such as IL-1β and TNF-α) results in the production of other inflammatory factors such as NF-κB, IL-6, and anti-inflammatory cytokines such as IL-10. An uncontrolled cytokine cascade will lead to sepsis and, in severe cases, to septic shock. Tissue/organ dysfunction or end-organ damage might occur following progressive cytokine imbalance. CLP: cecal ligation and puncture; IL: interleukin; TNF: tumor necrosis factor.

(80 mg/kg) and xylazine (10 mg/kg). A 2 cm midline laparotomy was performed longitudinally and medially on the anterior abdomen. The distal 20% was ligated by 3.0 silk sutures below the ileocecal valve to make a closed-loop and was perforated two times with a sterile 21-gauge needle. The loop (cecum) was manually and gently squeezed to extrude fecal material from the punctures, and then placed back into the abdominal cavity. The peritoneum and skin were sutured in two layers. After surgery, all groups were resuscitated with 5 mL NS by subcutaneous injection. A thermoregulated heating pad and overhead heating lamp were used to maintain core body temperature (37°C). The sham group underwent surgery identical to CLP, with the exception that ligation and puncture procedures were not performed.

2.4. Bicinchoninic Acid Assay (BCA). Total amounts of serum and liver tissue protein were assayed using a BCA protein quantification kit (ParsTous, Tehran, Iran) according to the manufacturer's instructions. Briefly, one part of copper reagent was added to 50 parts of BCA reagent to prepare the working solution. The serial dilutions of bovine serum albumin (BSA) standard were used to prepare the standard curve. Standards and sample solutions were pipetted into wells. The working solution was added into all the wells. The wells were incubated for 60 minutes at 60°C. Optical density (OD) was measured at 562 nm using an enzyme-linked immunosorbent assay (ELISA) plate reader (BioTek, Winooski, VT, USA). The blank OD was subtracted from all standard and sample OD values. Each sample protein concentration was determined using the standard curve.

2.5. Assessment of Liver Damage. Serum levels of AST and ALT were determined using commercially available ELISA kits (Pars Azmoon Inc., Tehran, Iran) and according to the manufacturer's instructions. The serum ALT levels were measured based on two parallel reactions. Firstly, ALT transfers the amino group of alanine to α-ketoglutaric acid. The products of this reaction are pyruvate and glutamate. Then, lactate dehydrogenase converts pyruvate to lactate while oxidizing NADH to NAD^+. This oxidation results in a decrease in absorbance at 340 nm, and this reduction is proportional to the ALT level in the sample [18]. Relatively similar reactions were used to measure the serum AST levels. AST transfers the amino group of aspartate to α-ketoglutaric acid to form oxaloacetate and glutamate. Then, malate dehydrogenase changes oxaloacetate to malate while oxidizing NADH to NAD^+ [19]. The absorbance was measured using an ELISA plate reader (BioTek, Winooski, VT, USA).

2.6. GSH Content. GSH levels were determined using Ellman's reagent (4 mg DTNB [5,5′-dithiobis-(2-nitrobenzoic acid)] in 10 mL sodium citrate 10%) [20]. In brief, equal volumes of 10% trichloroacetic acid were added to liver homogenates. The mixtures were then vortexed and centrifuged at 15,000 g for 10 min at 4°C. Following centrifugation, 100 μL of the resulting supernatants was added to a 96-well microplate. Subsequently, 200 μL of Ellman's reagent was added to each well. The absorbance was measured at 412 nm using an ELISA plate reader (BioTek, Winooski, VT, USA).

2.7. Detection and Quantitation of Cytokines. Following euthanasia, blood samples were collected in sterile blood-collecting tubes by cardiac puncture and allowed to clot for 2 h at room temperature. Following the protocol, serum was removed and stored at ≤-20°C. All samples were centrifuged for 20 minutes at 1000 g. IL-1β, IL-6, and IL-10 concentrations were then measured using ELISA kits specific for rats (R&D Systems, Minneapolis, MN, USA). All reagents, standard dilutions, controls, and samples were prepared according to the manufacturer's instructions. 50 μL of assay diluent (specific for each cytokine) was added to each well. Then, 50 μL of standards, controls, or samples was added to each well. The plates were covered with an adhesive strip and incubated for 2 h at room temperature. The standards, controls, and samples were recorded on a plate layout. Each well was aspirated and washed five times by filling with wash buffer (400 μL). After removing any remaining wash buffer, the plates were inverted and blotted against clean paper towels. 100 μL of rat IL-1β, IL-6, or IL-10 was added to each well. The plates were covered with an adhesive strip and incubated for another 2 h at room temperature. Each well was aspirated and washed five times as previously described. 100 μL of substrate solution was added to each well and incubated at room temperature for 30 minutes away from light. For the last step, 100 μL of stop solution was added to each well, and after 30 minutes, the ODs were determined at 450 nm and 540 nm. The readings at 540 nm were subtracted from 450 nm to correct optical imperfections in the plates. Spectrophotometric readings were taken using the BioTek Synergy 4 microplate reader (BioTek, Winooski, VT, USA). Data obtained from ELISA were then normalized to the total protein in each serum sample, which was measured by the BCA method (Section 2.4).

2.8. Selection of Reference and Target Genes and Design. GAPDH has been shown to be a suitable reference gene for use in normalizing liver tissue gene expression values obtained through RT-qPCR [21]. DNA sequences of GAPDH and target genes were obtained from the GenBank database, and corresponding primer sequences (Table 1) were designed using Primer-BLAST from NCBI. The primers were designed in exon-exon junctions to minimize genomic DNA contamination.

Primers were synthesized at the highest quality (Sinaclon, Tehran, Iran), and primer specificity was confirmed by melt curve analysis. RT-qPCR products were evaluated by electrophoresis in a 2% agarose gel to confirm the quality of products.

2.9. RT-qPCR. The expression of TNF-α and NF-κBi mRNA was determined by RT-qPCR. RNA samples were extracted from liver tissue following the TriPure isolation reagent protocol (Roche, Basel, Switzerland). RNA OD was measured using Eppendorf BioPhotometer (Eppendorf, Hamburg, Germany). RNA extracts were then used as templates for cDNA synthesis. Considering obtained RNA OD values, cDNA synthesis was performed with the PrimeScript™ RT reagent kit (Takara Biotechnology, Shiga, Japan) according to the manufacturer's instructions, using 5 μL of RNA (corresponding to 1 μg), 10 μL of RT-premix, 1 μL of random hexamers, and 4 μL of DEPC-RNase/DNase-free water. The primer sequences used in this study are listed in Table 1. RT-qPCR was conducted using Applied Biosystems StepOnePlus (Thermo Fisher, Waltham, MA, USA) and the SYBR Premix Ex Taq™ II kit (Takara Biotechnology, Shiga, Japan). Reactions were prepared in a total volume of 10 μL, each containing 3 μL of template cDNA (corresponding to 1 μg RNA), 0.5 μL of each primer (forward and reverse with concentrations equal to 5 pmol/μL), 5 μL of SYBR Green master mix, 0.2 μL of ROX reference dye, and 0.8 μL of RNase/DNase-free sterile water. After 5 min of room temperature incubation, the cDNA synthesis cycle (42°C for 90 min, followed by 95°C for 10 min) was performed on an Applied BioSystems 96-well thermal cycler. PCR was conducted with an initial single heating cycle (95°C for 10 min) followed by 45 amplification cycles (95°C for 5 s, 60°C for 40 s). All samples were analyzed in a single analytical run (RT-qPCR reaction) to exclude any potential variation. Finally, for each primer pair, product specificity and the absence of primer dimer formation were confirmed using a dissociation protocol with a heat gradient ranging from 60°C to 95°C. In order to control DNA contamination, no-template control (NTC) reactions were included in each experiment. Reactions were performed three times for each gene, and the mean value was used for statistical analyses using Applied Biosystems StepOnePlus (Thermo Fisher, Waltham, MA, USA). GAPDH was used as the housekeeping gene. The expression levels of TNF-α and NF-κBi mRNA were normalized to that of GAPDH as an internal control. All data were then normalized to the sham group [22, 23].

2.10. Statistical Analysis. GraphPad Prism version 8 for Windows was used for statistical analysis. Data are presented as the mean ± standard deviation (SD). One-way analysis of variance (ANOVA) was used to compare the sham, CLP, DX, and βS groups 48 h postsurgery. Post hoc comparisons were made with Tukey's post hoc test. Unpaired t-test was used to compare the IMI and IMI+βS groups 72 h postsurgery. The Kaplan-Meier method was used to estimate survival rates at 48 h postsurgery, and the log-rank test was used to compare the study groups. Significance was defined as $p < 0.05$.

3. Results

3.1. Serum Levels of AST and ALT. AST and ALT are effective modalities and biomarkers of liver function. The CLP group demonstrated significantly higher levels of both AST and

Table 1: Reference and target genes and the corresponding primers used in RT-qPCR.

Symbol	Gene name	Mechanism	GenBank ID	Primer sequences	Amplicon length (bp)
GAPDH	Glyceraldehyde-3-phosphate dehydrogenase	Glycolytic enzyme	NM 017008	FP: 5′-AGTGCCAGCCTCGTCTCATA-3′ RP: 5′-GGTAACCAGGCGTCCGATA-3′	77
TNF-α	Tumor necrosis factor-alpha	Proinflammatory cytokine	NM 012675	FP: 5′-TGGGCTCCCTCTCATCAGTT-3′ RP: 5′-CTTGGTGGTTTGCTACGACG-3′	104
NF-κBi	Nuclear factor kappa B inhibitor-alpha	Inhibitory enzyme	NM001105720	FP: 5′-GTGACTTTGGGTGCTGATGT-3′ RP: 5′-ACACTTCAACAGGAGCGAGA-3′	111

bp: base pair; FP: forward primer; RP: reverse primer.

ALT ($p < 0.0001$) in comparison to the sham group (Figures 2(a) and 2(b)). Both AST and ALT levels were markedly lower in groups that were treated with either DX or βS ($p < 0.0001$). ALT level was lower in the βS group than in the DX group; however, the difference was not statistically significant. The addition of βS to IMI (IMI+βS) resulted in markedly lower levels of AST and ALT compared with IMI-only treatment ($p < 0.001$ and $p < 0.0001$, respectively).

3.2. GSH Content of Liver Tissue. GSH is a pivotal antioxidant that acts as a scavenger of reactive oxygen species (ROS). GSH content was assessed as an indicator of oxidative stress. Significant depletion of GSH was observed in the CLP group compared to the sham group ($p < 0.0001$, Figure 2(c)). GSH content was higher in the DX- and βS-treated groups compared to the CLP group ($p < 0.001$ and $p < 0.0001$, respectively). GSH level was higher in βS-treated rats compared with the DX group ($p < 0.01$). Moreover, the addition of βS to IMI (IMI+βS group) resulted in significantly higher levels of GSH ($p < 0.05$).

3.3. Serum Concentrations of IL-1β, IL-6, and IL-10. Rats in the CLP group had remarkably higher serum levels of IL-1β, IL-6, and IL-10 compared with the sham group ($p < 0.0001$). Treatment with βS resulted in considerably lower levels of these cytokines compared with the CLP group (IL-1β, $p < 0.0001$; IL-6, $p < 0.0001$; and IL-10, $p < 0.0001$) (Figure 3). DX-treated rats showed lower levels of IL-1β and IL-6 compared with the CLP group ($p < 0.0001$ and $p < 0.05$, respectively). βS treatment resulted in considerably lower serum IL-6 levels as compared with DX treatment ($p < 0.01$). Although the differences in the levels of IL-1β and IL-6 between the IMI and IMI+βS groups were not statistically significant ($p > 0.05$), IL-10 levels were significantly lower in IMI+βS compared with the IMI group ($p < 0.001$).

3.4. Liver Expression of TNF-α and NF-κBi. Liver levels of TNF-α and NF-κBi mRNAs were determined by RT-qPCR. Higher concentrations of TNF-α and NF-κBi mRNAs were observed in the CLP group (Figure 4; data are presented relative to the sham group). Treatment with DX ($p < 0.0001$) and βS ($p < 0.0001$) resulted in remarkably lower TNF-α expression levels compared with the CLP group (Figure 4(a)). IMI+βS treatment led to lower levels of TNF-α mRNA compared with the IMI group, but the difference was not statistically significant. DX ($p < 0.0001$) and βS ($p < 0.0001$) treatments resulted in significantly lower levels of NF-κBi mRNA compared with the CLP group, and interestingly, the addition of βS to IMI led to significantly lower levels of NF-κBi mRNA ($p < 0.05$) compared with IMI-only treatment (Figure 4(b)).

3.5. Survival Rates. Survival rates were compared using the Kaplan-Meier method (Figure 5). The survival rates were 60% (3/5 rats) in the CLP group and 80% (4/5 rats) in the DX and IMI groups by day two. Survival rates in the sham, βS, and IMI+βS groups were 100% 48 h after surgery. According to the log-rank (Mantel-Cox) test, the survival curves were not significantly different between groups ($p > 0.05$).

4. Discussion

Inflammatory responses are believed to play a critical role in the underlying mechanisms of inflammatory diseases like sepsis. Hence, a combination of anti-inflammatory drugs and antibiotics is recommended to improve sepsis severity and prognosis [24]. Here, IMI was used as the antibiotic agent, as it has a broad-spectrum antibacterial activity [25, 26]. DX, a glucocorticoid drug that is widely used for sepsis patients, was also considered [24]. The physiological roles of phytosterols in the inflammatory processes have yet to be elucidated. Therefore, in the present study, we aimed to evaluate the association between βS administration and inflammatory cytokines by conducting an in vivo research using the gold standard method of sepsis induction, CLP.

Our study provides considerable insight into the anti-inflammatory properties of βS. We observed lower levels of IL-1β, IL-6, and IL-10 serum levels in the βS-treated group compared with the CLP group. Although adding βS to IMI treatment did not significantly alter IL-1β and IL-6 levels, it resulted in a remarkable decrease in IL-10 serum level compared with IMI alone, suggesting that βS might help to control the inflammation caused by cytokine cascade via modulation of anti-inflammatory cytokines. Furthermore, βS treatment caused a significantly greater reduction in IL-6 level compared with DX. Glucocorticoids such as DX are proven anti-inflammatory agents in sepsis management. Glucocorticoid therapy interferes with the production of

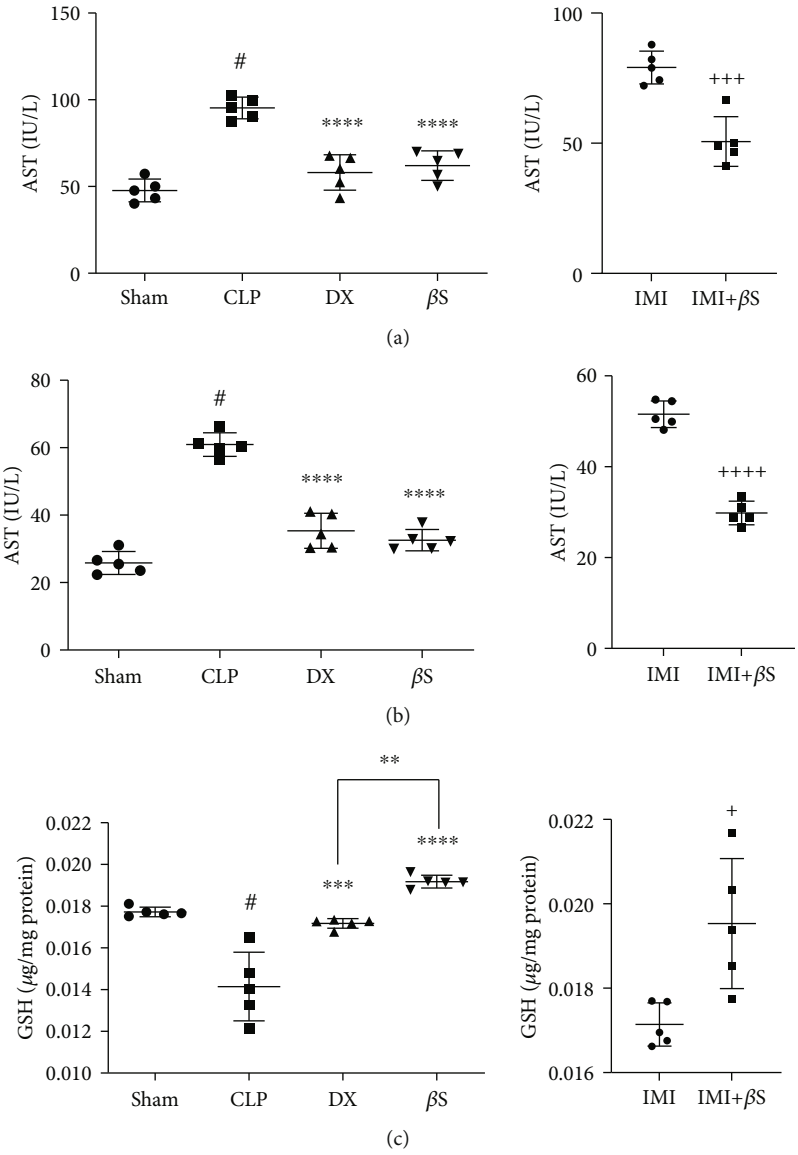

Figure 2: Measurement of AST (a) and ALT (b) serum levels and GSH content of liver tissue (c) using ELISA ($n = 5$/group). Measurements were performed 48 h after surgery in the sham, CLP, DX, and βS groups, and 72 h after surgery in the IMI and IMI+βS groups. All data are expressed as the mean ± SD. Data were analyzed by ANOVA, followed by Tukey's post hoc test for sham, CLP, DX, and βS comparison. The IMI and IMI+βS groups were analyzed separately using unpaired t-test. $^{\#}$Significant difference compared with the sham group ($p < 0.0001$). **Significant difference compared with the DX group ($p < 0.01$). ***Significant difference compared with the CLP group ($p < 0.001$). ****Significant difference compared with the CLP group ($p < 0.0001$). $^{+}$Significant difference compared with the IMI group ($p < 0.05$). $^{+++}$Significant difference compared with the IMI group ($p < 0.001$). $^{++++}$Significant difference compared with the IMI group ($p < 0.0001$). βS: β-sitosterol; CLP: cecal ligation and puncture; DX: dexamethasone; IMI: imipenem.

various proinflammatory cytokines such as IL-6. Schmidt et al. [27] reported that DX administration decreased IL-6 production in a CLP-induced sepsis study. Given this context, the statistically distinct reduction of IL-6 by βS supports the potential usefulness of βS in sepsis-induced inflammation. Our observations on the effects of βS on inflammatory cytokines are in agreement with several other studies. One recent study suggested a negative correlation between βS and IL-6 levels in an animal model of obesity-related chronic inflammation [28]. Another study revealed a decrease in IL-1β levels in murine-activated neutrophils following βS therapy [29]. However, our data on the effects of βS on serum levels of IL-6 and IL-10 is not in agreement with a study conducted by Alappat et al. [30] on the immune function of macrophages. Their findings demonstrated higher serum concentrations of IL-6 and IL-10 in the βS group compared with the sham group. These contradictory results might be due to different dosages, times of sampling, and the type of experimental study (i.e., *in vitro* vs. *in vivo*). Although IL-10 is an anti-inflammatory mediator

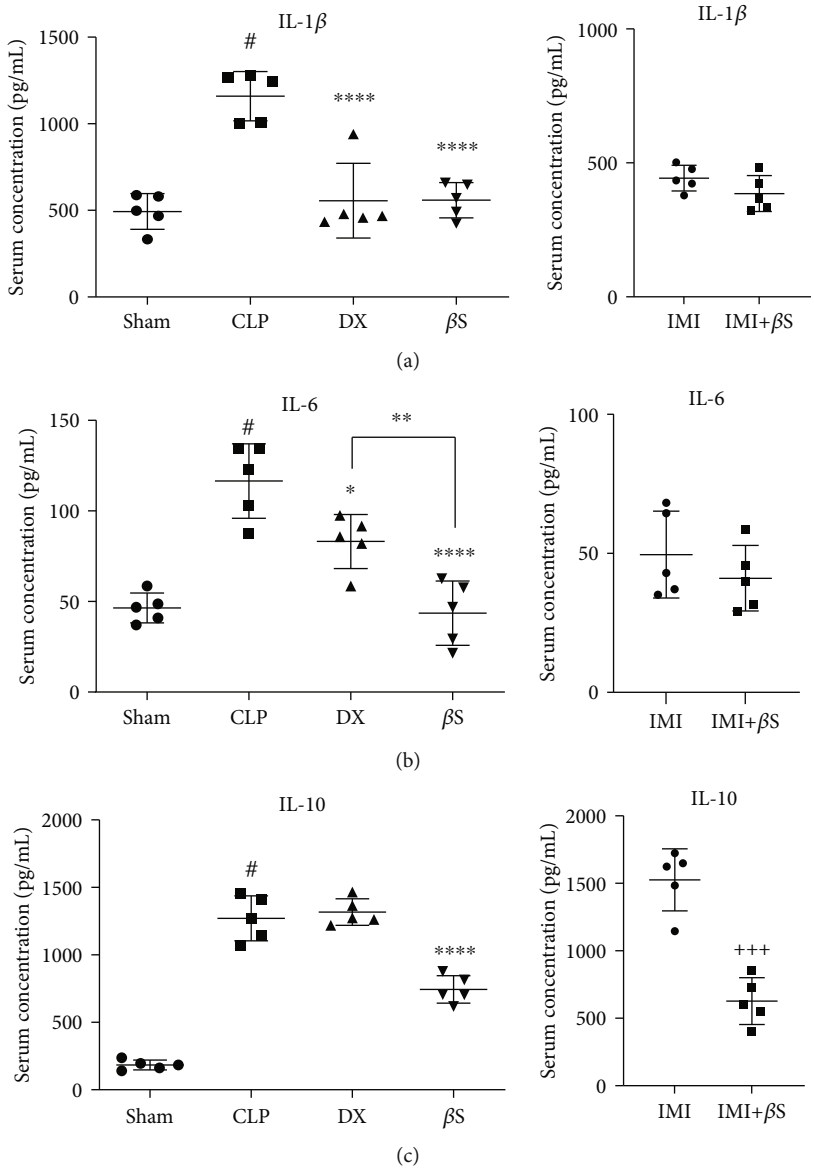

FIGURE 3: Measurement of IL-1β (a), IL-6 (b), and IL-10 (c) serum levels using ELISA ($n = 5$/group). Measurements were performed 48 h after surgery in the sham, CLP, DX, and βS groups, and 72 h after surgery in the IMI and IMI+βS groups. All data are normalized to the total protein levels measured by BCA assay (mean ± SD of 0.205 ± 0.0001, 0.205 ± 0.0001, 0.204 ± 0.0001, 0.204 ± 0.0001, 0.204 ± 0.0001, and 0.205 ± 0.0003 pg/mL in the sham, CLP, DX, βS, IMI, and IMI+βS groups, respectively), and expressed as the mean ± SD. Data were analyzed by ANOVA, followed by Tukey's post hoc test for sham, CLP, DX, and βS comparison. The IMI and IMI+βS groups were analyzed separately using unpaired t-test. $^{\#}$Significant difference compared with the sham group ($p < 0.0001$). *Significant difference compared with the CLP group ($p < 0.05$). **Significant difference compared with the DX group ($p < 0.01$). ****Significant difference compared with the CLP group ($p < 0.0001$). $^{+++}$Significant difference compared with the IMI group ($p < 0.001$). βS: β-sitosterol; CLP: cecal ligation and puncture; DX: dexamethasone; IMI: imipenem.

and could potentially suppress the cytokine cascade, the higher levels may lead to organ dysfunction, as previously confirmed by other studies [31, 32].

Rats treated with βS showed lower expression levels of TNF-α mRNA and NF-κBi mRNA in the liver compared with the CLP group, which is in line with the IL-1β and IL-6 lower levels in serum samples. βS also exerts beneficial effects on the cytokine cascade by targeting NF-κB. The inhibition of NF-κB by βS has been extensively investigated, with published findings that are in line with our data [13, 33, 34]. The immunoblot and confocal analyses of lipopolysaccharide- (LPS-) stimulated intestinal and peritoneal mouse macrophages by Kim et al. [33] showed that βS inhibits the phosphorylation and nuclear translocation of the p65 subunit of NF-κB. Similarly, ImageStream cytometry analysis by Valerio and Awad [34] showed that 24 h treatment of mouse macrophages with 4 μM βS and stimulation with LPS for the last 6 h resulted in 45% lower

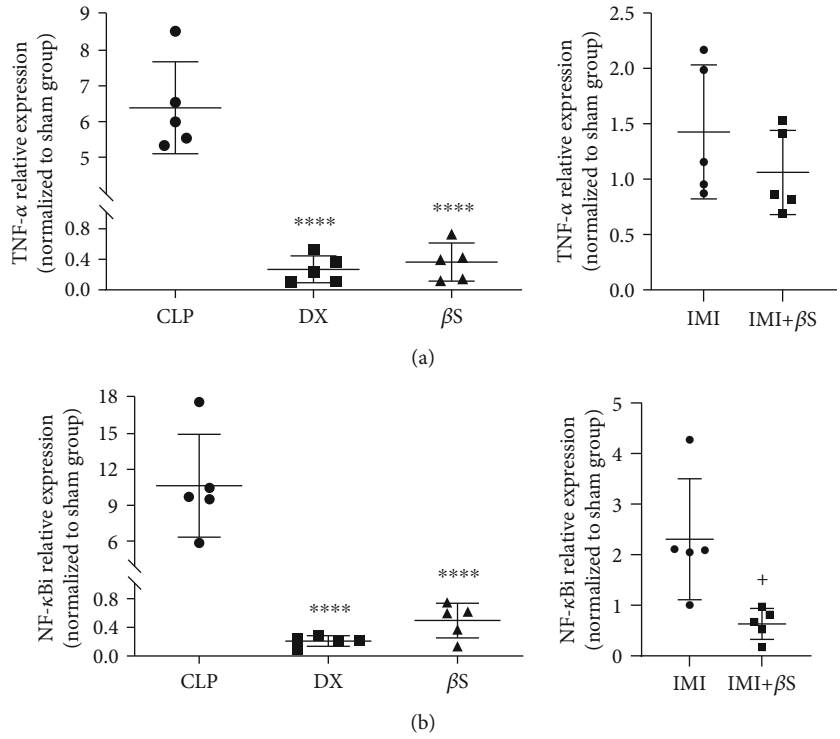

Figure 4: mRNA expression of TNF-α and NF-κBi in liver tissue. TNF-α and NF-κBi mRNA expression was assessed using predeveloped assays for RT-qPCR. Values were calculated using a comparative CT method ($2^{-\Delta\Delta CT}$) according to the manufacturer's instructions. GAPDH was used as an internal control gene. Data are presented as the mean ± SD normalized to the sham group. Statistical analysis was performed using one-way ANOVA and Tukey's multiple comparisons test for sham, CLP, DX, and βS comparison. The IMI and IMI+βS groups were analyzed separately using unpaired t-test. ****Significant difference compared with the CLP group ($p < 0.0001$). $^{+}$Significant difference compared with the IMI group ($p < 0.05$). βS: β-sitosterol; CLP: cecal ligation and puncture; DX: dexamethasone; IMI: imipenem.

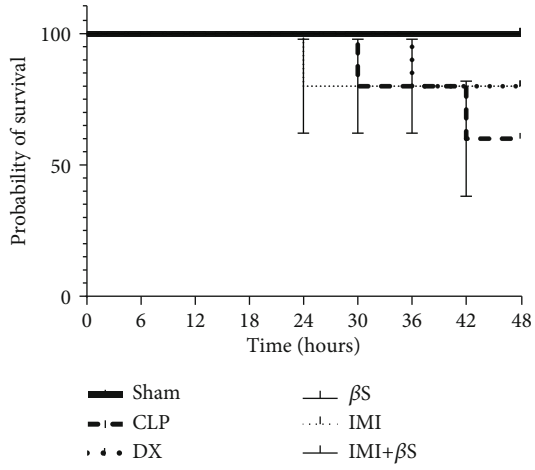

Figure 5: Survival rates over the 48 h period after surgery (observations every 6 h). There was no statistically significant difference in survival rates between the study groups ($p > 0.05$). βS: β-sitosterol; CLP: cecal ligation and puncture; DX: dexamethasone; IMI: imipenem.

translocation of NF-κB to the nucleus compared to the LPS alone. The stabilization of NF-κBi mRNA by βS is believed to be the mechanism underlying TNF-α downregulation, reducing its phosphorylation, and consecutively depleting the nuclear NF-κB complex [35]. The most striking result that emerges from our data is that the administration of βS and DX both resulted in significantly lower levels of TNF-α and NF-κBi mRNA expression compared to the CLP group ($p < 0.0001$), and the level of expression was the same between the βS and DX groups as confirmed by Tukey's multiple comparisons test ($p > 0.05$). This further supports that βS could be considered as an effective intervention for controlling sepsis-induced inflammation.

Liver injury is common among sepsis patients. The incidence of liver dysfunction varies in different studies from 34% to 46% [36]. Along with the sepsis-associated liver injury, other liver injuries such as diseases caused by hepatitis B and C viruses, alcoholic liver disease, nonalcoholic fatty liver disease, and drug-induced injuries are also common among sepsis patients [37]. Elevation of serum AST and ALT and reduction of liver GSH are signs of liver malfunction [3]. In our experiment, compared with the sham group, CLP rats had significantly higher levels of AST and ALT. These levels were markedly lower in the βS-treated rats. Similarly, compared with the sham group, liver GSH content was significantly lower in the CLP group, and βS treatment restored the GSH content. Furthermore, the level of GSH in the βS group was significantly greater than that in the DX group. The addition of βS to IMI (IMI+βS group) also resulted in significantly lower levels of ALT and significantly

higher levels of liver GSH content compared to the IMI-only group. These results suggest that βS could provide advantageous effects on liver function and also demonstrate its possible antioxidant activity. Our data confirm the results provided by Wong et al. [38], which demonstrated the favorable effects of βS against carbon tetrachloride-induced hepatotoxicity with significant improvements in AST, ALT, and GSH levels. Liver dysfunction during sepsis is associated with an increased risk of multiple organ failure and death. Mortality occurs in up to 68% of sepsis patients with liver dysfunction [36]. Data from our study, showing reduced serum levels of AST and ALT, suggest that βS may improve liver function in sepsis. Redox imbalance and severe oxidative stress occur in critically ill sepsis patients and can cause multiple organ failure [39, 40]. Glutathione is the primary antioxidant in cells, meaning that the lower the glutathione content, the greater the risk of organ failure becomes [41]. Thus, increased liver GSH content with βS treatment indicates that it may improve prognosis and limit liver dysfunction in sepsis.

We additionally investigated the survival rates over the 48 h period after treatment (observed every 6 h). CLP-induced rats exhibited 60% survival. All animals in the sham, βS, and IMI+βS groups survived up to 48 h, while the IMI and DX groups had a lower survival rate of 80%. Based on the Kaplan-Meier curves, these differences in survival rates were not statistically significant. Our data do not allow drawing any clear conclusions about the impact of βS on survival rate.

Doğan et al. [42] evaluated the antibacterial effects of different steroid substances. While they did not find any significant antibacterial activity for progesterone, estrone, and stigmasterol, they reported that βS inhibits the growth of *Staphylococcus aureus* with a minimum inhibitory concentration (MIC) value of 32 μg/mL. In another study by Sen et al. [43], the antibacterial activity of βS was examined using the agar disk diffusion method. βS was found to be effective against *Escherichia coli*, *Pseudomonas aeruginosa*, *Staphylococcus aureus*, and *Klebsiella pneumoniae*. They reported that the antibacterial activity of βS (20 μg/mL) was almost equivalent to that of gentamicin (20 μg/mL). Similarly, Burčová et al. [44] demonstrated the bacteriostatic effects of βS on *Escherichia coli*, *Bacillus cereus*, *Pseudomonas aeruginosa*, *Bacillus subtilis*, and *Listeria monocytogenes*. A wide range of bacteria were affected by βS in these studies, and this can potentially provide additional benefits for sepsis patients. More pharmacokinetic and pharmacodynamic studies are required to fully evaluate the antibacterial properties of βS in sepsis.

Here, we demonstrated the beneficial impacts of βS administration on inflammatory responses and liver function tests in septic rats. By dampening the hyperinflammatory damage, βS may provide some benefits in diseases with molecular patterns similar to sepsis, such as the coronavirus disease 2019 (COVID-19). It has been demonstrated that the extensive release of inflammatory mediators such as TNF-α, IL-6, and IL-10 is associated with increased mortality risk in COVID-19 patients [45]. Moreover, this cytokine storm may lead to liver dysfunction in these patients as elevated AST/ALT levels are widely reported in the literature [46]. The potential benefits of βS supplementation in COVID-19 could be investigated in future research. The disturbance of immune cells, including a drastic depletion of CD4 and CD8 lymphocytes, occurs in sepsis patients [47]. The evaluation of the effects of βS on the status of immune cells is warranted in future studies.

5. Conclusions

Overproduction of proinflammatory cytokines contributes to high mortality rates in sepsis patients. In our study, we observed that treatment with βS at a dose of 1 mg/kg for two days results in a significant reduction of proinflammatory cytokines in the sera of CLP-induced septic rats. Liver expression of TNF-α and NF-κBi was also reduced in rats treated with βS. Similarly, the addition of βS to IMI led to an improvement in the serum and liver inflammatory markers compared to IMI alone at three days after sepsis induction. We concluded that βS has noticeable potential for consideration as an anti-inflammatory supplement in hyperinflammatory conditions such as sepsis. Our findings would seem to suggest that βS targets NF-κB as a major regulator of cytokine cascade and inhibits inflammatory response to a great extent. Liver dysfunction is common among sepsis patients and is associated with a poor prognosis. Here, we found that βS treatment effectively lowered the levels of serum biomarkers of liver dysfunction (AST and ALT) and increased the liver GSH content in septic rats. Thus, βS could alleviate liver oxidative stress and could inhibit possible organ dysfunction. The results so far are encouraging and promising, and this could eventually lead to a better understanding of the beneficial effects of βS against hyperinflammation. Future research should provide further insight into the potential use of βS in sepsis and similar clinical conditions with systemic inflammation.

Data Availability

The data supporting the conclusions of this study are available from the corresponding author upon request.

Conflicts of Interest

The authors declare that there is no conflict of interest regarding the publication of this article.

Acknowledgments

This study was supported by a grant from the Vice Chancellor for Research, Tehran University of Medical Sciences, Tehran, Iran (grant no. 30955).

References

[1] WHO, "Sepsis: World Health Organization," https://www.who.int/news-room/fact-sheets/detail/sepsis.

[2] W. Schulte, J. Bernhagen, and R. Bucala, "Cytokines in sepsis: potent immunoregulators and potential therapeutic

targets—an updated view," *Mediators of Inflammation*, vol. 2013, 16 pages, 2013.

[3] D. Wang, Y. Yin, and Y. Yao, "Advances in sepsis-associated liver dysfunction," *Burns & Trauma.*, vol. 2, no. 3, pp. 97–105, 2014.

[4] T. Blackwell and J. Christman, "Sepsis and cytokines: current status," *British Journal of Anaesthesia*, vol. 77, no. 1, pp. 110–117, 1996.

[5] A. A. Shalmani, M. H. Ghahremani, F. Jeivad et al., "Monomethyl fumarate alleviates sepsis-induced hepatic dysfunction by regulating TLR-4/NF-κB signalling pathway," *Life Sciences*, vol. 215, pp. 152–158, 2018.

[6] J. M. Prince, R. M. Levy, R. Yang et al., "Toll-like receptor-4 signaling mediates hepatic injury and systemic inflammation in hemorrhagic shock," *Journal of the American College of Surgeons*, vol. 202, no. 3, pp. 407–417, 2006.

[7] P. DAMA, D. LEDOUX, M. NYS et al., "Cytokine serum level during severe sepsis in human IL-6 as a marker of severity," *Annals of Surgery*, vol. 215, no. 4, pp. 356–362, 1992.

[8] E. Girardin, G. E. Grau, J.-M. Dayer, and P. Roux-Lombard, "Tumor necrosis factor and interleuktn-1 in the serum of children with severe infectious purpura," *New England Journal of Medicine*, vol. 319, no. 7, pp. 397–400, 1988.

[9] B. Derkx, A. Marchant, M. Goldman, R. Bijlmer, and S. van Deventer, "High levels of interleukin-10 during the initial phase of fulminant meningococcal septic shock," *Journal of Infectious Diseases*, vol. 171, no. 1, pp. 229–232, 1995.

[10] J. Gomez-Jimenez, M. Martin, R. Sauri et al., "Interleukin-10 and the monocyte/macrophage-induced inflammatory response in septic shock," *Journal of Infectious Diseases*, vol. 171, no. 2, pp. 472–475, 1995.

[11] G. S. El-Tanbouly, M. S. El-Awady, N. A. Megahed, H. A. Salem, and H. A. El-Kashef, "The NF-κB inhibitor celastrol attenuates acute hepatic dysfunction induced by cecal ligation and puncture in rats," *Environmental Toxicology and Pharmacology*, vol. 50, pp. 175–182, 2017.

[12] R. E. Ostlund Jr., "Phytosterols in human nutrition," *Annual Review of Nutrition*, vol. 22, no. 1, pp. 533–549, 2002.

[13] S. Loizou, I. Lekakis, G. P. Chrousos, and P. Moutsatsou, "β-Sitosterol exhibits anti-inflammatory activity in human aortic endothelial cells," *Molecular Nutrition & Food Research*, vol. 54, no. 4, pp. 551–558, 2010.

[14] P. Bouic and J. H. Lamprecht, "Plant sterols and sterolins: a review of their immune-modulating properties," *Alternative Medicine Review*, vol. 4, no. 3, pp. 170–177, 1999.

[15] L. Fraile, E. Crisci, L. Córdoba, M. A. Navarro, J. Osada, and M. Montoya, "Immunomodulatory properties of beta-sitosterol in pig immune responses," *International Immunopharmacology*, vol. 13, no. 3, pp. 316–321, 2012.

[16] J. M. Prieto, M. C. Recio, and R. M. Giner, "Anti-inflammatory activity of β-sitosterol in a model of oxazoloneinduced contact-delayed-type hypersensitivity," *Boletin Latinoamericano y del Caribe de Plantas Medicinales y Aromaticas*, vol. 5, no. 3, pp. 57–62, 2006.

[17] J. E. Yuk, J. S. Woo, C.-Y. Yun et al., "Effects of lactose-β-sitosterol and β-sitosterol on ovalbumin-induced lung inflammation in actively sensitized mice," *International Immunopharmacology*, vol. 7, no. 12, pp. 1517–1527, 2007.

[18] A. Farahnak, F. Amni, T. Golmohammadi, M. R. Eshraghian, and M. B. Molaei Rad, "The effect of triclabendazole on ALT enzyme activity in Fasciola hepatica helminths and parasitized sheep liver tissues," *Journal of Medical Microbiology and Infectious Diseases.*, vol. 3, no. 1, pp. 1–5, 2015.

[19] X.-J. Huang, Y.-K. Choi, H.-S. Im, O. Yarimaga, E. Yoon, and H.-S. Kim, "Aspartate aminotransferase (AST/GOT) and alanine aminotransferase (ALT/GPT) detection techniques," *Sensors*, vol. 6, no. 7, pp. 756–782, 2006.

[20] M. R. Sepand, M. H. Ghahremani, K. Razavi-Azarkhiavi et al., "Ellagic acid confers protection against gentamicin-induced oxidative damage, mitochondrial dysfunction and apoptosis-related nephrotoxicity," *Journal of Pharmacy and Pharmacology*, vol. 68, no. 9, pp. 1222–1232, 2016.

[21] A. Radonić, S. Thulke, I. M. Mackay, O. Landt, W. Siegert, and A. Nitsche, "Guideline to reference gene selection for quantitative real-time PCR," *Biochemical and Biophysical Research Communications*, vol. 313, no. 4, pp. 856–862, 2004.

[22] A. J. Siddiqui, J. Bhardwaj, and S. K. Puri, "mRNA expression of cytokines and its impact on outcomes after infection with lethal and nonlethal Plasmodium vinckei parasites," *Parasitology Research*, vol. 110, no. 4, pp. 1517–1524, 2012.

[23] A. J. Siddiqui, J. Bhardwaj, M. Goyal et al., "Immune responses in liver and spleen against Plasmodium yoelii pre-erythrocytic stages in Swiss mice model," *Journal of Advanced Research*, vol. 24, pp. 29–41, 2020.

[24] I. Martin-Loeches, M. M. Levy, and A. Artigas, "Management of severe sepsis: advances, challenges, and current status," *Drug Design, Development and Therapy*, vol. 9, p. 2079, 2015.

[25] K. C. Doerschug, L. S. Powers, M. M. Monick, P. S. Thorne, and G. W. Hunninghake, "Antibiotics delay but do not prevent bacteremia and lung injury in murine sepsis," *Critical Care Medicine*, vol. 32, no. 2, pp. 489–494, 2004.

[26] V. T. Enoh, C. Y. Lin, T. K. Varma, and E. R. Sherwood, "Differential effect of imipenem treatment on injury caused by cecal ligation and puncture in wild-type and NK cell-deficient β2-microgloblin knockout mice," *American Journal of Physiology. Gastrointestinal and Liver Physiology*, vol. 290, no. 2, pp. G277–G284, 2006.

[27] C. Schmidt, B. Kurt, K. Höcherl, and M. Bucher, "Inhibition of NF-κB activity prevents downregulation of α1-adrenergic receptors and circulatory failure during CLP-induced sepsis," *Shock*, vol. 32, no. 3, pp. 239–246, 2009.

[28] M. Kurano, K. Hasegawa, M. Kunimi et al., "Sitosterol prevents obesity-related chronic inflammation," *Molecular and Cell Biology of Lipids*, vol. 1863, no. 2, pp. 191–198, 2018.

[29] R. Liz, L. Zanatta, G. O. dos Reis et al., "Acute effect of β-sitosterol on calcium uptake mediates anti-inflammatory effect in murine activated neutrophils," *Journal of Pharmacy and Pharmacology*, vol. 65, no. 1, pp. 115–122, 2012.

[30] L. Alappat, M. Valerio, and A. B. Awad, "Effect of vitamin D and β-sitosterol on immune function of macrophages," *International Immunopharmacology*, vol. 10, no. 11, pp. 1390–1396, 2010.

[31] G. Monneret, M.-E. Finck, F. Venet et al., "The anti-inflammatory response dominates after septic shock: association of low monocyte HLA-DR expression and high interleukin-10 concentration," *Immunology Letters*, vol. 95, no. 2, pp. 193–198, 2004.

[32] C. Wunder, O. Eichelbrönner, and N. Roewer, "Are IL-6, IL-10 and PCT plasma concentrations reliable for outcome prediction in severe sepsis? A comparison with APACHE III and

SAPS II," *Inflammation Research*, vol. 53, no. 4, pp. 158–163, 2004.

[33] K. A. Kim, I. A. Lee, W. Gu, S. R. Hyam, and D. H. Kim, "β-Sitosterol attenuates high-fat diet-induced intestinal inflammation in mice by inhibiting the binding of lipopolysaccharide to Toll-like receptor 4 in the NF-κB pathway," *Molecular Nutrition & Food Research*, vol. 58, no. 5, pp. 963–972, 2014.

[34] M. Valerio and A. B. Awad, "β-Sitosterol down-regulates some pro-inflammatory signal transduction pathways by increasing the activity of tyrosine phosphatase SHP-1 in J774A. 1 murine macrophages," *International Immunopharmacology*, vol. 11, no. 8, pp. 1012–1017, 2011.

[35] A. Wullaert, K. Heyninck, and R. Beyaert, "Mechanisms of crosstalk between TNF-induced NF-κB and JNK activation in hepatocytes," *Biochemical Pharmacology*, vol. 72, no. 9, pp. 1090–1101, 2006.

[36] J. Yan, S. Li, and S. Li, "The role of the liver in sepsis," *International Reviews of Immunology*, vol. 33, no. 6, pp. 498–510, 2014.

[37] H. Kobashi, J. Toshimori, and K. Yamamoto, "Sepsis-associated liver injury: incidence, classification and the clinical significance," *Hepatology Research*, vol. 43, no. 3, pp. 255–266, 2013.

[38] H. S. Wong, J. H. Chen, P. K. Leong, H. Y. Leung, W. M. Chan, and K. M. Ko, "β-Sitosterol protects against carbon tetrachloride hepatotoxicity but not gentamicin nephrotoxicity in rats via the induction of mitochondrial glutathione redox cycling," *Molecules*, vol. 19, no. 11, pp. 17649–17662, 2014.

[39] K. Mantzarlis, V. Tsolaki, and E. Zakynthinos, "Role of oxidative stress and mitochondrial dysfunction in sepsis and potential therapies," *Oxidative Medicine and Cellular Longevity*, vol. 2017, 10 pages, 2017.

[40] C. Goodyear-Bruch and J. D. Pierce, "Oxidative stress in critically ill patients," *American Journal of Critical Care*, vol. 11, no. 6, pp. 543–551, 2002.

[41] G. Biolo, R. Antonione, and M. De Cicco, "Glutathione metabolism in sepsis," *Critical Care Medicine*, vol. 35, Suppl, pp. S591–S595, 2007.

[42] A. DOĞAN, S. OTLU, Ö. ÇELEBİ et al., "An investigation of antibacterial effects of steroids," *Turkish Journal of Veterinary and Animal Sciences*, vol. 41, no. 2, pp. 302–305, 2017.

[43] A. Sen, P. Dhavan, K. K. Shukla, S. Singh, and G. Tejovathi, "Analysis of IR, NMR and antimicrobial activity of β-sitosterol isolated from Momordica charantia," *Sci Secure J Biotechnol*, vol. 1, no. 1, pp. 9–13, 2012.

[44] Z. Burčová, F. Kreps, M. Greifová et al., "Antibacterial and antifungal activity of phytosterols and methyl dehydroabietate of Norway spruce bark extracts," *Journal of Biotechnology*, vol. 282, pp. 18–24, 2018.

[45] G. Chen, D. Wu, W. Guo et al., "Clinical and immunological features of severe and moderate coronavirus disease 2019," *The Journal of Clinical Investigation.*, vol. 130, no. 5, pp. 2620–2629, 2020.

[46] N. A. Fierro, "COVID-19 and the liver: what do we know after six months of the pandemic?," *Annals of Hepatology*, vol. 19, no. 6, pp. 590-591, 2020.

[47] R. de Pablo, J. Monserrat, A. Prieto, and M. Alvarez-Mon, "Role of circulating lymphocytes in patients with sepsis," *BioMed Research International*, vol. 2014, 11 pages, 2014.

Hindawi
BioMed Research International
Volume 2021, Article ID 5516940, 7 pages
https://doi.org/10.1155/2021/5516940

Review Article

Interleukin-27 as a Diagnostic Biomarker for Patients with Sepsis: A Meta-Analysis

Ying Wang[1], **Jingyi Zhao**[2], **Yinhui Yao**[1], **Dan Zhao**[3] **and Shiquan Liu**[4]

[1]*Department of Pharmacy, The Affiliated Hospital of Chengde Medical College, Chengde 067000, China*
[2]*Department of Functional Center, Chengde Medical College, Chengde 067000, China*
[3]*Department of Intensive Care Unit, The Affiliated Hospital of Chengde Medical College, Chengde 067000, China*
[4]*Department of Thoracic Surgery, The Affiliated Hospital of Chengde Medical College, Chengde 067000, China*

Correspondence should be addressed to Yinhui Yao; yaoyh_gc@163.com

Received 17 February 2021; Revised 13 March 2021; Accepted 29 March 2021; Published 14 April 2021

Academic Editor: Vijay Kumar Srivastava

Background. The present study was aimed to investigate the value of blood interleukin-27 (IL-27) as a diagnostic biomarker of sepsis. *Methods*. We searched PubMed, EMBASE, the Cochrane Library, and the reference lists of relevant articles. All studies published up to October 21, 2020, which evaluated the accuracy of IL-27 levels for the diagnosis of sepsis were included. All the selected papers were assessed using the Quality Assessment of Diagnostic Accuracy Studies-2 (QUADAS-2). We used a bivariate random effects model to estimate sensitivity, specificity, diagnostic odds ratios (DOR), and a summary receiver operating characteristic curve (SROC). Deeks' funnel plot was used to illustrate the potential presence of publication bias. *Results*. This meta-analysis included seven articles. The pooled sensitivity, specificity, and DOR were 0.85 (95% CI, 0.72-0.93), 0.72 (95% CI, 0.42-0.90), and 15 (95% CI, 3-72), respectively. The area under the summary receiver operating characteristic curve was 0.88 (95% CI, 0.84-0.90). The pooled I^2 statistic was 96.05 for the sensitivity and 96.65 for the specificity in the heterogeneity analysis. Deeks' funnel plot indicated no publication bias in this meta-analysis ($P = 0.07$). *Conclusions*. The present results showed that IL-27 is a reliable diagnostic biomarker of sepsis, but it should be investigated in combination with other clinical tests and results.

1. Introduction

Sepsis is a severe complication of severe infection, severe trauma, burns, shock, and surgery, and it can lead to septic shock and multiple organ dysfunction syndromes (MODS) [1, 2]. Currently, sepsis poses a significant public health effect in all parts of the world as it is associated with high morbidity and mortality. The morbidity rate in patients with sepsis is 29.5% in the hospital and 47% in the intensive care unit (ICU), and the mortality rate in patients with sepsis is 25.8% in the ICU and 35.3% in the hospital [3, 4]. When shock is present, the rates can increase to 40%~50% [5, 6]. Presently, the gold standard in diagnosing sepsis is microbiologic cultures, in spite of this is a delay between the clinical manifestations and the results from such cultures. As a result, patients do not receive timely antibacterial treatment, often leading to unfavorable outcomes [7–9]. Therefore, diagnostic biomarkers that can indicate a diagnosis of sepsis before the microbiological cultures are complete are needed.

Among the current diagnostic biomarkers used for sepsis, procalcitonin (PCT) is the most common. Several meta-analyses of the utility of PCT in diagnosing infection and sepsis have been performed. However, the usefulness of PCT is variable, and PCT is insufficient to distinguish between infected and uninfected critically ill patients [10–13]. Many studies have shown the efficacy of interleukin-27 (IL-27) for the differential diagnosis of sepsis and nonsepsis [14–18]. IL-27 is produced by antigen-presenting cells exposed to inflammatory stimuli and other conditions, and it is composed of EBI3 (an IL-12p40-related protein) and p28 (an IL-12p35-related polypeptide) joined with disulfide bonds. IL-27 induces the proliferation of naive CD4+ T cells and causes both proinflammatory and anti-inflammatory reactions [19, 20]. IL-27 plays a remarkable role in the evolution of various diseases

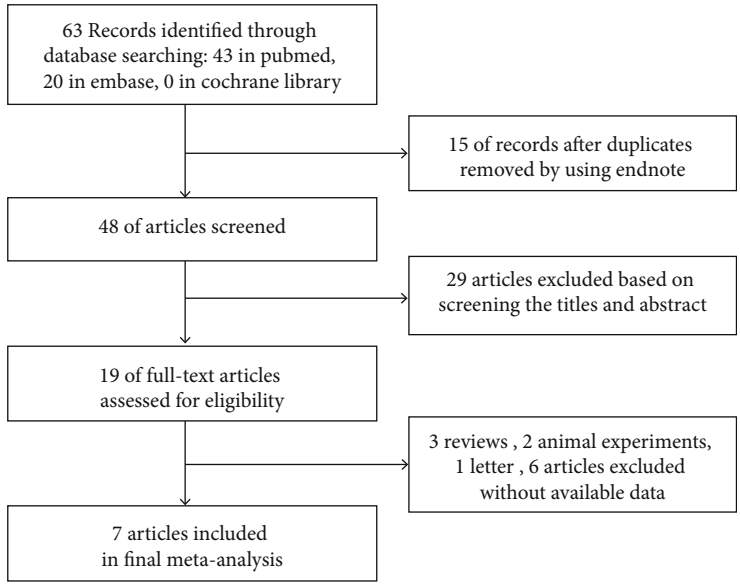

Figure 1: Seven studies collection flow chart.

Table 1: Characteristics of the included studies.

Author	Year	Country	Cases/controls	Cutoff, ng/mL	TP	FN	FP	TN	Sensitivity	Specificity	Population
Wong HR [24]	2012	USA	130/101	2	120	10	66	35	92%	35%	Children
Wong HR [14]	2013	France	145/125	1	128	17	96	29	88%	23%	Adults
Wong HR [16]	2014	USA	109/78	1	94	15	34	44	86%	56%	Adults
Fu J [25]	2015	China	45/66	3.6	18	27	10	56	40%	85%	Adults
He Y [15]	2017	China	68/83	1	48	20	24	59	70.59%	71.08%	Neonates
Abo El Magd NM [26]	2018	Egypt	45/45	485.56	43	2	0	45	95.56%	100%	Neonates
Fahmy EM [27]	2020	Egypt	47/37	—	44	3	7	30	93.6%	81.1%	Neonates

through its involvement in antitumor immunity and anti-infection immunity. In animal experiments, neutralizing the biological function of IL-27 improves the survival time of mice with sepsis [21]. Hence, it is biologically feasible to use IL-27 as a diagnostic marker for sepsis.

To date, there has been no meta-analysis on the effectiveness of IL-27 as a biological marker for sepsis diagnosis. Therefore, this meta-analysis was the first to make a judgment about the diagnostic accuracy of IL-27 in sepsis and to evaluate the associated specificity and sensitivity.

2. Methods

2.1. Search Strategy. A systematic search was performed for relevant literature in three databases (the Cochrane Library, EMBASE, and PubMed). The correlational studies reported that IL-27 is a useful biomarker for the differential diagnosis of patients with sepsis and nonsepsis, and they were published prior to October 21, 2020. The search keywords were as follows: (interleukin-27 or IL-27) in combination with "sepsis" and "biomarker". There were no language or publication-type restrictions. We checked the reference lists of correlational articles to confirm additional eligible studies not included in the databases. All the relevant articles were published.

2.2. Selection Criteria. In the meta-analysis, case-control studies using IL-27 for the differential diagnosis of patients with sepsis and nonsepsis were included. Then, the case-control studies provided details of data to construct 2×2 contingency tables. The exclusion criteria used were as follows: (1) meta-analyses, conference abstracts, correspondences, letters, case reports, editorials, animal experiments, and reviews; and (2) unavailable or insufficient data.

2.3. Data Extraction and Quality Assessment. Two authors, including the first author, independently extracted the following information from the eligible studies: the country where the research was conducted, the publication year, the numbers of cases and controls, biomarkers, and the data for the meta-analysis (true positive (TP), true negative (TN), false positive (FP), false negative (FN), sensitivity and specificity). We evaluated the quality of the included literature with the QUADAS-2 tool [22].

2.4. Statistical Analysis. To obtain the diagnostic accuracy of IL-27 for sepsis, we pooled the sensitivity, specificity, PLR,

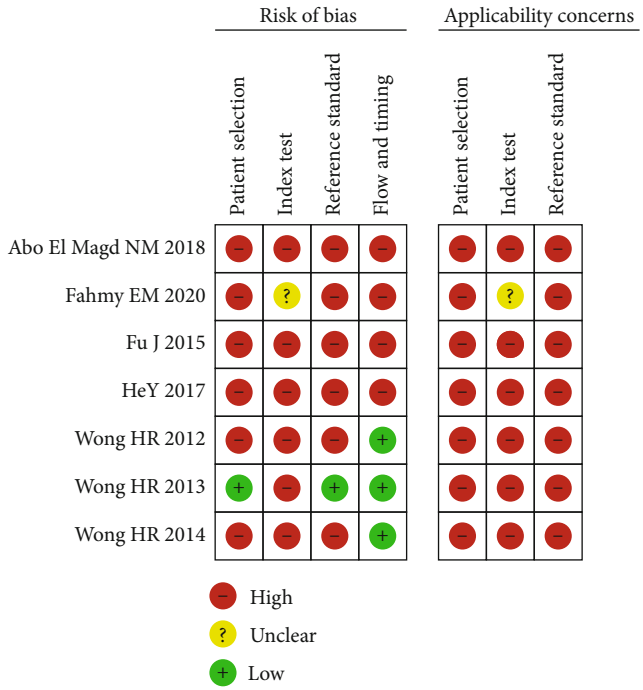

Figure 2: Risk of bias and applicability concerns of the included studies.

NLR, and DOR; we constructed a SROC curve and computed the area under the curve (AUC) with Meta-disc 1.4 (XI Cochrane Colloquium, Barcelona, Spain) and Stata 14.0 (StataCorp, College Station, TX) software. We assessed the statistical heterogeneity using I^2 statistics and identified the impact of potential heterogeneity on the specificity and sensitivity through threshold analysis, and we evaluated the publication bias of the included studies by Deeks' regression test of funnel plot asymmetry [23]. $P < 0.05$ or $I^2 > 50\%$ indicated statistically significant heterogeneity.

3. Results

3.1. Data Selection and Study Characteristics. The initial search retrieved 63 articles from the databases. After the duplicates were removed and the titles and abstracts were screened, we excluded 48 articles and provisionally included 19 articles. We made a full-text review of 7 articles and eliminated 12 articles [14–16, 24–27]. Finally, seven articles were used in our analysis (Figure 1). Seven studies included 589 sepsis patients and 535 controls, and they were performed in the USA, France, China, and Egypt. The included patient populations were neonates, children, and adults. The detailed characteristics of the seven studies included in our meta-analysis are listed in Table 1.

3.2. Quality of the Included Studies. The QUADAS-2 tool was applied to evaluate the quality of the seven studies about IL-27 for differential diagnosis in patients with sepsis, and the detailed results are shown in Figure 2.

3.3. Diagnostic Accuracy. The following results were computed using the Stata 14.0 software: 0.85 (95% CI, 0.72-0.93) for sensitivity, 0.72 (95% CI, 0.42-0.90) for specificity (Figure 3), 15 (95% CI, 3-72) for DOR, 3.0 (95% CI, 1.2-7.7) for PLR, and 0.20 (95% CI, 0.09-0.46) for NLR. The pooled AUC was 0.88 (95% CI, 0.84-0.90), suggesting that IL-27 is a highly accurate diagnostic biomarker for sepsis (Figure 4).

3.4. Heterogeneity Analysis. We performed a heterogeneity analysis with the seven studies, and the I^2 was 96.05 (95% CI, 94.28-97.82) for sensitivity and 96.65 (95% CI, 95.22-98.08) for specificity, indicating heterogeneity among the studies. The threshold analysis P value was 0.76, indicating no heterogeneity in our meta-analysis.

3.5. Publication Bias. We evaluated publication bias through Deeks' funnel plot asymmetry test, which clearly demonstrated that no significant publication bias existed in this meta-analysis ($P = 0.07$) (Figure 5).

4. Discussion

Currently, PCT is a biomarker that is broadly used in clinical diagnosing for bacterial infection, but it cannot be used to distinguish sepsis from noninfectious causes of systemic inflammatory response syndrome (SIRS) in critical patients [11]. Genome-wide expression analysis has indicated that IL-27 combined with PCT is a better predictor of infection than either biomarker alone [24]. Moreover, Eckerle et al. showed that IL-27 is more effective than PCT in diagnosing bacterial infections in pediatric emergencies [28]. Studies have shown that IL-27 also links up with suppression of inflammation and that IL-27 is a therapeutic target for limiting neonatal susceptibility to sepsis and improving infection outcomes [29–32]. Wong et al. calculated the AUC and cut-off points, and they showed that IL-27 is comprehensively superior to PCT as a biomarker for diagnosing sepsis [24]. Therefore, our meta-analysis included seven articles to investigate the value of IL-27 in diagnosing patients with sepsis. The results of our study clearly demonstrated that IL-27 was an accurate diagnostic biomarker for sepsis with the potential for clinical applicability. In our meta-analysis, the sensitivity was 0.84, and the specificity was 0.71, indicating an adequate overall diagnostic accuracy. The SROC provides reliable summarized data of diagnostic studies, showing the intuitive trade-off between specificity and sensitivity. According to the results of SROC, the AUC was 0.88, which further heralded that the overall accuracy was good. The sensitivity, specificity, and AUC of IL-27 in our study showed similarities with PCT (0.77, 0.79, and 0.85, respectively) [12], IL-6 (0.73, 0.76, and 0.81, respectively) [33], and presepsin (0.77, 0.73, and 0.86, respectively) [13], which are valuable diagnostic markers for sepsis in published studies. Thus, IL-27 may develop into a biological marker in diagnosing sepsis in the future.

To evaluate the overall accuracy, the DOR integrates the sensitivity and specificity into a readily interpretable number [34]. The DOR represents the ratio of the probability of the

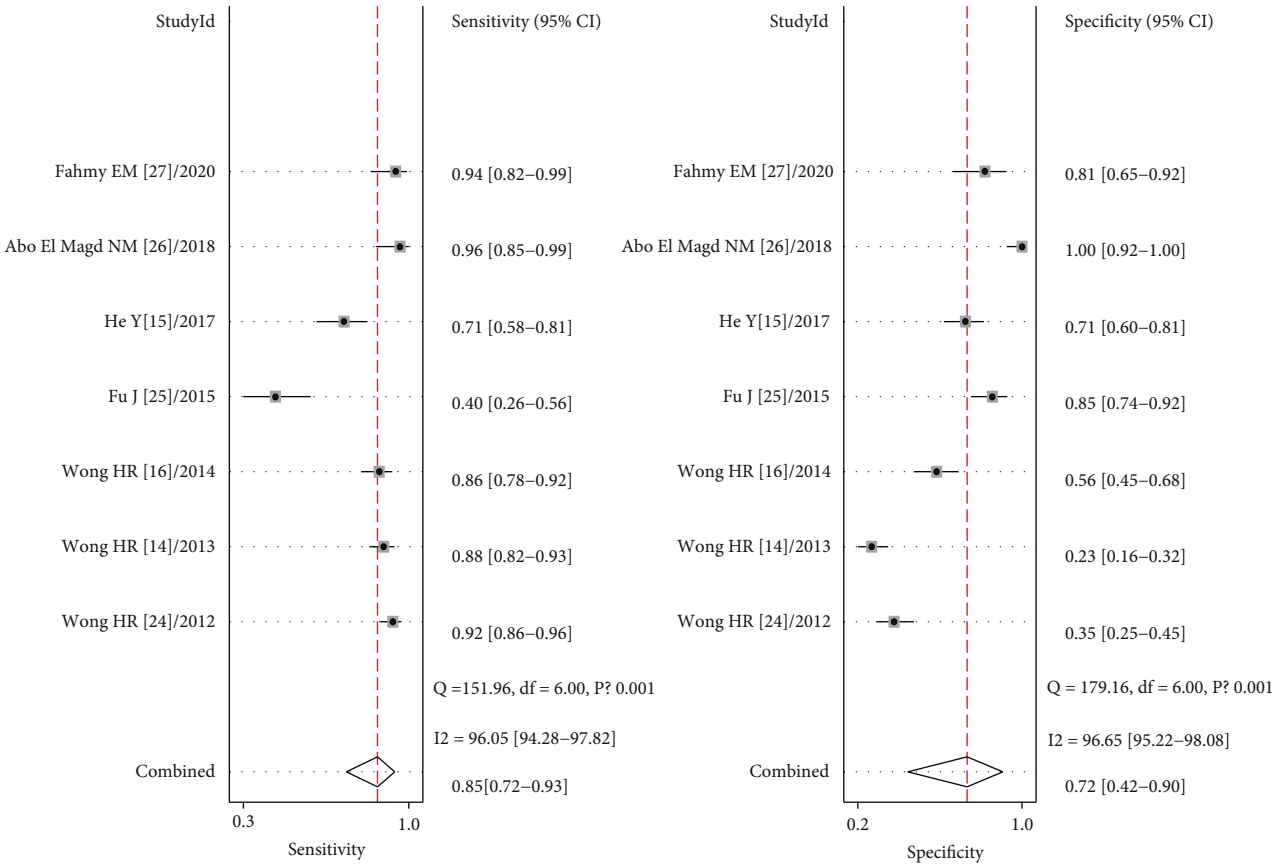

Figure 3: Forest plots of the sensitivity and specificity of interleukin-27 as a diagnostic biomarker for sepsis.

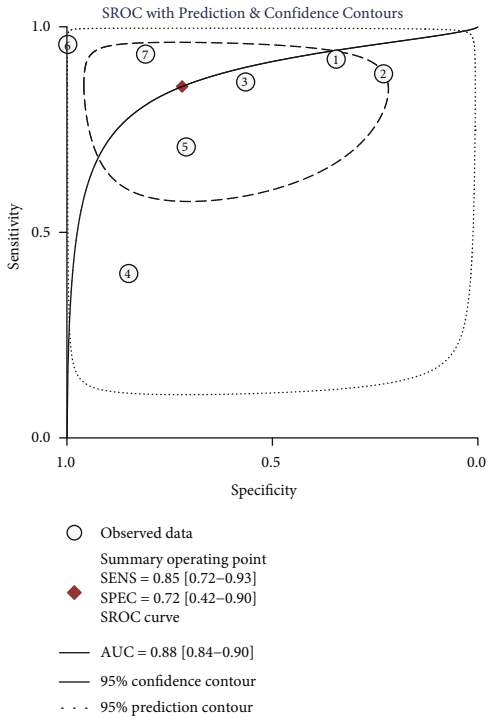

Figure 4: Symmetrical summary receiver operator curve (SROC) for interleukin-27 in all seven studies.

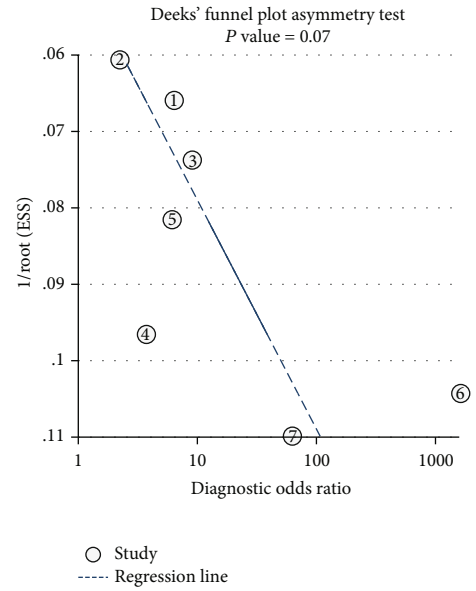

Figure 5: Deeks' funnel plot.

positive results between the conditional group and unconditional group. The DOR varies from 0 to infinity and DOR values with a larger notice better diagnosis. When the value of DOR is less than 1.0, it indicates that the test is unable to distinguish the patients with or without the condition. In

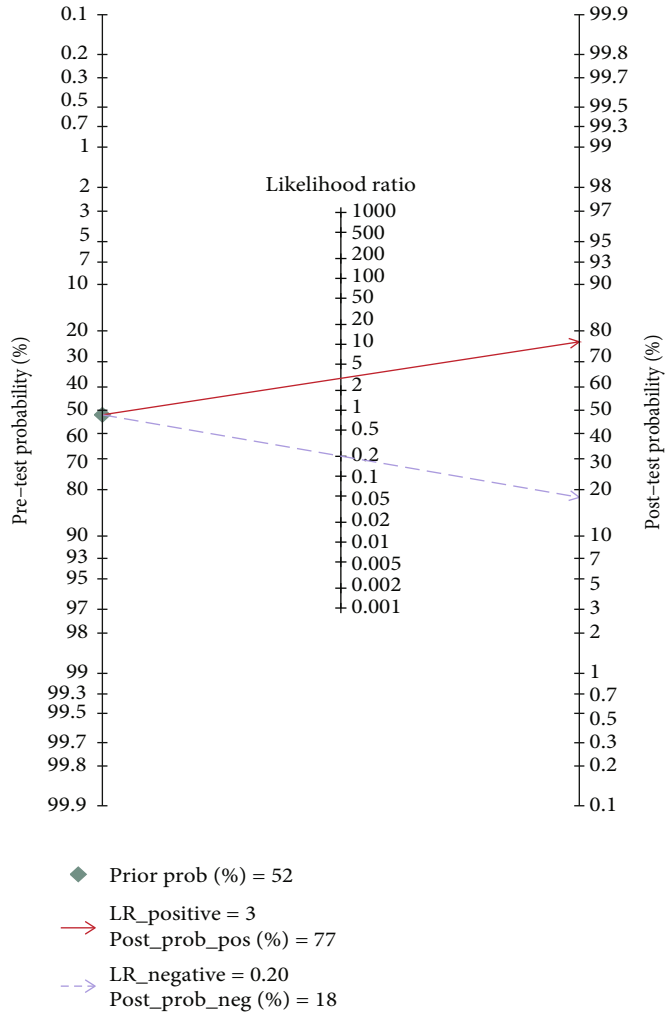

Figure 6: Fagan nomogram of interleukin-27 for the diagnosis of sepsis.

our meta-analysis, the calculated DOR was 15 (95% CI, 3-72), suggesting a high overall accuracy of IL-27 as a biological marker for differential diagnosis of sepsis.

We also performed a heterogeneity analysis to discover the existence of heterogeneity among the studies. The I^2 value was 96.05 for sensitivity and 96.65 for specificity, indicating a high degree of heterogeneity among the studies. Several factors may have contributed to this high degree of heterogeneity. First, the age distributions of the subjects differed as adults, neonates, and children were included. Different populations have different pathophysiological characteristics. A previous study has shown that the average IL-27 levels in the plasma of children with sepsis are higher than those in adults because the upregulation of IL-27 expression in answer to infection is more robust in children [14, 16]. Thus, IL-27 may be a more useful diagnostic biomarker in patients with sepsis who were not yet an adult. Second, seven studies were performed in different regions, including the USA, France, China, and Egypt. The inclusion of different ethnicities can contribute to heterogeneity. Third, sepsis was defined differently in various studies [35]. The new definition of sepsis was published in 2016 [1]; four studies used the pre-2016 report, and two studies used the latest information. For clinically septic but culture-negative patients, the lack of a harmonized definition may lead to a high degree of heterogeneity. Fourth, the pathogenic bacteria differed among the patients. The post hoc analyses showed that the AUC for IL-27 in patients with secondary sepsis infection caused by a Gram-positive bacterium and Gram-negative bacterium was 0.639 and 0.768, respectively [14, 16]. Therefore, the bacterial etiology of sepsis should be considered as a source of heterogeneity.

To increase the clinical applicability of the results of IL-27 in this meta-analysis, we used LRs to calculate the posttest probabilities according to Fagan's nomogram. Given a pretest probability of 52%, the pooled PLR of 3 increased the posttest likelihood (positive predictive value) to 77%. Thus, 77 of 100 patients with positive IL-27 results could be expected to have a confirmed diagnosis of sepsis. Moreover, the pooled NLR of 0.20 reduced the posttest probability to 18%. Thus, only 18 of 100 patients with negative IL-27 results may ultimately be diagnosed with sepsis (Figure 6). These results indicated that IL-27 is a useful diagnostic indicator for sepsis.

In this meta-analysis, several limitations attracted our attention and should be discussed. Primarily, the degree of

heterogeneity should be considered. Due to the small sample size and the limited data available, we could not perform a meta-regression analysis. Therefore, we only analyzed factors underlying the existence of heterogeneity. Second, all databases used to identify the studies were in English. Therefore, some publications may have been overlooked, which may have been one of the causes of the bias in this meta-analysis. To overcome the above problems, the authors repeated the search to include more studies but did not find additional relevant articles or available data.

5. Conclusions

In conclusion, IL-27 can be used as a candidate biomarker for the diagnosis of patients with sepsis. Although IL-27 has the potential for clinical applicability for identifying sepsis in critical patients, the test results of IL-27 should be explained in combination with clinical and other test factors. Further studies with a large sample size are needed to be designed to reduce the heterogeneity in the analysis of the utility of IL-27 for discrimination between sepsis and nonsepsis.

Data Availability

The data of Table 1 used to support the findings of our study are included within the article (see References).

Conflicts of Interest

No conflicts of interest were declared.

Acknowledgments

The present work was supported by the Science and Technology Plan Project of Chengde (202006A049). We also thanked American Journal Experts for proofreading this meta-analysis.

References

[1] M. Singer, C. S. Deutschman, C. W. Seymour et al., "The third international consensus definitions for sepsis and septic shock (Sepsis-3)," *JAMA*, vol. 315, no. 8, pp. 801–810, 2016.

[2] X. Gao, Y. Liu, F. Xu et al., "Assessment of apoptosis inhibitor of macrophage/CD5L as a biomarker to predict mortality in the critically ill with sepsis," *Chest*, vol. 156, no. 4, pp. 696–705, 2019.

[3] L. M. Napolitano, "Sepsis 2018: definitions and guideline changes," *Surgical Infections*, vol. 19, no. 2, pp. 117–125, 2018.

[4] A. Teggert, H. Datta, and Z. Ali, "Biomarkers for point-of-care diagnosis of sepsis," *Micromachines*, vol. 11, no. 3, p. 286, 2020.

[5] T. van der Poll, F. L. van de Veerdonk, B. P. Scicluna, and M. G. Netea, "The immunopathology of sepsis and potential therapeutic targets," *Nature Reviews. Immunology*, vol. 17, no. 7, pp. 407–420, 2017.

[6] J. Hou, Q. Chen, X. Wu et al., "S1PR3 signaling drives bacterial killing and is required for survival in bacterial Sepsis," *American Journal of Respiratory and Critical Care Medicine*, vol. 196, no. 12, pp. 1559–1570, 2017.

[7] R. S. Samraj, B. Zingarelli, and H. R. Wong, "Role of biomarkers in sepsis care," *Shock*, vol. 40, no. 5, pp. 358–365, 2013.

[8] S. L. Weiss, J. C. Fitzgerald, F. Balamuth et al., "Delayed antimicrobial therapy increases mortality and organ dysfunction duration in pediatric sepsis," *Critical Care Medicine*, vol. 42, no. 11, pp. 2409–2417, 2014.

[9] M. A. Puskarich, S. Trzeciak, N. I. Shapiro et al., "Association between timing of antibiotic administration and mortality from septic shock in patients treated with a quantitative resuscitation protocol," *Critical Care Medicine*, vol. 39, no. 9, pp. 2066–2071, 2011.

[10] R. Arkader, E. J. Troster, M. R. Lopes et al., "Procalcitonin does discriminate between sepsis and systemic inflammatory response syndrome," *Archives of Disease in Childhood*, vol. 91, no. 2, pp. 117–120, 2006.

[11] B. M. Tang, G. D. Eslick, J. C. Craig, and A. S. McLean, "Accuracy of procalcitonin for sepsis diagnosis in critically ill patients: systematic review and meta-analysis," *The Lancet Infectious Diseases*, vol. 7, no. 3, pp. 210–217, 2007.

[12] C. Wacker, A. Prkno, F. M. Brunkhorst, and P. Schlattmann, "Procalcitonin as a diagnostic marker for sepsis: a systematic review and meta-analysis," *The Lancet Infectious Diseases*, vol. 13, no. 5, pp. 426–435, 2013.

[13] Z. Zheng, L. Jiang, L. Ye, Y. Gao, L. Tang, and M. Zhang, "The accuracy of presepsin for the diagnosis of sepsis from SIRS: a systematic review and meta-analysis," *Annals of Intensive Care*, vol. 5, no. 1, p. 48, 2015.

[14] H. R. Wong, C. J. Lindsell, P. Lahni, K. W. Hart, and S. Gibot, "Interleukin 27 as a sepsis diagnostic biomarker in critically ill adults," *Shock*, vol. 40, no. 5, pp. 382–386, 2013.

[15] Y. He, W. . du, H. Y. Jiang et al., "Multiplex cytokine profiling identifies interleukin-27 as a novel biomarker for neonatal early onset sepsis," *Shock*, vol. 47, no. 2, pp. 140–147, 2017.

[16] H. R. Wong, K. D. Liu, K. N. Kangelaris, P. Lahni, and C. S. Calfee, "Performance of interleukin-27 as a sepsis diagnostic biomarker in critically ill adults," *Journal of Critical Care*, vol. 29, no. 5, pp. 718–722, 2014.

[17] W. J. Hanna, Z. Berrens, T. Langner, P. Lahni, and H. R. Wong, "Interleukin-27: a novel biomarker in predicting bacterial infection among the critically ill," *Critical Care*, vol. 19, no. 1, p. 378, 2015.

[18] A. V. Raveendran, A. Kumar, and S. Gangadharan, "Biomarkers and newer laboratory investigations in the diagnosis of sepsis," *The Journal of the Royal College of Physicians of Edinburgh*, vol. 49, no. 3, pp. 207–216, 2019.

[19] S. Pflanz, J. C. Timans, J. Cheung et al., "IL-27, a heterodimeric cytokine composed of EBI3 and p28 protein, induces proliferation of naive $CD4^+$ T cells," *Immunity*, vol. 16, no. 6, pp. 779–790, 2002.

[20] A. V. Villarino, J. Larkin 3rd, C. J. Saris et al., "Positive and negative regulation of the IL-27 receptor during lymphoid cell activation," *Journal of Immunology*, vol. 174, no. 12, pp. 7684–7691, 2005.

[21] S. Wirtz, I. Tubbe, P. R. Galle et al., "Protection from lethal septic peritonitis by neutralizing the biological function of interleukin 27," *The Journal of Experimental Medicine*, vol. 203, no. 8, pp. 1875–1881, 2006.

[22] P. F. Whiting, A. W. Rutjes, M. E. Westwood et al., "QUADAS-2: a revised tool for the quality assessment of diagnostic

accuracy studies," *Annals of Internal Medicine*, vol. 155, no. 8, pp. 529–536, 2011.

[23] J. J. Deeks, P. Macaskill, and L. Irwig, "The performance of tests of publication bias and other sample size effects in systematic reviews of diagnostic test accuracy was assessed," *Journal of Clinical Epidemiology*, vol. 58, no. 9, pp. 882–893, 2005.

[24] H. R. Wong, N. Z. Cvijanovich, M. Hall et al., "Interleukin-27 is a novel candidate diagnostic biomarker for bacterial infection in critically ill children," *Critical Care*, vol. 16, no. 5, p. R213, 2012.

[25] J. Fu, Y. Wang, P. Zeng, and S. Niu, "Value of interleukin-27 as a diagnostic biomarker of sepsis in critically ill adults," *Zhonghua Wei Zhong Bing Ji Jiu Yi Xue*, vol. 27, no. 6, pp. 460–464, 2015.

[26] N. M. Abo El Magd, S. A. Abdel Salam, Y. A. Aly, and N. A. Fahim, "The role of serum interleukin-27 as a diagnostic biomarker for diagnosis of neonatal sepsis," *The Egyptian Journal of Immunology*, vol. 25, no. 2, pp. 87–95, 2018.

[27] E. M. Fahmy, N. M. Kamel, A. Abdelsadik et al., "Assessment of interleukin-27 and chemokine RANTES as biomarkers for early onset neonatal sepsis," *The Egyptian Journal of Immunology*, vol. 27, no. 1, pp. 9–18, 2020.

[28] M. Eckerle, P. Lahni, and H. Wong, "Estimating the probability of bacterial infection using a novel biomarker among pediatric patients in the emergency department," *Biomarkers*, vol. 21, no. 5, pp. 404–408, 2016.

[29] B. G. Seman, J. K. Vance, T. W. Rawson et al., "Elevated levels of interleukin-27 in early life compromise protective immunity in a mouse model of Gram-negative neonatal sepsis," *Infection and Immunity*, vol. 88, no. 3, 2020.

[30] M. Gleave Parson, J. Grimmett, J. K. Vance et al., "Murine myeloid-derived suppressor cells are a source of elevated levels of interleukin-27 in early life and compromise control of bacterial infection," *Immunology and Cell Biology*, vol. 97, no. 5, pp. 445–456, 2019.

[31] J. He, Q. Zhang, W. Zhang et al., "The interleukin-27-964A>G polymorphism enhances sepsis-induced inflammatory responses and confers susceptibility to the development of sepsis," *Critical Care*, vol. 22, no. 1, p. 248, 2018.

[32] J. Fan, Y. C. Zhang, D. F. Zheng et al., "IL-27 is elevated in sepsis with acute hepatic injury and promotes hepatic damage and inflammation in the CLP model," *Cytokine*, vol. 127, p. 154936, 2020.

[33] S. Iwase, T. A. Nakada, N. Hattori et al., "Interleukin-6 as a diagnostic marker for infection in critically ill patients: a systematic review and meta-analysis," *The American Journal of Emergency Medicine*, vol. 37, no. 2, pp. 260–265, 2019.

[34] A. S. Glas, J. G. Lijmer, M. H. Prins, G. J. Bonsel, and P. M. Bossuyt, "The diagnostic odds ratio: a single indicator of test performance," *Journal of Clinical Epidemiology*, vol. 56, no. 11, pp. 1129–1135, 2003.

[35] M. E. Nunnally and A. Patel, "Sepsis-what's new in 2019?," *Current Opinion in Anaesthesiology*, vol. 32, no. 2, pp. 163–168, 2019.

Hindawi
BioMed Research International
Volume 2021, Article ID 9927498, 6 pages
https://doi.org/10.1155/2021/9927498

Research Article

Percutaneous Nephrolithotomy Can Reduce the Incidence of Sepsis Compared with Flexible Ureteroscopy in Treating Solitary Proximal Ureteral Stone Patients with Positive Urine Culture

Qi-Dong Xia, Yu-Feng Wang, Chen-Qian Liu, Jin-Zhou Xu, Jian-Xuan Sun, Yang Xun, Cong Li, Jia Hu, Jun-Lin Lu, and Shao-Gang Wang

Department of Urology, Tongji Hospital, Tongji Medical College, Huazhong University of Science and Technology, Wuhan, China

Correspondence should be addressed to Jun-Lin Lu; lujunlintjm@hust.edu.cn and Shao-Gang Wang; sgwangtjm@163.com

Received 4 March 2021; Revised 25 March 2021; Accepted 29 March 2021; Published 13 April 2021

Academic Editor: Manash K. Paul

Background. Sepsis is a potentially lethal complication for both flexible ureteroscopy (fURS) and percutaneous nephrolithotomy (PCNL). This study is aimed at comparing the sepsis rate after fURS and PCNL and the risk factors for sepsis in patients with solitary proximal ureteral stone. *Methods*. We reviewed the data of patients with calculi between 10 mm to 20 mm who underwent fURS or PCNL surgery from Tongji Hospital's database. A total of 910 patients were eligible with 412 fURS cases and 498 PCNL cases. We used univariate analysis and multivariate logistic regression analysis to identify the risk factors for sepsis. Subgroup analysis was performed using logistic regression analysis. *Results*. In the cohort, 27 (6.6%) and 19 (3.8%) patients developed sepsis after fURS and PCNL, respectively. Multivariate analysis shows that the risk factors for sepsis are fURS (OR = 3.160, $P = 0.004$), serum WBC ≥ 10,000 cells/μL (OR = 3.490, $P = 0.008$), albumin − globulin ratio < 1.2 (OR = 2.192, $P = 0.029$), positive urine culture (OR = 6.145, $P < 0.001$), and prolonged operation time (OR = 1.010, $P = 0.046$). Subgroup analysis was conducted using potential risk factors: stone size, serum WBC, urine culture, and albumin-globulin ratio (AGR). In subgroup of positive urine culture, patients were more likely to develop sepsis after fURS than PCNL. *Conclusions*. PCNL may be a better choice than fURS to reduce postoperative sepsis, especially for patients with positive urine culture.

1. Introduction

Urolithiasis is one of the most common diseases in the urinary system. It affects patients globally because of its high incidence rate that is 7-13% in North America, 5-9% in Europe, and 1-5% in Asia [1–3]. Surgery is the main treatment for urolithiasis: extracorporeal shock wave lithotripsy, endoscopic surgery, or laparoscopic surgery. Among them, percutaneous nephrolithotomy (PCNL) and flexible ureteroscopy (fURS) are both recommended to remove 10-20 mm ureteral stone [4].

Sepsis is one of the most intractable surgery complications, which leads to a longer length of stay and even lethal sepsis shock in some cases [5]. According to previous studies, postoperative sepsis is the primary complication with an incidence of 0.3-7.4% in fURS and 0.9-5.9% in PCNL [6–8]. It seems that different surgical procedures may lead to different incidence rate of sepsis. Thus, urologists make efforts to discover risk factors or preoperative predicting factors for postoperative sepsis. There have been several preoperative features identified as risk factors such as positive urine culture, female sex, and diabetes [9]. However, though the preoperative risk factor has been identified, it is hardly helpful for clinicians to make a clinical decision about which surgical procedure to choose, PCNL or fURS. Thus, we aim to compare the occurrence of postoperative sepsis between fURS and PCNL and analyze the difference of risk factors.

Besides, PCNL is usually utilized to treat larger stone than fURS [10, 11]. Considering the heterogeneity of the stone size between patients may influence the sepsis incidence, we conducted a retrospective clinical data collection of patients with solitary proximal ureteral stone with stone size between 10 and 20 mm. We performed univariate and multivariate analyses to discover the risk factors for postoperative sepsis in our

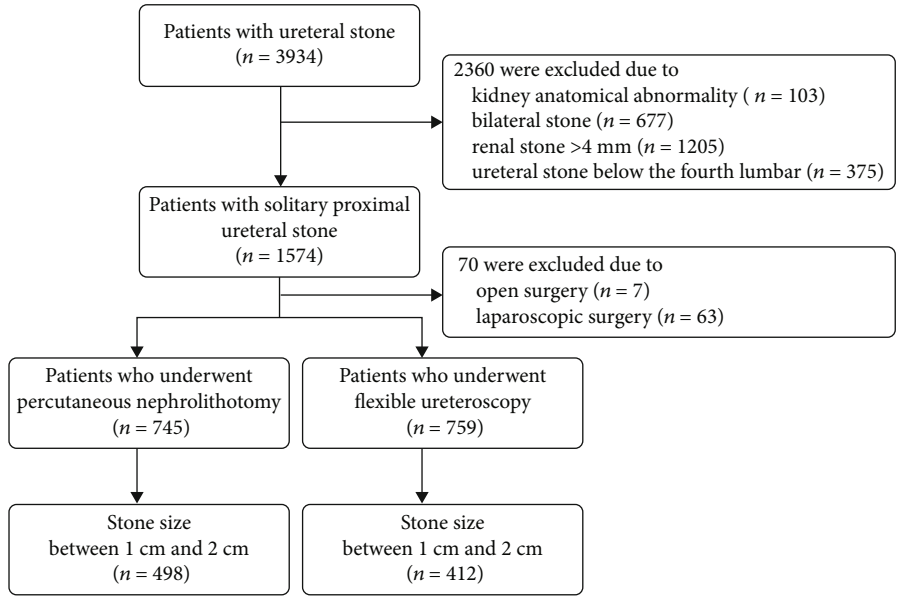

Figure 1: The screening flow chart.

cohort. Our works may provide evidence for clinicians to make surgical choice.

2. Materials and Methods

The research was approved by the Ethics Committee of Tongji Medical College (2019S1035). The retrospective study included patients from January 2012 to December 2018. The inclusion criteria were (1) unilateral, solitary, and proximal ureteral stones; (2) PCNL or fURS to treat urolithiasis; (3) stone size ranging from 10 mm to 20 mm; (4) patient age ≥ 18 years. The exclusion criteria were anatomical abnormality: solitary kidney, horseshoe kidney, transplant kidney, and kidney duplication.

The primary outcome was postoperative sepsis. According to the 2001 International Sepsis Definitions Conference, postoperative sepsis was defined as the concurrence of infection and at least two of the following criteria with 48 hours of surgery: (1) heart rate > 90/minute, (2) respiratory rate > 20 /minute, (3) body temperature > 38°C, and leukocyte count < 4,000 cells/μL or >12,000 cells/μL.

The patient data was retrospectively collected from the hospital's database. Preoperative factors were recorded such as patient age, sex, body mass index (BMI), comorbidities (diabetes, coronary heart disease, paraplegia, and hypertension), stone size and laterality, presence of hydronephrosis and indwelling stent, hematological tests (serum white blood cell [WBC], neutrophil, and lymphocyte), biochemical tests (creatinine, cholesterol, albumin, and globulin), urine tests (urine WBC and urine nitrite), urine culture, and American Society of Anesthesiologists (ASA) score. Size of ureteral access sheath and flexible ureteroscope for fURS and size of sheath and nephroscope for PCNL were also recorded. Operation time was documented from the commencement of operation to the end of anesthesia. The laboratory tests were routinely performed and obtained for all patients. Patients who have infectious indicators (fever, high serum WBC proportion, or positive urine culture) received at least a full antibiotic regimen for seven days until the tests turned negative. Otherwise, one dose of antibiotics was applied for prophylactic purpose.

Statistical analysis was conducted using Statistical Product and Service Solutions (SPSS) version 24.0. The Student's t-test was used to compare continuous variables (expressed by mean ± standard deviation) with a normal distribution. Continuous variables with a skewed distribution were showed as median (interquartile range [IQR]) and compared by the Mann-Whitney U test. The chi-square test or Fisher's exact test was utilized to detect the difference between groups with categorical variables (expressed by proportions). The logistic regression method was used to identify the risk factors of sepsis. The difference was considered statistically significant when P value <0.05.

3. Results

After reviewing 3934 patients with ureteral stone, 2360 were excluded primarily due to kidney anatomical abnormality ($n = 103$), bilateral stone ($n = 677$), renal stone > 4 mm ($n = 1205$), and ureteral stone below the fourth lumbar ($n = 375$). Finally, a total of 910 patients with 10-20 mm solitary proximal ureteral stone were eligible for analysis (Figure 1). Among them, 412 patients underwent fURS, whereas 498 patients received PCNL.

The detailed basic information of the eligible patients is shown in Table 1. Patients who received PCNL had higher rate of hydronephrosis, larger stone size, and longer operation time. The rough sepsis rate of fURS (6.6%) is higher than that of PCNL (3.8%). But the difference is not significant ($P = 0.061$). The multivariate analysis indicates that five variables are independent risk factors of sepsis (Table 2): fURS (OR = 3.160, $P = 0.004$), serum WBC ≥ 10,000 cells/μL

Table 1: Basic characteristics of including patients.

Variables	All patients ($n = 910$)	fURS ($n = 412$)	PCNL ($n = 498$)	P value
Age (years)	50.0 ± 12.4	49.1 ± 13.2	50.6 ± 11.6	0.074
Male, *n* (%)	588 (64.6)	271 (65.8)	317 (63.7)	0.505
BMI (kg/m^2)	24.0 ± 3.1	24.2 ± 3.3	23.9 ± 3.0	0.163
Preoperative urological condition, n (%)				
Hydronephrosis	131 (14.4)	34 (8.3)	97 (19.5)	<0.001
Indwelling stent	63 (6.9)	29 (7.0)	34 (6.8)	0.900
Stone characteristics				
Stone size (mm)	13.3 ± 3.2	12.4 ± 2.8	14.1 ± 3.2	<0.001
Left side, *n* (%)	476 (52.3)	208 (50.5)	268 (53.8)	0.317
Comorbidities, n (%)				
Diabetes	74 (8.1)	39 (9.5)	35 (7.0)	0.180
Coronary heart disease	15 (1.6)	6 (1.5)	9 (1.8)	0.679
Hypertension	210 (23.1)	90 (21.8)	120 (24.1)	0.422
Urine test				
Urine WBC, median (IQR) (cells/hpf)	52.0 (19.6-163.7)	46.0 (17.1-127.4)	59.0 (21.3-193.4)	0.024
Positive urine nitrite, *n* (%)	55 (6.0)	23 (5.6)	32 (6.4)	0.595
Positive urine culture, *n* (%)	100 (11.0)	38 (9.2)	62 (12.4)	0.121
Hematological test (10^{9}cells/L)				
Serum WBC	6.8 ± 2.8	6.9 ± 3.2	6.6 ± 2.5	0.164
Neutrophil	4.1 ± 2.7	4.3 ± 3.0	4.0 ± 2.4	0.169
Lymphocyte	1.9 ± 0.6	1.9 ± 0.6	1.9 ± 0.6	0.943
Biochemical test				
Albumin (g/L)	39.5 ± 4.2	39.8 ± 4.3	39.3 ± 4.3	0.662
Globulin (g/L)	29.2 ± 4.6	29.2 ± 4.4	29.2 ± 4.8	0.061
AGR	1.39 ± 0.28	1.39 ± 0.27	1.39 ± 0.29	0.051
Creatinine, median (IQR) (μmoI/L)	85.0 (69.0-108.0)	83.0 (68.0-108.0)	86.0 (70.0-109.0)	0.680
Cholesterol (mmol/L)	4.1 ± 0.9	4.1 ± 0.9	4.1 ± 0.9	0.848
ASA, n (%)				0.150
I	378 (41.5)	157 (38.1)	221 (44.4)	
II	510 (56.0)	243 (59.0)	267 (53.6)	
III	21 (2.3)	12 (2.9)	9 (1.8)	
IV	1 (0.1)	0 (0.0)	1 (0.2)	
Operation time, median (IQR) (min)	85.0 (66.0-110.0)	72.5 (58.0-89.0)	98.0 (78.0-120.0)	<0.001
Postoperative sepsis, *n* (%)	46 (5.1)	27 (6.6)	19 (3.8)	0.061

(OR = 3.490, $P = 0.008$), albumin − globulin ratio < 1.2 (OR = 2.192, $P = 0.029$), positive urine culture (OR = 6.145, $P < 0.001$), and prolonged operation time (OR = 1.010, $P = 0.046$). Sex ($P = 0.354$) and stone size ($P = 0.716$) are not considered as independent risk factors.

Urologists are more likely to choose PCNL to treat larger stones. We divided patients into a larger stone size group (15-20 mm) and a smaller stone size group (10-15 mm) to evaluate the sepsis rate between fURS and PCNL (Figure 2). Both groups are not of statistical difference: $P = 0.160$ for smaller stone size group and $P = 0.205$ for larger stone size group. Subgroup analysis using sepsis risk factors is also performed: serum WBC, urine culture, and albumin-globulin ratio (AGR). In the positive urine culture group, patients who receive fURS have 5.71 times the risk of developing sepsis than patients who receive PCNL ($P < 0.001$).

4. Discussion

Sepsis is one of the most severe complications in patients who underwent lithotomy, which may both occur after PCNL or fURS [12, 13]. It has been reported that the occurrence rate of sepsis post-fURS or post-PCNL was different. According to previous research, the sepsis rate after fURS reaches

Table 2: Multivariate analysis for the risk factors of sepsis.

Variables	B	OR	95% CI	*P* value
Surgery (ref. PCNL)	1.151	3.160	(1.459 to 6.842)	0.004
Sex (ref. male)	0.324	1.383	(0.697 to 2.747)	0.354
Age (years)	0.019	1.019	(0.990 to 1.048)	0.200
BMI (kg/m^2)	0.013	1.014	(0.910 to 1.129)	0.807
Stone size (mm)	0.020	1.021	(0.915 to 1.139)	0.716
Indwelling stent	-0.038	0.962	(0.338 to 2.739)	0.943
Diabetes	-0.431	0.650	(0.181 to 2.334)	0.509
Hydronephrosis	-0.519	0.595	(0.168 to 2.107)	0.421
Serum WBC ≥ 10,000 cells/μL	1.250	3.490	(1.391 to 8.758)	0.008
AGR < 1.2	0.785	2.192	(1.082 to 4.442)	0.029
Positive urine culture	1.816	6.145	(2.541 to 14.859)	<0.001
Urine WBC ≥ 50 cells/hpf	0.185	1.203	(0.531 to 2.726)	0.659
Positive urine nitrite	0.676	1.967	(0.750 to 5.157)	0.169
Operation time (min)	0.010	1.010	(1.000 to 1.020)	0.046

Abbreviations: PCNL: percutaneous nephrolithotomy; BMI: body mass index; WBC: white blood cell; AGR: albumin globulin ratio.

Patient status	PCNL		fURS		Odds ratio [95%CI]	*P* value	Odds ratio [95%CI]
	Sepsis	Total	Sepsis	Total			
Stone size							
<15mm	11	278	19	301	1.64 [0.76 to 3.50]	0.160	
≥15mm	8	220	8	111	2.06 [0.75 to 5.64]	0.205	
Serum WBC							
<10,000 cells/μL	14	459	22	379	1.96 [0.99 to 3.88]	0.054	
≥10,000 cells/μL	5	39	5	33	1.21 [0.32 to 4.62]	0.776	
Urine culture							
Positive	7	62	16	38	5.71 [2.07 to 15.79]	<0.001	
Negative	12	436	11	374	1.07 [0.47 to 2.46]	0.872	
AGR							
<1.2	11	126	14	87	2.00 [0.86 to 4.66]	0.106	
≥1.2	8	372	13	325	1.90 [0.78 to 4.63]	0.161	

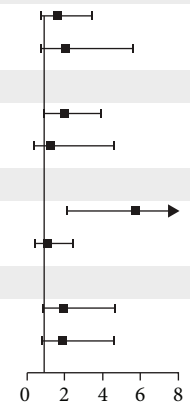

Figure 2: Subgroup analysis to compare sepsis rate between PCNL and fURS.

0.3%-7.4% [6, 7], and the sepsis rate after PCNL reaches 0.9%-5.9% [8]. In our study, sepsis after PCNL was 3.8% (19/498) and 6.6% (27/412) after fURS, which shows a consistency with previous studies. Based on the multivariate logistic analysis, we find that surgical option, positive urine culture, serum WBC, and operation time are independent predictors of postoperative sepsis. Patients with positive urine culture are more likely to suffer sepsis after fUSR than PCNL. However, no significant difference in sepsis rate is indicated between PCNL and fURS when urine culture is negative.

We previously report that positive urine culture is an independent predictor for post-fURS sepsis and assemble a nomogram to predict the occurrence of post-fURS sepsis [14]. Uchinda [15] et al. and Blackmur et al. [7] explored the role of bladder urine culture in infectious complications that it is an independent risk factor increasing 3.53 to 4.88 times the risk of infectious complications. It may be because the high intrarenal pressure during the fURS promotes local pathogens and toxins into blood circulation. AGR usually plays a role as a predictor of cancer progression or cancer-specific survival because it reflects patients' nutrition, inflammation, and immunity [16]. We also find it as a predictor of sepsis after endourological stone surgery [14, 17]. In this study, both low AGR and high AGR groups, PCNL, and fURS have similar sepsis rates. From the aspect of reducing operative sepsis, the level of AGR may have little influence on surgical option.

Kreydin and Eisner have systemically summarized the risk factors for sepsis after PCNL [18], and the pre-PCNL factors included positive urine culture, female, nephrostomy, urinary diversion, stone size, hydronephrosis, diabetes, and

complicated calculi. Meanwhile, the local urinary system condition is considered the most critical factor related to infectious complications. Besides, more novel predictors for post-PCNL sepsis are identified by researchers. For example, C-reactive protein, albumin, and procalcitonin are considered predictors reflecting the systematic condition of patients [8, 19].

Positive urine culture is a predictor of postoperative sepsis for both fURS and PCNL. The evidence reveals that urine culture can be an essential reference factor for surgical choice to reduce the incidence of sepsis. In patients with 10-20 mm ureteral stone, we find that PCNL is better than fURS when patients have a positive urine culture. Our works can optimize the surgery strategy for patients with a high risk of infection [20, 21].

The main limitation of the study is the single-center retrospective nature, which may cause selection bias. We include a relatively large number of patients to stabilize the results. Subgroup analysis is also performed to compare sepsis incidence in patients with different conditions. Further prospective and multicenter studies are needed.

5. Conclusions

In summary, we find that PCNL might be a better choice than fURS to reduce postoperative sepsis, especially when patients have a positive urine culture.

Abbreviations

fURS: Flexible ureteroscopy
PCNL: Percutaneous nephrolithotomy
BMI: Body mass index
WBC: White blood cell
AGR: Albumin-globulin ratio
ASA: American Society of Anesthesiologists
SPSS: Statistical Product and Service Solutions
IQR: Interquartile range.

Data Availability

All data that supports the findings of this study is available from the corresponding author upon reasonable request.

Ethical Approval

The authors are accountable for all aspects of the work in ensuring that questions related to the accuracy or integrity of any part of the work are appropriately investigated and resolved. The authors are accountable for all aspects of the work in ensuring that questions related to the accuracy or integrity of any part of the work are appropriately investigated and resolved. The study was conducted in accordance with the Declaration of Helsinki (as revised in 2013). The study was approved by the Ethics Committee of Tongji Medical College, Huazhong University of Science and Technology (IORG No: IORG0003571).

Consent

Individual consent for this retrospective analysis was waived.

Conflicts of Interest

The authors declare that they have no conflicts of interest.

Authors' Contributions

(I) Conception and design was carried out by XQD, WYF, LJL, and WSG. (II) LC, HJ, and WSG contributed to the administrative support. (III) Provision of study materials or patients was done by LC and XY. (IV) Collection and assembly of data was performed by LJL and XQD. (V) LJL, WYF, and XQD contributed to the data analysis and interpretation. (VI) Manuscript writing and final approval of manuscript were done by all authors. Qi-Dong Xia and Yu-Feng Wang share co-first authorship.

Acknowledgments

This research is supported by grants from the National key research and development program (2017YFB1302804).

References

[1] M. J. Favus, "Epidemiology of Nephrolithiasis," in *Primer on the Metabolic Bone Diseases and Disorders of Mineral Metabolism: Eighth Edition*, pp. 856–859, Wiley Blackwell, 2013.

[2] I. Pinduli, R. Spivacow, E. Del Valle et al., "Prevalence of urolithiasis in the autonomous city of Buenos Aires, Argentina," *Urological Research*, vol. 34, no. 1, pp. 8–11, 2006.

[3] M. Medina-Escobedo, M. Zaidi, E. Real-de León, and S. Orozco-Rivadeneyra, "Urolithiasis prevalence and risk factors in Yucatan, Mexico," *Salud Pública de México*, vol. 44, no. 6, pp. 541–545, 2002.

[4] C. C. Wen and S. Y. Nakada, "Treatment selection and outcomes: renal calculi," *Urologic Clinics of North America*, vol. 34, no. 3, pp. 409–419, 2007.

[5] A. Heinze, A. S. Gozen, and J. Rassweiler, "Tract sizes in percutaneous nephrolithotomy: does miniaturization improve outcome?," *Current Opinion in Urology*, vol. 29, no. 2, pp. 118–123, 2019.

[6] B. K. Somani, G. Giusti, Y. Sun et al., "Complications associated with ureterorenoscopy (URS) related to treatment of urolithiasis: the Clinical Research Office of Endourological Society URS Global study," *World Journal of Urology*, vol. 35, no. 4, pp. 675–681, 2017.

[7] J. P. Blackmur, N. U. Maitra, R. R. Marri, F. Housami, M. Malki, and C. Mcilhenny, "Analysis of factors' association with risk of postoperative urosepsis in patients undergoing ureteroscopy for treatment of stone disease," *Journal of Endourology*, vol. 30, no. 9, pp. 963–969, 2016.

[8] M. Rivera, B. Viers, P. Cockerill, D. Agarwal, R. Mehta, and A. Krambeck, "Pre- and postoperative predictors of infection-related complications in patients undergoing percutaneous nephrolithotomy," *Journal of Endourology*, vol. 30, no. 9, pp. 982–986, 2016.

[9] Y. Xun, Y. Yang, X. Yu, C. Li, J. Lu, and S. Wang, "A preoperative nomogram for sepsis in percutaneous nephrolithotomy

treating solitary, unilateral and proximal ureteral stones," *PeerJ*, vol. 6, article e9435, 2020.

[10] C. Türk, A. Petřík, K. Sarica et al., "EAU guidelines on interventional treatment for urolithiasis," *European Urology*, vol. 69, no. 3, pp. 475–482, 2016.

[11] G. M. Preminger, D. G. Assimos, J. E. Lingeman, S. Y. Nakada, M. S. Pearle, and J. S. Wolf, "Chapter 1: AUA guideline on management of staghorn calculi: diagnosis and treatment recommendations," *The Journal of Urology*, vol. 173, no. 6, pp. 1991–2000, 2005.

[12] T. Tokas, T. R. W. Herrmann, A. Skolarikos, and U. Nagele, "Pressure matters: intrarenal pressures during normal and pathological conditions, and impact of increased values to renal physiology," *World Journal of Urology*, vol. 37, no. 1, pp. 125–131, 2019.

[13] P. J. S. Osther, "Risks of flexible ureterorenoscopy: pathophysiology and prevention," *Urolithiasis*, vol. 46, no. 1, pp. 59–67, 2018.

[14] J. Lu, Y. Xun, X. Yu et al., "Albumin-globulin ratio: a novel predictor of sepsis after flexible ureteroscopy in patients with solitary proximal ureteral stones," *Translational Andrology and Urology*, vol. 9, no. 5, pp. 1980–1989, 2020.

[15] Y. Uchida, R. Takazawa, S. Kitayama, and T. Tsujii, "Predictive risk factors for systemic inflammatory response syndrome following ureteroscopic laser lithotripsy," *Urolithiasis*, vol. 46, no. 4, pp. 375–381, 2018.

[16] G. Y. Lv, L. An, X. D. Sun, Y. L. Hu, and D. W. Sun, "Pretreatment albumin to globulin ratio can serve as a prognostic marker in human cancers: a meta-analysis," *Clinica Chimica Acta*, vol. 476, pp. 81–91, 2018.

[17] T. Yang, S. Liu, J. Hu, L. Wang, and H. Jiang, "The evaluation of risk factors for postoperative infectious complications after percutaneous nephrolithotomy," *BioMed Research International*, vol. 2017, Article ID 4832051, 7 pages, 2017.

[18] E. I. Kreydin and B. H. Eisner, "Risk factors for sepsis after percutaneous renal stone surgery," *Nature Reviews Urology*, vol. 10, no. 10, pp. 598–605, 2013.

[19] C. G. Xu and Y. L. Guo, "Diagnostic and prognostic values of BMPER in patients with urosepsis following ureteroscopic lithotripsy," *BioMed Research International*, vol. 2019, Article ID 8078139, 9 pages, 2019.

[20] S. Chugh, A. Pietropaolo, E. Montanari, K. Sarica, and B. K. Somani, "Predictors of urinary infections and urosepsis after ureteroscopy for stone disease: a systematic review from EAU section of urolithiasis (EULIS)," *Current Urology Reports*, vol. 21, no. 4, p. 16, 2020.

[21] D. Chen, C. Jiang, X. Liang et al., "Early and rapid prediction of postoperative infections following percutaneous nephrolithotomy in patients with complex kidney stones," *BJU International*, vol. 123, no. 6, pp. 1041–1047, 2019.